Università degli Studi di Pavia
Dottorato di Ricerca in Fisica – XXIII Ciclo

Modeling the fluctuations effects on radiofrequency current drive in toroidal plasmas

Lorenzo Morini

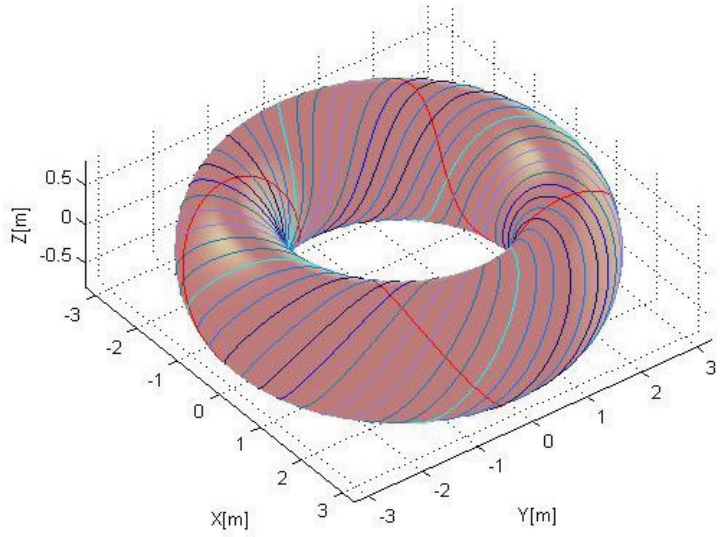

Supervisors: Dr. Y. Peysson
Prof. M. Carfora

Referee: Dr. C. Castaldo

Tesi per il conseguimento del titolo

Università
degli Studi
di Pavia

Dipartimento di
Fisica
"A. Volta"

DOTTORATO DI RICERCA IN FISICA – XXIII CICLO

Modeling the fluctuations effects on radiofrequency current drive in toroidal plasmas

dissertation submitted by

Lorenzo Morini

to obtain the degree of

DOTTORE DI RICERCA IN FISICA

Supervisors: Dr. Y. Peysson (CEA, Cadarache, France)
Prof. M. Carfora (Università degli Studi di Pavia)

Referee: Dr. C. Castaldo (Associazione EURATOM/ENEA sulla Fusione, Centro Ricerche Frascati)

Cover: Iso-fluctuations lines corresponding to different values of the drift -induced equilibrium perturbations, reported using the blue colormap and compared with a single equilibrium magnetic field line (red line). More details can be found in Fig.3.2 of this thesis on page 39.

Modeling the fluctuations effects on radiofrequency current drive in toroidal plasmas
Lorenzo Morini
PhD thesis – University of Pavia
Printed in Pavia, Italy, November 2010
ISBN 978-88-95767-43-7

Alla mia famiglia e a Carla,
perchè anche quando non era facile,
loro c'erano...

"Che hai fatto in questi anni, Noodles?"
"Sono andato a letto presto!"
Tratto dal film *"C'era una volta in America"*,
regia di Sergio Leone, 1984.

"La vera autenticità non sta nell'essere come si è, ma nel riuscire a somigliare il più possibile al sogno che ognuno ha di se stesso."
Tratto dal film *"Tutto su mia madre"*,
regia di Pedro Almodovar, 1999.

Contents

Introduction

In magnetically confined plasma devices and expecially in tokamak experiments fluctuations of several equilibrium quantities (density of the species, temperature, magnetic field) have been detected and measured with various techniques [1, 2, 3, 4, 5]. The effects of these fluctuations on high frequencies electromagnetic waves propagation has been extensively studied, principally with the purpose to develop active diagnostics with laser and microwaves (reflectrometry, Thomson scattering) [6, 7, 8]. However, fluctuations of the medium may affect strongly also the propagation and the absorption of radiofrequency (rf) waves used to generate toroidal current in non-inductive way (non-inductive current drive). The effects of plasmas fluctuations on Lower Hybrid waves have been investigated in several studies [9, 10, 11, 12]. The wave vector of lower hybrid waves has been identified to be potentially very sensitive to fluctuations, consequently the cumulative effects of these small equilibrium perturbations may affects strongly the wave damping and modify significantly the profiles of the current generated. More recently, it has been shown that plasma edge fluctuations in ITER tokamak scenarios can generate a spreading of the Electron Cyclotron wave beam launched for driving current enough localized for stabilizing NTM modes in high β regimes [13, 14]. The initial spreading can be amplified dramatically by the long distance between the mirrors where the wave enters and the magnetic flux on which the mode is growing, and this can compromise the stabilization procedure.
The precise estimation of fluctuations effects on propagation and absorption of radiofrequency waves can thus have a great relevance in the interpretation and comprehension of data from current drive experiments, which in many cases, expecially for lower hybrid current drive, are in poor agreement with theoretical predictions [15, 16]. Furthermore, an accurate analysis of conditions in which fluctuations effects are relevant is determinant for the project of efficient rf current drive systems and for the design of operative scenarios in future tokamak devices (ITER). Radiofrequency current drive modeling in toroidal plasmas requires the evaluation of the equilibrium distribution function of the particles, which is solution of the Boltzmann kinetic equation coupled with Maxwell's equations governing the evolution of the electromagnetic field in-

duced by the waves [17, 18]. The several time scales present in the plasma can be divided into two fundamental categories [17]: the fast time scales, corresponding to waves propagation and to electron gyromotion, and the slow time scales, associated to wave damping, bounced particles motion and collisions [19]. The equilibrium distribution function evolves in slow time scales and in order to study the continuative effects of the radiofrequency fields on this function an average of the Boltzmann kinetic equation on the fast time scales is performed. The drift kinetic equation governing the evolution of the distribution on the collisional timescales is derived [19]. This equation is solved by Fokker Planck routines coupled with wave propagation codes which evaluate the radiofrequency fields by means of fullwave techniques or various asymptotic methods (raytracing, beamtracing, quasioptics). Fullwave simulations are performed for low frequency waves (essentally ion cyclotron waves with f of the order of 100MHz), while for high frequency waves like lower hybrid (f of the order of few GHz) and electron cyclotron (f of the order of 100GHz) calculations become extremely long and require great computational resources, and asymptotic methods, which conditions of applicabity are satisfied in most cases of practical interest, provide very powerfull tools for the solution of Maxwell's equation. The aim of this work is to incorporate the fluctuations effects in these sofisticated numerical tools for calculation of current drive by high frequencies waves (lower hybrid and electron cyclotron) based on raytracing-Fokker Planck techniques, preserving in a consistent way the conditions of validity and applicability of this approach: the WKB approximation, which makes possible the utilization of raytracing techniques [18], the weak damping limit, which separates the propagation problem from the absorption [20], and the quasilinear description of wave-particle interaction processes [17, 18]. For this reason, instead of modeling the interaction of the radiofrequency waves with fluctuations in term of a sequence of scattering processes, as it has been proposed in many works [9, 11, 12, 13, 14], the effects of the fluctuations are described by introducing directly time-dependent perturbations of the magnetic equilibrium. The fast universal toroidal ray-tracing code C3PO [21] has been modified to incorporate the effects of equilibrium perturbations on ray trajectories. The modified raytracing tool is then coupled with the 3-D linearized bounce-averaged relativistic electron kinetic solver LUKE [22] in order to estimate the modification of the generated current profiles due to the perturbations. The approach proposed is general and can be used to describe the effects on high frequencies waves current drive of all fluctuations which properties preserve the conditions of validity of raytracing-Fokker Planck modeling techniques of wave-particle interaction. Fluctuations of all the equilibrium functions (density of the species, magnetic field, temperature) which satisfy this condition can be accounted in the propagation and the absorption of waves of various range of frequencies (lower hybrid and electron cyclotron), without any further restriction, and preserving the overall structure of the highly benchmarked existing tools.

This thesis is organized as follows. In chapter 1 a brief overview of radiofrequency current drive theory is given: the wave equation and the bounce-averaged kinetic equation are introduced and the raytracing technique for the calculation of the rf fields is illustrated. In chapter 2 the proposed general model for studying the fluctuations effects is described: generic time-dependent perturbation of the equilibrium are introduced and their inclusion in the raytracing-Fokker Planck routine is discussed in details. In chapter 3 are illustrated two examples of fluctuations processes which can be described in the framework of this model: drift-like stochastic fluctuations of the electronic density and of the magnetic field, and toroidal magnetic ripple field, which can be interpreted as a static perturbation of the magnetic equilibrium. The physical characteristics of these processes are discussed in details, and explicit expressions for the perturbations generated by these fluctuations are derived and explained using some simple examples. In the fourth chapter, after a brief description of lower hybrid and electron cyclotron characteristics in a cold plasma and a brief introduction to lower hybrid and electron cyclotron current drive, some examples of lower hybrid (LHCD) and electron cyclotron current drive (ECCD) calculations performed considering fluctuations are reported: the perturbations of the ray trajectories are shown using a simple analytical equilibrium with parameters typical of JET tokamak [21, 23], while the effects on the current profiles are tested in ITER tokamak scenarios. In the last chapter, conclusions and future perspectives regarding the thesis work are summerized. In appendix A the several sets of curvilinear coordinates system used for describing waves propagation and absorption in thesis work are illustrated in details. Finally in appendix B explicit expressions for the equilibrium derivatives used in modified raytracing equations are reported.

Chapter 1

Elements of radiofrequency current drive theory

Generating and driving toroidal current in a non-inductive way is necessary for a fusion reactor to operate in steady state conditions. Several methods for non-inductive plasma current drive have been proposed and extensively studied, both in theory and experiments, one of the most successful is based on the use of radiofrequency electromagnetic waves of several frequency regimes (Ion Cyclotron, Lower Hybrid, Electron Cyclotron, Electron Bernstein). These electromagnetic waves are excited into the plasma by external antennas or mirrors and exchange momentum as well as energy with the particles by means of various wave-particle resonance mechanisms. Using rf waves both plasma heating and current drive can be obtained. If the population of resonant particles is accelerated by the radiofrequency field along a particular direction, there is an unidirectional change in the velocity of resonant particles which generates a current flowing in the plasma. The equilibrium distribution function of the particles, initially Maxwellian and determined by the Coulomb collisions, is then modified and the new distribution function results from the competition between the acceleration due to the wave and the collisions that tend to re-establish a Maxwellian distribution.
In this chapter the theoretical issues for modeling this complex physical process, known as radiofrequency current drive, are briefly introduced. In the first section the different time scales involved in the process are illustrated and discussed in details: the fast scales associated to the wave propagation and the slow scales (bounce, collisional and wave damping scales) correspondent to the electron distribution function variation. Only the wave-electron interactions are considered, the ions dynamics is neglected. The basic evolution equations of the system are introduced: the Maxwell's equations coupled with the linearized Vlasov equation describe the fast evolution of the radiofrequency wave field, while the electron distribution function is given by the solution of the bounce-averaged relativistic kinetic equation, which is the balance equation between the diffusion term due to the radiofrequency wave effects and the col-

lisional operator associated to various collisional processes [17, 18]. The current induced into the plasma depends by the distribution function, as a consequence the numerical solution of the kinetic equation is necessary for estimating the radiofrequency current drive. The radiofrequency diffusion operator depends explicitely by the electric field induced by the wave, then the bounce-averaged kinetic equation is coupled with the linearized Maxwell-Vlasov system which governs the evolution of this field. In the second section the raytracing method for solving Maxwell's equations is presented. It is based on WKB approximation, that implies the reduction of the Maxwell's equations to a set of ordinary differential equations, the ray equations, which numerical integration is less expensive in terms of computational resources. Integrating the ray equations makes possible to estimate the ray contribution to the total power flow of the wave and then to evaluate the quasilinear diffusion operator. Once the diffusion operator has been calculated, the kinetic equation can be solved and the effects of the radiofrequency wave on the electron distribution function can be estimated.

1.1 Kinetic description of wave-particle interaction

The radiofrequency electromagnetic field is damped into the plasma by means of several Doppler resonant mechanisms and transfers energy and momentum to the resonant particles. Considering only the damping on the electrons, the general relativistic wave-particle resonance condition is:

$$\omega - k_{\parallel} v_{\parallel} = n\frac{\omega_{ce}}{\gamma} \qquad n = 0, \pm 1, \pm 2 \tag{1.1}$$

Where ω is the frequency of the wave, $k_{\parallel}$ is the component of the wave vector parallel to the magnetic field, $v_{\parallel}$ is the component of electron velocity parallel to the magnetic field, $\omega_{ce} = q_e B/m_e$ is the electron cyclotron frequency and n is the harmonic number, each different value of n corresponds to a different damping mechanism, (Landau damping and magnetic pumping correspond to $n = 0$, while cyclotron damping to $n = 1$).
The current induced by the wave is calculated using the relation:

$$\mathbf{J}(\mathbf{X}, t) = q_e \iiint \mathbf{v} f(\mathbf{X}, \mathbf{p}, t) d^3\mathbf{p} \tag{1.2}$$

where $f(\mathbf{X}, \mathbf{p}, t)$ is the electron distribution function in the phase space, $\mathbf{X}$ is the position and $\mathbf{v}$ is the electron velocity, and $\mathbf{p} = \gamma\mathbf{v}$. The electromagnetic field into the plasma is solution of the Maxwell's equations:

$$\nabla_{\mathbf{X}} \times \mathbf{E} = -\frac{\partial \mathbf{B}}{\partial t} \tag{1.3}$$

$$\nabla_{\mathbf{X}} \times \mathbf{B} = \mu_0 \varepsilon_0 \frac{\partial \mathbf{E}}{\partial t} + \mu_0 \mathbf{J} \tag{1.4}$$

where $\nabla_{\mathbf{X}}$ is the gradient operator in the configurations space. The electron distribution function $f(\mathbf{r}, \mathbf{p}, t)$ is solution of the Boltzmann kinetic equation:

$$\frac{\partial f}{\partial t} + \mathbf{v} \cdot \nabla_{\mathbf{X}} f + q_e(\mathbf{E} + \mathbf{v} \times \mathbf{B}) \cdot \nabla_{\mathbf{p}} f = \left(\frac{\partial f}{\partial t}\right)_C \tag{1.5}$$

Where $\nabla_{\mathbf{p}}$ is the gradient in the momentum space and $(\partial f/\partial t)_C$ is the Coulomb collision operator. The Maxwell's equations and the kinetic equation form a system of nonlinear coupled differential equations: the distribution function is solution of the kinetic equation, which presents a nonlinear term dependent by the electric and magnetic field, then it is necessary to evaluate an expression for these fields solving the Maxwell's equations. The total electric and magnetic field are composed by the equilibrium fields $\overline{\mathbf{E}}(\mathbf{X}, t)$ and $\overline{\mathbf{B}}(\mathbf{X}, t)$ and by the oscillating contributions due to the radiofrequency wave, $\widetilde{\mathbf{E}}(\mathbf{X}, t)$ and $\widetilde{\mathbf{B}}(\mathbf{X}, t)$. Assuming that the rf fields amplitude is small compared to the total fields amplitude, it is possible to consider $\widetilde{\mathbf{E}}(\mathbf{X}, t)$ and $\widetilde{\mathbf{B}}(\mathbf{X}, t)$ as first order perturbative corrections of the equilibrium fields:

$$\mathbf{E} = \overline{\mathbf{E}} + \widetilde{\mathbf{E}} \tag{1.6}$$

$$\mathbf{B} = \overline{\mathbf{B}} + \widetilde{\mathbf{B}} \tag{1.7}$$

$$\tag{1.8}$$

The perturbations are assumed to be harmonic:

$$\widetilde{\mathbf{E}}(\mathbf{X}, t) = \int d\omega \iiint d^3\mathbf{k} \widetilde{\mathbf{E}}_{\mathbf{k},\omega} e^{i(\mathbf{k}\cdot\mathbf{X} - \omega t)} \tag{1.9}$$

$$\widetilde{\mathbf{B}}(\mathbf{X}, t) = \int d\omega \iiint d^3\mathbf{k} \widetilde{\mathbf{B}}_{\mathbf{k},\omega} e^{i(\mathbf{k}\cdot\mathbf{X} - \omega t)} \tag{1.10}$$

The distribution function and the current are respectively:

$$\begin{aligned} f &= \overline{f} + \widetilde{f} \\ \mathbf{J} &= \overline{\mathbf{J}} + \widetilde{\mathbf{J}} \end{aligned} \tag{1.11}$$

Where $\widetilde{f}$ and $\widetilde{\mathbf{J}}$ are the perturbations of the equilibrium distribution function and of the current due to the wave fields. The equilibrium quantities evolve at time scales much slower than the wave propagation times (of the order of $\tau_\omega = 2\pi/\omega$), this means that during the rf field evolution $\overline{\mathbf{E}}, \overline{\mathbf{B}}, \overline{f}$ and $\overline{\mathbf{J}}$ do not vary in time[17, 18]. The collision frequency ν_c ($\nu_{ee} \approx 1$KHz) is much smaller than the wave frequency ω ($\omega/2\pi =$ 1GHz for LH and $\omega/2\pi \approx 100$GHz for EC), and the gyro-frequency ω_{ce} ($\omega_{ce}/2\pi \approx 10$GHz for $\gamma \approx 1$). This means that the collisions are not enough frequent to affect the rf fields evolution and the electron gyromotion, and if the equations are referred to the wave or to the gyromotion time scales, the collisional effects can be neglected.
In tokamak devices the electrons moving in slowly varying magnetic field have

an adiabatic invariant: their magnetic moment μ. The electrons perpendicular gyro-motion presents a magnetic potential energy given by the relation:

$$W_\perp = \mu B \tag{1.12}$$

If the magnetic field intensity B varies along the field lines, the electron energy conservation law, defined as follows:

$$\frac{m_e}{2} v_\parallel^2 + \mu B = E \tag{1.13}$$

Where $v_\parallel$ is the electron velocity parallel to the magnetic field, leads to electrons trapping in the field well created by the potential μB: the electrons which have not enough kinetic energy to escape from the well generated by the magnetic potential start to move in closed trapped orbits known as "banana orbits", while the electrons having sufficient velocity to escape from the well (passing electrons) continue to circulate along their originary trajectories of motion. The frequency of the electron motion in the closed orbits is the bounce frequency ω_b and is small compared to ω and to ω_{ce}. The Coulomb collisions deviate the electrons from their original orbits, but the collision frequency ν_c is much smaller than bounce frequency ($\nu_{ee} \approx 1$KHz), so the time required by the collisions to deflect the motion is too long respect to the bouncing period and the electrons trapped or escaping are able to complete their orbits [17, 22]. In practice:

$$\nu_c \ll \omega_b/2\pi \ll \omega/2\pi, \omega_{ce}/2\pi \tag{1.14}$$

Using the periods:

$$\tau_\omega, \tau_{ce} \ll \tau_b \ll \tau_c \tag{1.15}$$

As a consequence, four different time scales, corresponding to different physical processes, are involved in the problem:

- The wave time scale, correspondent to the rf wave dynamics, with characteristic time length $\tau_\omega = 2\pi/\omega$;
- The gyromotion time scale, associated with the electron gyromotion, with characteristic time length $\tau_{ce} = 2\pi/\Omega_e$
- The bounce time scale, associated to the trapped or passing electron motion along the field lines, with characteristic time length $\tau_b = 2\pi/\omega_b$;
- The collisional time scale with characteristic time length $\tau_c = 1/\nu_c$;

The wave dynamics can be studied specializing the Maxwell-Boltzmann system to the wave time scales and deriving the orders zero and one of the perturbative developing using the expressions (1.8) and (1.11), this procedure is illustrated in the next subsection and makes possible the linearization of the kinetic equation. The solution of this equation gives an expression for $\widetilde{f}$ in function of $\overline{f}$ and of the rf fields, and using this expression into the Faraday's law is possible

to obtain a linear constitutive relation depending by the equilibrium distribution function, which is stationary respect to the fast time scales [17, 18]. The estimation of the equilibrium distribution function is necessary for calculating the current coupled to the plasma, as a consequence the low time scales modification of $\overline{f}$ due to the rf fields must be considered. These effects are described by the quasilinear term of the Bounce-averaged Fokker-Planck equation, illustrated in subsection 1.1.2, which governs the evolution of $\overline{f}$ on the slow time scales. The numerical solution of this equation is essential for all current drive calculations [17, 18, 22].

1.1.1 Linearized Vlasov equation

Considering the dynamics at the fast time scales, correspondent to the wave and to the gyromotion, as just discussed, the collisions can be neglected. The Boltzmann kinetic equation (1.5) in the non-collisional limit becomes the Vlasov equation:

$$\frac{\partial f}{\partial t} + \mathbf{v} \cdot \nabla_{\mathbf{X}} f + q_e(\mathbf{E} + \mathbf{v} \times \mathbf{B}) \cdot \nabla_{\mathbf{p}} f = 0 \tag{1.16}$$

The system constituted by the Vlasov and the Maxwell's equations describes in a self-consistent way the rf wave dynamics. Using the perturbative expressions (1.8) and (1.11) the equation (1.16) can be linearized. The solution of the zero-order Vlasov equation gives the equilibrium distribution function, which is stationary respect to this fast time scales, in function of the equilibrium fields:

$$\mathbf{v} \cdot \nabla_{\mathbf{X}} \overline{f} + q_e(\overline{\mathbf{E}} + \mathbf{v} \times \overline{\mathbf{B}}) \cdot \nabla_{\mathbf{p}} \overline{f} = 0 \tag{1.17}$$

While the zero-order Ampere's law is:

$$\nabla_{\mathbf{X}} \times \overline{\mathbf{B}} = \mu_0 \overline{\mathbf{J}} \tag{1.18}$$

Where $\mathbf{J}$ is the first order moment of the equilibrium distribution function:

$$\overline{\mathbf{J}} = q_e \iiint \mathbf{v} \overline{f}(\mathbf{X}, \mathbf{p}, t) d^3\mathbf{p} \tag{1.19}$$

The first order kinetic equation is known as the linearized Vlasov equation:

$$\frac{\partial \widetilde{f}}{\partial t} + \mathbf{v} \cdot \nabla_{\mathbf{p}} \widetilde{f} + q_e(\overline{\mathbf{E}} + \mathbf{v} \times \overline{\mathbf{B}}) \cdot \nabla_{\mathbf{p}} \widetilde{f} = -q_e(\widetilde{\mathbf{E}} + \mathbf{v} \times \widetilde{\mathbf{B}}) \cdot \nabla_{\mathbf{p}} \overline{f} \tag{1.20}$$

This equation describes the evolution of the perturbation of the distribution function $\widetilde{f}$ generated by the rf fields $\widetilde{\mathbf{E}}$ and $\widetilde{\mathbf{B}}$, which are solution of the first order Maxwell's equations:

$$\nabla_{\mathbf{X}} \times \widetilde{\mathbf{E}} = -\frac{\partial \widetilde{\mathbf{B}}}{\partial t} \tag{1.21}$$

$$\nabla_{\mathbf{X}} \times \widetilde{\mathbf{B}} = \mu_0 \varepsilon_0 \frac{\partial \widetilde{\mathbf{E}}}{\partial t} + \mu_0 \widetilde{\mathbf{J}} \tag{1.22}$$

The linearized Vlasov equation can be solved with the method of the characteristics, integrating along the unperturbed particle orbits, this procedure is illustrated and discussed in details in several manuals of plasma waves kinetic theory [17, 18], and it gives an expression of $\widetilde{f}$ in function of $\nabla_{\mathbf{p}}\widetilde{f}$ and of the equilibrium fields:

$$\widetilde{f}(\mathbf{X}, \mathbf{p}, t) = -q_e \int_{-\infty}^{t} dt' [\overline{\mathbf{E}}(\mathbf{X}', t') + \mathbf{v} \times \overline{\mathbf{B}}(\mathbf{X}', t')] \cdot \nabla_{\mathbf{p}} \overline{f} \tag{1.23}$$

Injecting this expression in the general definition of current, and assuming that the response of the plasma to the wave fields is linear ($\mathbf{J} \propto \mathbf{E}$) [17], the following linear constitutive relation is derived:

$$\widetilde{\mathbf{J}} = q_e \iiint \mathbf{v} \widetilde{f}(\mathbf{X}, \mathbf{p}, t) d^3\mathbf{p} \equiv \mathbb{S}(\overline{f}) \cdot \widetilde{\mathbf{E}} \tag{1.24}$$

Where $\mathbb{S}(\overline{f})$ is the conductivity tensor, related to the dielectric tensor by the relation:

$$\mathbb{K}(\overline{f}) = \mathbb{I} + \frac{i}{\varepsilon_0 \omega} \mathbb{S}(\overline{f}) \tag{1.25}$$

The integration along the unperturbed orbits gives an explicit expression for the conductivity tensor or for the diectric tensor in function of the equilibrium distribution function $\overline{f}$, these tensors describe the response of the plasma to the sollecitations due to the rf waves electromagnetic fields. Inserting the constitutive relation (1.24) into the Ampere's law (1.21) and injecting this equation in the Faraday's law (1.22), yields to the wave equation:

$$\nabla_{\mathbf{X}} \times \nabla_{\mathbf{X}} \times \widetilde{\mathbf{E}} + \mu_0 \mathbb{S}(\overline{f}) \cdot \frac{\partial \widetilde{\mathbf{E}}}{\partial t} + \varepsilon_0 \mu_0 \frac{\partial^2 \widetilde{\mathbf{E}}}{\partial t^2} = 0 \tag{1.26}$$

Solving this equation makes possible to calculate the electric field induced by the rf wave. The rf wave dynamics is completely described by the linearized Maxwell-Vlasov system, which solution in closed form gives explicit expressions for the rf waves fields and for the perturbations of the current and of the distribution function associated with the wave. This system is referred to the waves and to the gyromotion time scales, the equilibrium distribution function is stationary respect to these scales, and infact it is obtained in function of the equilibrium fields as solution of the zero-order steady state Vlasov equation 1.17, but considering the effects of the wave fields on the slow time scales, correspondent to the bounce and collisional periods, is necessary for evaluating $\overline{f}$ in a correct and consistent way.

1.1.2 Bounce averaged kinetic equation

In order to derive an equation adequate for describing the evolution of the equilibrium distribution function on the slow time scales, which correspond

to the bounce and the collisional times, the Boltzmann kinetic equation (1.5) must be averaged over the wave and the gyromotion time scales. This implies an averaging operation over a period $\tau = 2\pi/\omega$ with ω rf waves frequency, and over the azimuthal angle in the momentum space φ (in the momentum space the cylindrical coordinates system $(p_\parallel, p_\perp, \varphi)$ where $p_\parallel$ is the component of the momentum parallel to the equilibrium magnetic field and $p_\perp$ is used). The average over φ is performed because a dependence of the equilibrium distribution function by the gyro-angle would imply a time variation on scales tipical of the gyromotion, of the order $\tau_{ce} = 2\pi/\omega_{ce}$. Introducing the perturbative expressions for the total fields (1.8) and for the total distribution function (1.11) into the equation (1.5) and performing the wave- and gyro-averaging, the resulting equation is:

$$\frac{\partial \overline{f}}{\partial t} + \mathbf{v}_{gc} \cdot \nabla_{\mathbf{X}} \overline{f} = \varepsilon(\overline{f}) + C(\overline{f}) + Q(\overline{f}) \tag{1.27}$$

Where $\mathbf{v}_{gc}$ is the electron guiding center velocity, the operator $\varepsilon(\overline{f})$ describes the action of the ohmic electric field on the distribution function, $C(\overline{f})$ is the Coulomb collision operator averaged over the fast time scales and $Q(\overline{f})$ is the quasilinear operator which describes the time-averaged effects of the nonlinear term of the kinetic equation on $\overline{f}$; in other words, it represents the effects of the radiofrequency wave fields on the distribution function averaged on the wave and on the gyromotion time scale [17, 18, 22]:

$$C(\overline{f}) = \int_0^{2\pi/\omega} dt \int_0^{2\pi} d\varphi \left(\frac{\partial f}{\partial t} \right)_C \tag{1.28}$$

$$Q(\overline{f}) = -\int_0^{2\pi/\omega} dt \int_0^{2\pi} d\varphi \left[q_e \left(\widetilde{\mathbf{E}} + \mathbf{v} \times \widetilde{\mathbf{B}} \right) \cdot \nabla_{\mathbf{p}} \widetilde{f} \right] \tag{1.29}$$

$$\varepsilon(\overline{f}) = -\int_0^{2\pi/\omega} dt \int_0^{2\pi} d\varphi q_e \overline{\mathbf{E}} \cdot \nabla_{\mathbf{p}} \overline{f} \tag{1.30}$$

The quasilinear operator can be expressed in the flux conservative form as a diffusion operator in the momentum space[17, 22]:

$$Q(\overline{f}) = -\nabla_{\mathbf{p}} \cdot (\mathbb{D}^{QL} \cdot \nabla_{\mathbf{p}} \overline{f}) \tag{1.31}$$

The diffusion tensor $\mathbb{D}^{QL}$ is function of $\left\| \widetilde{\mathbf{E}} \right\|^2$, then the wave- and gyro-averaged kinetic equation (1.27) is nonlinearly coupled with the wave equation (1.26) and the estimation of the rf electric field is necessary to evaluate the quasilinear operator. The gyro-averaged equilibrium distribution function $\overline{f}(\mathbf{r}, \mathbf{p}, t)$ in plasmas with axisymmetric configuration is function of four coordinates: two in the momentum space $(p_\parallel, p_\perp)$, and two in the configuration space, which using the flux coordinates system described in section 2.2 are (ψ, θ), while the dependence by the toroidal angle ϕ is dropped for effect of the axisymmetry. The time dependence is referred to the bounce and the collisional time scales. Remembering the discussion at the beginning of the section, in the low collisional limit the collisions frequency is much less than the bounce frequency,

then the time required by the collisions to deflect the electrons orbits is too long respect to the bounce period and the electrons trajectories along the magnetic field lines are not perturbed significantly, as a consequence it is possible to perform the averaging of the kinetic equation over a bounce period, the result is the bounce averaged kinetic equation:

$$\frac{\partial \left\{\overline{f}\right\}}{\partial t} = \left\{\varepsilon(\overline{f})\right\} + \left\{C(\overline{f})\right\} + \left\{Q(\overline{f})\right\} \tag{1.32}$$

The bounce average of the drift term present in the gyro-averaged vanishes and the bounce averaged distribution function is uniform along the field line and independent by the poloidal angle θ, then $\left\{\overline{f}\right\} = \left\{\overline{f}\right\}(\psi, p_{\parallel}, p_{\perp}, t)$ and the equation 1.32 is a 3-D partial differential equation which time dependence is referred to the collisions time scale. The numerical solution of this equation makes possible the estimation of the continuative effects of the rf induced fields on the equilibrium distribution function.

1.2 RF Waves Dynamics

Since the quasilinear diffusion tensor $\mathbb{D}^{QL}$ is function of $\left\|\widetilde{\mathbf{E}}\right\|^2$, the kinetic equation (1.32) is nonlinearly coupled with the wave equation (1.26), and radiofrequency current drive calculations require the evaluation of the waves induced field $\widetilde{\mathbf{E}}$. The calculation of this field using full wave methods is a complex problem, and requires very powerful computational resources, however, if the wavelength and the wave period are small compared to the typical time and space variations scale length of the medium, (propagation in a slowly varying medium), the waves propagation and absorption can be described using the geometrical optics techniques, based on the asymptotic solution of the equation (1.26), obtained by the eikonal ansatz. Remembering that the equilibrium varies at very slow time scales respect to the waves fields the plasma is assumed to be stationary respect to the wave, and the general conditions of applicability of the eikonal approximation in a slowly non-homogeneous plasma state that the wavelength λ must be much shorter than the equilibrium scale length L:

$$\lambda \ll L \tag{1.33}$$

And that the wave characteristics also varies slowly:

$$\|\nabla \mathbf{k}\|^2 \gg \|\nabla k\| \tag{1.34}$$

These two conditions imply that the wave properties valid for a uniform plasma (Fourier analysis, group velocity, local conductivity tensor) can be applied locally also in a slowly non-homogeneous plasma, and that the wave vector $\mathbf{k}$ is a slowly varying function of the space. If the transverse size of the radiofrequency beam d satisfies the inequality:

$$\lambda \ll d \tag{1.35}$$

The beam can be represented also as a quasi-plane wave and the electric field can be expressed as a wave packet [19]. In practice, if:

$$\lambda \ll d \ll L \tag{1.36}$$

Both the eikonal approximation than the quasi-plane wave representation are valid and the radiofrequency electric field $\widetilde{\mathbf{E}}$ can be expressed as follows:

$$\widetilde{\mathbf{E}}(\mathbf{X},t) = \widetilde{\mathbf{E}}_{\mathbf{k},\omega}(\mathbf{X},t)e^{i(\mathbf{k}(\mathbf{X})\cdot\mathbf{X}-\omega t)} \tag{1.37}$$

The wave vector $\mathbf{k}$ is much larger than the variations of the amplitude $\widetilde{\mathbf{E}}_{\mathbf{k},\omega}$ in the direction perpendicular to the group velocity, in this case the spectral width in this direction is very small, diffraction effects are negligibles and raytracing techniques can be used to study the evolution of $\mathbf{k}$ and $\widetilde{\mathbf{E}}_{\mathbf{k},\omega}$.

1.2.1 Weak damping approximation

The weak damping approximation assumes that the electric field amplitude varies slowly in space and in time in the direction of the group velocity compared respectively to the wavelength and to the wave period [18], in this case the following relations are satisfied:

$$\frac{\left\|\nabla_{\mathbf{X}}\widetilde{\mathbf{E}}_{\mathbf{k},\omega}\cdot\mathbf{v}_G\right\|}{\left\|\widetilde{\mathbf{E}}_{\mathbf{k},\omega}\cdot\mathbf{v}_G\right\|} \ll \|\mathbf{k}\| \tag{1.38}$$

$$\frac{\left\|\partial\widetilde{\mathbf{E}}_{\mathbf{k},\omega}/\partial t\cdot\mathbf{v}_G\right\|}{\left\|\widetilde{\mathbf{E}}_{\mathbf{k},\omega}\cdot\mathbf{v}_G\right\|} \ll \omega \tag{1.39}$$

Assuming the validity of the weak damping approximation and using the expression (1.37) for the rf field, the wave equation (1.26) becomes [1][19]:

$$\mathbb{D}_{\mathbf{k},\omega}\cdot\widetilde{\mathbf{E}}_{\mathbf{k},\omega} = i\nabla_{\mathbf{k}}\mathbb{D}_{\mathbf{k},\omega} : \nabla_{\mathbf{X}}\widetilde{\mathbf{E}}_{\mathbf{k},\omega} \tag{1.40}$$

Where $\mathbb{D}_{\mathbf{k},\omega}$ is the dispersion tensor in the Fourier space, defined as follows:

$$\mathbb{D}_{\mathbf{k},\omega} = \mathbf{NN} - N^2\mathbb{I} + i\frac{\mathbb{S}_{\mathbf{k},\omega}(\overline{f})}{\varepsilon_0\omega} \tag{1.41}$$

$\mathbb{S}_{\mathbf{k},\omega}$ is the Fourier transform of the conductivity tensor, and it is still a function of the equilibrium distribution function $\overline{f}$, while $\mathbf{N}$ is the wave refractive index, given by the expression:

$$\mathbf{N} \equiv \frac{c}{\omega}\mathbf{k} \tag{1.42}$$

[1] the double dot product is defined as: $\nabla_{\mathbf{k}}\cdot\left(\mathbb{D}_{\mathbf{k},\omega}\cdot\nabla_{\mathbf{X}}\widetilde{\mathbf{E}}_{\mathbf{k},\omega}\right) = \nabla_{\mathbf{k}}\mathbb{D}_{\mathbf{k},\omega} : \nabla_{\mathbf{X}}\widetilde{\mathbf{E}}_{\mathbf{k},\omega} + \nabla_{\mathbf{k}}\left(\nabla_{\mathbf{X}}\widetilde{\mathbf{E}}_{\mathbf{k},\omega}\right) : \mathbb{D}_{\mathbf{k},\omega} = \nabla_{\mathbf{k}}\mathbb{D}_{\mathbf{k},\omega} : \nabla_{\mathbf{X}}\widetilde{\mathbf{E}}_{\mathbf{k},\omega}$

The susceptibility tensor of the plasma $\mathbb{X}_{\mathbf{k},\omega}$ and then the dielectric tensor $\mathbb{K}_{\mathbf{k},\omega}$ are defined in function of $\mathbb{S}_{\mathbf{k},\omega}$:

$$\mathbb{X}_{\mathbf{k},\omega}(\overline{f}) = \frac{i}{\varepsilon_0\omega}\mathbb{S}_{\mathbf{k},\omega}(\overline{f}) \tag{1.43}$$

$$\mathbb{K}_{\mathbf{k},\omega}(\overline{f}) = \mathbb{I} + \mathbb{X}_{\mathbf{k},\omega}(\overline{f}) \tag{1.44}$$

The dielectric tensor represents the response of the plasma to the electromagnetic waves sollecitations, and the dispersion tensor can be rewritten as follows:

$$\mathbb{D}_{\mathbf{k},\omega} = \mathbf{NN} - N^2\mathbb{I} + \mathbb{K}_{\mathbf{k},\omega}(\overline{f}) \tag{1.45}$$

Considering a cylindrical symmetry respect to the magnetic field axis $\mathbf{b} = \mathbf{B}/B$, the components of the refractive index parallel and perpendicular to $\mathbf{b}$ are defined respectively:

$$N_\parallel = \mathbf{N}\cdot\mathbf{b} \tag{1.46}$$

$$N_\perp = \|\mathbf{N}\times\mathbf{b}\| \tag{1.47}$$

The component $N_\parallel$ and the wave frequency ω are assumed to be given real quantities (only propagative modes are considered), while the unknown quantity $N_\perp$ presents in the general case a real and an imaginary part:

$$N_\perp = N_{\perp r} + iN_{\perp i} \tag{1.48}$$

As a consequence, the dispersion tensor $\mathbb{D}_{\mathbf{k},\omega}$ may be decomposed as follows:

$$\mathbb{D}_{\mathbf{k},\omega} = \mathbb{D}^H_{\mathbf{k},\omega} + i\mathbb{D}^A_{\mathbf{k},\omega} \tag{1.49}$$

Where $\mathbb{D}^H_{\mathbf{k},\omega}$ and $\mathbb{D}^A_{\mathbf{k},\omega}$ are respectively the hermitian and the antihermitian part, given by the expressions:

$$\mathbb{D}^H_{\mathbf{k},\omega} = \frac{\mathbb{D}_{\mathbf{k},\omega} + \mathbb{D}^*_{\mathbf{k},\omega}}{2} \tag{1.50}$$

$$\mathbb{D}^A_{\mathbf{k},\omega} = \frac{\mathbb{D}_{\mathbf{k},\omega} - \mathbb{D}^*_{\mathbf{k},\omega}}{2i} \tag{1.51}$$

In the weak damping limit, the condition $|\mathbb{D}^A_{ij}| \ll |\mathbb{D}^H_{ij}|$ must be satisfied, where $\mathbb{D}^H_{ij}$ and $\mathbb{D}^A_{ij}$ are respectively the elements of the hermitian and of the antihermitian part of the dispersion tensor, and this conditions implies that $|N_{\perp i}| \ll |N_{\perp r}|$. Taking $\delta \simeq |\mathbb{D}^A_{ij}|/|\mathbb{D}^H_{ij}| \ll 1$ as a small expansion parameter, the perpendicular index of refraction, the dispersion tensor and the polarization vectors $\widetilde{\mathbf{e}}_{\mathbf{k},\omega} = \widetilde{\mathbf{E}}_{\mathbf{k},\omega}/||\widetilde{\mathbf{E}}_{\mathbf{k},\omega}||$ can be expanded in powers of δ [19, 20]:

$$\begin{aligned} N_\perp &= N_{\perp 0} + N_{\perp 1} + \cdots \\ \widetilde{\mathbf{e}}_{\mathbf{k},\omega} &= \widetilde{\mathbf{e}}_{\mathbf{k},\omega,0} + \widetilde{\mathbf{e}}_{\mathbf{k},\omega,1} + \cdots \\ \mathbb{D}_{\mathbf{k},\omega} &= \mathbb{D}_{\mathbf{k},\omega}\left(N_{\perp 0}\right) + N_{\perp 1}\frac{\partial \mathbb{D}_{\mathbf{k},\omega}}{\partial N_{\perp r}}\bigg|_{N_\perp = N_{\perp 0}} + \cdots \end{aligned} \tag{1.52}$$

The Taylor expansion of $\mathbb{D}_{\mathbf{k},\omega}$ is possible because $\mathbb{D}_{\mathbf{k},\omega}(N_\perp)$ is analytical. Substituing these expressions in the (1.40), the wave equation can be ordered in powers of δ. At the zero-order the following equation is obtained:

$$\mathbb{D}_{\mathbf{k},\omega}\left(N_{\perp 0}\right)\cdot\widetilde{\mathbf{e}}_{\mathbf{k},\omega,0}=0 \tag{1.53}$$

This equation possesses non-trivial solutions if and only if the determinant of the dispersion tensor $\mathbb{D}^H_{\mathbf{k},\omega}$ is zero, this condition defines the dispersion relation:

$$\mathcal{D}(N_{\perp 0},N_\parallel,\omega)\equiv \det\mathbb{D}^H_{\mathbf{k},\omega}\left(N_{\perp 0}\right)=0 \tag{1.54}$$

This scalar equation gives the local electromagnetic eigenmodes that can be excited independently in an homogeneous and stationary plasma. It can be solved for $N_{\perp 0}(N_\parallel,\omega)$, and considering only propagative modes $N_{\perp 0}=N_{\perp r0}$ is real, since $\mathbb{D}^H_{\mathbf{k},\omega}$ is hermitian. At the first order the equation for the wave amplitude in direction of the beam is derived [19]:

$$\mathbf{v}_G\cdot\nabla_{\mathbf{X}}\left\|\widetilde{\mathbf{E}}_{\mathbf{k},\omega}\right\|+\frac{\widetilde{\mathbf{e}}^*_{\mathbf{k},\omega,0}\cdot\mathbb{D}^A_{\mathbf{k},\omega}\cdot\widetilde{\mathbf{e}}_{\mathbf{k},\omega,0}}{\partial\left(\widetilde{\mathbf{e}}^*_{\mathbf{k},\omega,0}\cdot\mathbb{D}^H_{\mathbf{k},\omega}\cdot\widetilde{\mathbf{e}}_{\mathbf{k},\omega,0}\right)/\partial\omega}\left\|\widetilde{\mathbf{E}}_{\mathbf{k},\omega}\right\|=0 \tag{1.55}$$

This equation describes the energy transfer between the wave and the resonant particles (in this case between the wave and the electrons). The propagative characteristics of the waves are fully described by the equation (1.53), while the damping due to the interaction with the resonant particles is governed by the (1.55). Since $N_{\perp 0}$ is real, the hermitian part of the dispersion tensor $\mathbb{D}^H_{\mathbf{k},\omega}$ depends by the principal value of the momentum space integral which determines the conductivity tensor $\mathbb{S}_{\mathbf{k},\omega}$ and the dielectric tensor $\mathbb{K}_{\mathbf{k},\omega}$, while the contribution of the resonant particles is contained in the antihermitian part $\mathbb{D}^A_{\mathbf{k},\omega}$, which depends by the antihermitian dielectric tensor $\mathbb{K}^A_{\mathbf{k},\omega}$. As a consequence, for studying waves propagation the resonant part of the dispersion tensor is ignored and $\mathbb{D}^H_{\mathbf{k},\omega}$ is almost dependent by the bulk of the distribution function, which is Maxwellian:

$$\mathbb{D}^H_{\mathbf{k},\omega}(\overline{f})\simeq\mathbb{D}^H_{\mathbf{k},\omega}(f_M) \tag{1.56}$$

The waves propagation can thus be studied under the limitative condition (1.36) using the raytracing techniques and assuming $\mathbb{D}^H_{\mathbf{k},\omega}(\overline{f})=\mathbb{D}^H_{\mathbf{k},\omega}(f_M)$. In the next subsection the ray equations are derived applying the characteristics method to the general expression of the dispersion equation (1.54).
The antihermitian part of the dispersion tensor $\mathbb{D}^A_{\mathbf{k},\omega}(\overline{f})$, instead, depends strongly by the variations of the equilibrium distribution function $\overline{f}$ generated by the interaction between the radiofrequency waves and the resonant electrons, consequently, for estimating the wave amplitude, the evaluation of the equilibrium distribution function by means of the numerical solution of the bounce-averaged kinetic equation (1.32) is required. The global consistency of this scheme is ensured by the equivalence between the energy lost by the wave,

which damping is described by the amplitude equation (1.55), and the energy gained by the resonant electrons, described by the quasilinear diffusion operator (1.31), equivalently, between the power dissipated by the wave, given by the relation:

$$P = \frac{\varepsilon_0 \omega}{2} \left\| \widetilde{\mathbf{E}}_{\mathbf{k},\omega} \right\|^2 \left(\widetilde{\mathbf{e}}^*_{\mathbf{k},\omega} \cdot \mathbb{D}^A_{\mathbf{k},\omega} \cdot \widetilde{\mathbf{e}}_{\mathbf{k},\omega} \right) \tag{1.57}$$

and the power gained by the electrons.

1.2.2 Ray equations

Assuming that the conditions of applicability (1.36) are satisfied, the propagative characteristics of the radiofrequency waves can be studied solving the equation (1.53) with the raytracing technique. The zero-order real perpendicular refractive index can be determined in function of $N_\parallel$ and ω solving the dispersion relation (1.54). Remembering that the hermitian part of the dispersion tensor is mostly determined by the bulk of the distribution function, it is assumed that $\mathbb{D}^H_{\mathbf{k},\omega}(\overline{f}) = \mathbb{D}^H_{\mathbf{k},\omega}(f_M)$, consequentely the susceptibility tensor $\mathbb{X}^H_{\mathbf{k},\omega}$ and the dielectric tensor $\mathbb{K}^H_{\mathbf{k},\omega}$ can be expressed in function of the following non-dimensional parameters: the refractive index $\mathbf{N}$, the thermal velocity normalized to the speed of the light $\beta_{T\alpha} = v_{T\alpha}/c$ where $v_{T\alpha} = \sqrt{kT_\alpha/m_\alpha}$, the ratios $\overline{\omega}_{p\alpha} = \omega_{p\alpha}/\omega$ and $\overline{\omega}_{c\alpha} = \omega_{c\alpha}/\omega$ of the plasma frequency $\omega_{p\alpha} = \sqrt{q_\alpha^2 n_\alpha/\varepsilon_0 m_\alpha}$ and of the cyclotron frequency $\omega_{c\alpha} = q_\alpha B/m_\alpha$ to the wave frequency ω. The dispersion tensor $\mathbb{D}^H_{\mathbf{k},\omega}$ can be rewritten as follows:

$$\mathbb{D}^H_{\mathbf{k},\omega} = \mathbf{NN} - N^2\mathbb{I} + \mathbb{K}^H_{\mathbf{k},\omega}(\mathbf{N}, \beta_{T\alpha}, \overline{\omega}_{p\alpha}, \overline{\omega}_{c\alpha}) \tag{1.58}$$

In this case, remembering that in the weak damping limit $|N_{\perp i}| \ll |N_{\perp r}|$ and assuming the zero-order approximation $N_{\perp r} = N_{\perp r0}$, the dispersion relation (1.54) becomes:

$$\mathcal{D}(N_\parallel, N_{\perp r}, \beta_{T\alpha}, \overline{\omega}_{p\alpha}, \overline{\omega}_{c\alpha}) \equiv \det \mathbb{D}^H_{\mathbf{k},\omega}(N_\parallel, N_{\perp r}, \beta_{T\alpha}, \overline{\omega}_{p\alpha}, \overline{\omega}_{c\alpha}) = 0 \tag{1.59}$$

From here in this subsection $\mathbf{N}$ and $\mathbf{k} = \omega\mathbf{N}/c$ will be referred to the zero-order real solution of this dispersion relation, which components are $N_\parallel$ and $N_\perp = N_{\perp r} = N_{\perp r0}$.
The ray equations in a plasma slowly varying in space and time are defined by the condition $\mathcal{D}(\mathbf{X}, t, \mathbf{k}, \omega) = 0$ along the ray trajectory, where $\mathcal{D}$ is the dispersion relation (1.59). Therefore, at each point along the ray trajectory the following condition must be satisfied:

$$\delta\mathcal{D} = \frac{\partial \mathcal{D}}{\partial \mathbf{X}} \cdot \delta\mathbf{X} + \frac{\partial \mathcal{D}}{\partial t}\delta t + \frac{\partial \mathcal{D}}{\partial \mathbf{k}} \cdot \delta\mathbf{k} + \frac{\partial \mathcal{D}}{\partial \omega}\delta\omega = 0 \tag{1.60}$$

This condition can be rewritten as follows:

$$\delta\mathcal{D} = \frac{\partial \mathcal{D}}{\partial \mathbf{X}} \cdot \dot{\mathbf{X}}\delta\tau + \frac{\partial \mathcal{D}}{\partial t}\dot{t}\delta\tau + \frac{\partial \mathcal{D}}{\partial \mathbf{k}} \cdot \dot{\mathbf{k}}\delta\tau + \frac{\partial \mathcal{D}}{\partial \omega}\dot{\omega}\delta\tau = 0 \tag{1.61}$$

Where τ is the curvilinear adimensional coordinate which represents the distance along the ray trajectory, and $\dot{\mathbf{X}} = d\mathbf{X}/d\tau, \dot{\mathbf{k}} = d\mathbf{k}/d\tau, \dot{t} = dt/d\tau, \dot{\omega} = d\omega/d\tau$. If the wave vector $\mathbf{k}$ is expressed in coordinates that are canonically conjugate to those of the position vector $\mathbf{X}$, the following relation is verified:

$$\{X_i, k_j\} = \delta_{ij} \tag{1.62}$$

Where $\{\cdots\}$ is the Poisson bracket, δ_{ij} is the Kronecker delta symbol, X_i and k_j the coordinates of the vectors $\mathbf{X}$ and $\mathbf{k}$ respectively. Since the frequency ω and the time t are also canonically conjugate, the dispersion relation can be seen as the "hamiltonian" of the ray, infact it is a function of a set of canonically conjugate coordinates and its value is constant along the trajectory, and the analogy with the conservation of the mechanical energy along the particle trajectories in classical mechanics [24] is total. Considering the Hamiltonian nature of $\mathcal{D}$, the following equations can be derived:

$$\begin{aligned} \frac{d\mathbf{X}}{d\tau} &= \frac{\partial \mathcal{D}}{\partial \mathbf{k}} \\ \frac{d\mathbf{k}}{d\tau} &= -\frac{\partial \mathcal{D}}{\partial \mathbf{X}} \\ \frac{dt}{d\tau} &= -\frac{\partial \mathcal{D}}{\partial \omega} \end{aligned} \tag{1.63}$$

$$\frac{d\omega}{d\tau} = \frac{\partial \mathcal{D}}{\partial t} \tag{1.64}$$

$$\tag{1.65}$$

Using these equations it is straightforward to see that the condition (1.61) is automatically satisfied. Consequentely these four equations are the ray equations. From these system an expression for the group velocity can be defined:

$$\frac{d\mathbf{X}}{dt} = -\frac{\partial \mathcal{D}}{\partial \mathbf{k}} \Big/ \frac{\partial \mathcal{D}}{\partial \omega} = \mathbf{v}_G \tag{1.66}$$

The group velocity indicates the direction of the energy flow, and from this expression it is shown that the ray is directed along $\mathbf{v}_G$. If the plasma equilibrium is constant in time or if it evolves at time scales very slow respect to the wave propagation, the dispersion relation is independent by the time, and the wave frequency ω is constant along the ray trajectory. In this case the time t is considered the evolution variable of the ray dynamics and the ray equations become:

$$\begin{aligned} \frac{d\mathbf{X}}{dt} &= -\frac{\partial \mathcal{D}}{\partial \mathbf{k}} \Big/ \frac{\partial \mathcal{D}}{\partial \omega} \\ \frac{d\mathbf{k}}{dt} &= \frac{\partial \mathcal{D}}{\partial \mathbf{X}} \Big/ \frac{\partial \mathcal{D}}{\partial \omega} \end{aligned} \tag{1.67}$$

This is the form of the ray equations commonly found in literature and describes the time evolution of the ray trajectory and of the wave vector along this trajectory [18].

Chapter 2

A general model for describing fluctuations effects on RF current drive

In this chapter a general model for describing the effects of the fluctuations on radiofrequency current drive in toroidal plasmas is presented. These effects are described by introducing a time-dependent perturbation of the magnetic equilibrium and then of the quantities dependent by the equilibrium, such as the field $\mathbf{B}$, the densities of the various species n_α and the temperatures T_α. The raytracing equations integrated by the fast 3D routine C3PO are modified including these perturbations and the effects of the fluctuations on ray trajectories are incorporated. Coupling the modified raytracing routine with the Fokker-Planck 3D code LUKE makes it possible to estimate the effects of the fluctuations on the power absorption profiles and on current drive. This model is general and can be used to study different kinds of fluctuations and their effects on RF waves of different ranges of frequencies (it is applicable to all high frequency waves), the only limitation is the preservation of the conditions of applicability of the raytracing Fokker-Planck description of the wave-particle interactions: the WKB approximation, the weak damping assumption and the quasilinear hypothesis. These conditions are well satisfied by fluctuations processes relevated in several tokamak experiments [1, 2] and are discussed in details in the first section. In the second section three alternative sets of coordinates appropriate to describe the waves propagation and absorption in toroidal geometry taking into account the magnetic equilibrium configuration are introduced. In the third section the general representation of the perturbed magnetic equilibrium is presented and in 2.4 the modified ray equations are illustrated. In section 2.5 the inclusion of the perturbations effects into the Fokker-Planck routine for current drive calculations is discussed, taking into account the possible random nature of the fluctuations processes.

2.1 Basic assumptions and limitations

In chapter 1, the different time scales involved in current drive calculations have been introduced and discussed. The radiofrequency wave period $\tau_\omega = 2\pi/\omega$ is much shorter than the bounce period $\tau_b = 2\pi/\omega_b$ which is much shorter than the collisional time scale, $\tau_c = 1/\nu_c$, required by collisions to deflect with cumulative effects an electron from its orbit by a significant angle:

$$\tau_\omega \ll \tau_b \ll \tau_c \tag{2.1}$$

Using the frequencies:

$$\nu_c \ll \omega_b/2\pi \ll \omega/2\pi \tag{2.2}$$

These inequalities are well satisfied for parameters of tokamaks like JET or Tore Supra (see chapter 1), and represent the limit of validity of the quasilinear theory of wave-particle interaction and of applicability of the bounce averaging procedure to the kinetic equation. Only fluctuations with characteristics that preserve the quasilinear assumptions and the bounce averaging procedure, incorporated in the relations (2.1) and (2.2), can be described by this model and then accounted in current drive calculations. Consequently fluctuations which respect this constraint have frequency $\widetilde{f} = \widetilde{\omega}/2\pi$ smaller than both RF wave frequency and bounce frequency, and time scales much slower than the wave field and the electron orbits. This means that the wave evolves much more rapidly and the effects of the fluctuations can be studied as small perturbations of the magnetic equilibrium: the wave field, represented by the rays, propagates into a plasma with a perturbed equilibrium configuration, but the time evolution of the fluctuations is slow and during the evolution of the ray the perturbation does not change. In practice, respect to the wave dynamics time scale, the perturbations have a stationary behaviour, the fluctuations structure remains constant while the rays propagate, and it change only after a time much longer than the wave period. On the other side, the fluctuations period is much longer than the bounce period, as a consequence trapped or circulating particles can move on their orbits and cover them several times without being deviate in a significative way for effect of the equilibrium perturbations, and the bounce-averaging procedure of the kinetic equation can be performed also including the equilibrium perturbations. These conditions may be incorporated into the relations (2.1) and (2.2):

$$\tau_\omega \ll \tau_b \ll \tau_c, \widetilde{\tau} \tag{2.3}$$

$$\nu_c, \widetilde{\omega}/2\pi \ll \omega_b/2\pi \ll \omega/2\pi \tag{2.4}$$

These inequalities include both the validity of the quasilinear bounce-averaged formulation of kinetic wave-particle interaction and the limit to the fluctuations frequency ranges that can be studied using this approach, and are well satisfied by the characteristics of the fluctuations investigated experimentally in many tokamak experiments, [1, 2], which frequencies are in the interval

1KHz $< \widetilde{f} <$ 1MHz. Most of them can then be decribed by the proposed model, preserving the structure of the raytracing Fokker-Planck routines commonly used for current drive calculations. Within this framework, for studying the fluctuations effects on the wave dynamics, the ray equations must be modified by including the corrections due to the perturbations, but remain independent by the time, since, as we have discussed, the spatial profile of this corrections does not change in a temporal interval comparable to the propagation scales. The temporal evolution of the fluctuations, instead, must be taken into account to estimate the effects of the perturbation on current profiles in a consistent way: the equilibrium electron distribution function, f_0, solution of the Fokker-Planck equation, varies in slow time scales, of the order of the collisional period, at these time scales the equilibrium perturbations evolve, so the time variation of the perturbations is not negligible compared to the quasilinear integration time step, and must be considered in the calculation of the current.

2.2 Toroidal coordinates systems

There are several sets of curvilinear coordinates appropriate for describing the toroidal plasma configuration, the most commonly used are:

- The toroidal coordinates system (R, Z, ϕ), illustrated in Fig.(2.1), where R is the distance from the axis of the torus, Z is the distance along the axis, and ϕ is the toroidal angle. This is an orthogonal system of coordinates and the basis vector $(\hat{R}, \hat{Z}, \hat{\phi})$ is defined in appendix A.

- The poloidal coordinates system (r, θ, ϕ), illustrated in Fig.(2.2), where the radial coordinate r and the poloidal angle θ are referred to a toroidal axis of constant position R_p, Z_p, which is the plasma magnetic axis, corresponding to the position of an extremum of the poloidal magnetic flux ψ (we commonly choose $\psi = 0$). Also the coordinates (r, θ, ϕ) are orthogonal and the basis $(\hat{r}, \hat{\theta}, \hat{\phi})$ is defined in appendix A.

- The flux coordinates system (ψ, s, ϕ), illustrated in Fig.(2.3), is the natural system for decribing the particle confined dynamics preserving the characteristics of the toroidal geometry. Infact, it takes into account both the properties of the toroidal symmetry than the structure of the magnetic configuration, based on the nested flux surfaces correspondent to different values of the poloidal magnetic flux function ψ [25]. This is an orthogonal system of coordinates corresponding to the basis vector $(\hat{\psi}, \hat{\mathbf{s}}, \hat{\phi})$ (see appendix A).The versor $\hat{\psi}$ is orthogonal to the flux surface, while $\hat{s}$ is parallel and it is on the poloidal plane. The coordinate s is the distance along the magnetic field lines, and its evolution is assumed counter-clockwise from the horizontal midplane, the origin is taken at

the position on minimum B-field amplitute within a flux surface:

$$B(\psi, s \equiv 0) = \min_s \{B(\psi, s)\} = B_0(\psi) \tag{2.5}$$

All the quantities with the subscript 0 are evaluated at the position of minimum B-field on a given flux surface.

- The set of coordinates (ψ, θ, ϕ) is an alternative to (ψ, s, ϕ) particularly convenient from a numerical point of view. This set decribes the equilibrium peculiarities and at the same time simplifies the numerical implementation, because makes possible the interpolation of the equilibrium using techniques based on the Fourier series, starting by a (ψ, θ) grid where θ is a periodic variable independent by ψ, on the other side, it the versors $\hat{\psi}$ and $\hat{\theta}$ are not orthogonal, and this makes the computation of the metric tensor more complicated (see appendix A). It is also possible to define a monotonic flux function $\rho(\psi)$ correspondent to the normalized radius on the horizontal Low Field Side (LFS) mid-plane. In an axisymmetric system using the functions $R(\psi, \theta)$ and $Z(\psi, \theta)$, ρ becomes:

$$\rho(\psi) = \frac{R(\psi, 0) - R_p}{R_{max} - R_p} \tag{2.6}$$

With $0 < \rho < 1$ and where $R_{max} = R(\psi_{max}, 0)$ is the value of R on the separatrix.

The system of coordinates (ρ, θ, ϕ) is particularly suitable for studying the ray propagation in an axisymmetric plasma with an arbitrary equilibrium. As just explained, $\rho(\psi)$ is a monotonic function of the poloidal magnetic flux coordinate ψ, which is defined by the following general expression for the equilibrium magnetic field [22, 25]:

$$\mathbf{B} = I(\psi)\nabla\phi + \nabla\phi \times \nabla\psi \tag{2.7}$$

Where $I(\psi)$ is a function related to the toroidal magnetic field, which account for the plasma para- or diamagnetism. Using the set of coordinates (ρ, θ, ϕ) the equilibrium magnetic field becomes [21]:

$$\mathbf{B} = \sigma_B B_T \hat{\phi} + \sigma_I B_P \hat{\mathbf{s}} \tag{2.8}$$

Where σ_B is the sign of B_P and σ_I is the sign of the toroidal current. The poloidal component $B_P = |I(\psi)|/R$ and the toroidal component $B_T = \|\nabla\psi\|/R$ are assumed to be positive. In this system the covariant coordinates of the radio frequency wave vector are:

$$k_i = (k_\rho, m, n) \tag{2.9}$$

And the contravariant basis of the system s:

$$\mathbf{e}^i = \left(\|\nabla\rho\| \hat{\rho}, \frac{\hat{\theta}}{r}, \frac{\hat{\phi}}{R} \right) \tag{2.10}$$

The expression for the wave vector is then:

$$\mathbf{k} = k_i e^i = k_\rho \left\| \nabla \rho \right\| \hat{\rho} + \frac{m}{r}\hat{\theta} + \frac{n}{R}\hat{\phi} \tag{2.11}$$

In the next sections $\mathbf{k}$ is expressed in this form and all the quantities introduced are functions of (ρ, θ, ϕ). It is important to say that for a magnetic equilibrium with non-circular and concentric flux surfaces $\hat{\rho}$ and $\hat{\mathbf{r}}$ are not coincident, and the angle α between the two versors is defined such that [21]:

$$\begin{aligned} \hat{\rho} \cdot \hat{\mathbf{r}} &= \cos\alpha \\ \hat{\rho} \cdot \hat{\theta} &= -\sin\alpha \\ \hat{\mathbf{s}} \cdot \hat{\mathbf{r}} &= \sin\alpha \\ \hat{\mathbf{s}} \cdot \hat{\theta} &= \cos\alpha \end{aligned} \tag{2.12}$$

From these expression $\hat{\rho}$ and $\hat{\mathbf{s}}$ can be expressed in function of $\hat{\mathbf{r}}$ and $\hat{\theta}$ or equivalently $\hat{\mathbf{r}}$ and $\hat{\theta}$ in function of $\hat{\rho}$ and $\hat{\mathbf{s}}$, and the following conditions of orthogonality are demonstrated [21]:

$$\begin{aligned} \hat{\rho} \cdot \hat{\mathbf{s}} &= 0 \\ \hat{\mathbf{r}} \cdot \hat{\theta} &= 0 \end{aligned} \tag{2.13}$$

Remembering that the toroidal versor $\hat{\phi}$ is perpendicular to the poloidal plane, two different systems of orthogonal coordinates are defined: (r, θ, ϕ) and (ρ, s, ϕ), while (ρ, θ, ϕ), as just discussed, are not orthogonal.

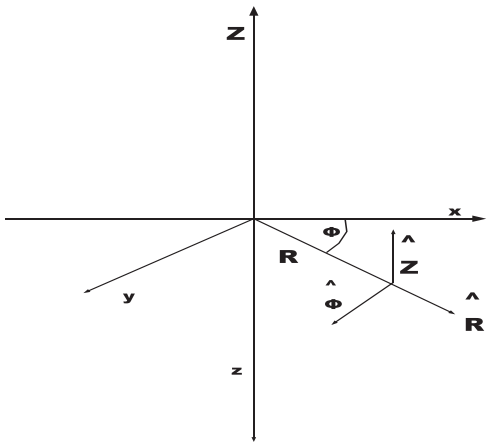

Figure 2.1: Coordinates system (R, Z, ϕ).

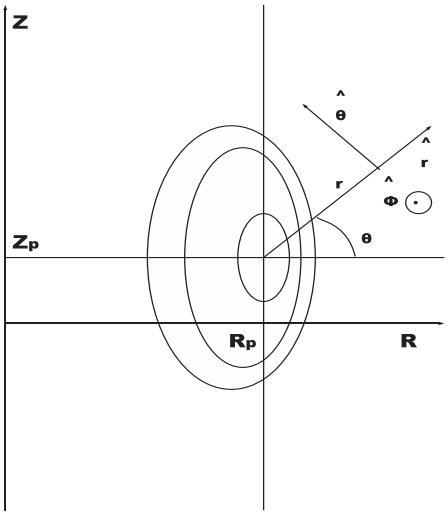

Figure 2.2: Coordinates system (r, θ, ϕ).

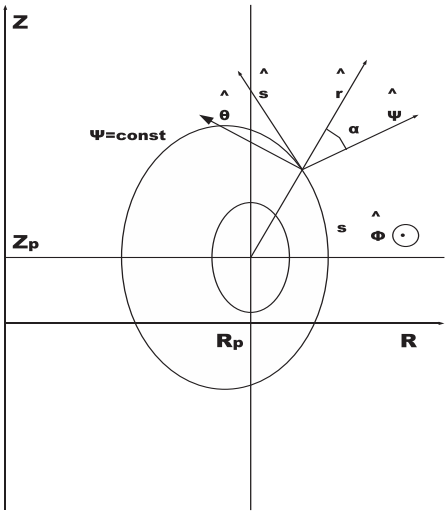

Figure 2.3: Coordinates system (ψ, s, ϕ).

2.3 Perturbed magnetic equilibrium

The fluctuations are represented by small perturbations of the magnetic equilibrium: any physical quantity g dependent by the equilibrium, which could be the density of a species n_α, the temperature T_α or a component of the magnetic field $\mathbf{B}$, may be expressed in the following form:

$$g(\rho,\theta,\phi,t) = \overline{g}(\rho,\theta) + \widetilde{g}(\rho,\theta,\phi,t) \tag{2.14}$$

Where (ρ,θ,ϕ) is the set of toroidal flux coordinates illustrated in details in section (2.2) with ρ generalized radial coordinate, θ poloidal angle and ϕ toroidal angle, and t is the time. The term $\overline{g}(\rho,\theta)$ corresponds to the unperturbed equilibrium while $\widetilde{g}(\rho,\theta,\phi,t)$ is the contribution due to the fluctuations. The unperturbed magnetic configuration is axisymmetric, while this axisymmetry is violated for effect of the fluctuations, as a consequence a dependence by the toroidal angle ϕ is introduced into the term correspondent to the perturbations, and including this correction the magnetic equilibrium becomes three-dimensional. The total perturbation is given by the sum of the contributions corresponding to several fluctuations mechanisms:

$$\widetilde{g}(\rho,\theta,\phi,t) = \sum_i \widetilde{g}_i(\rho,\theta,\phi,t) \tag{2.15}$$

Each contribution $\widetilde{g}_i$ is the sum of a finite set of oscillations with frequency $\widetilde{\omega}$ and wave vector $\widetilde{\mathbf{k}}$, then it can be expressed using the general harmonic form:

$$\widetilde{g}_i(\rho,\theta,\phi,t) = \sum_{\widetilde{\mathbf{k}}} \widetilde{g}^0_{i,\widetilde{\mathbf{k}}}(\rho,\theta)\cos\Phi_{\widetilde{\mathbf{k}}}(\rho,\theta,\phi,t) \tag{2.16}$$

The general expression for the phase is:

$$\Phi_{\widetilde{\mathbf{k}}} = \Phi_{\widetilde{\mathbf{k}}0} + \Phi^G_{\widetilde{\mathbf{k}}}(\rho,\theta,\phi) + \widetilde{\omega}(\widetilde{\mathbf{k}})t \tag{2.17}$$

Where $\Phi_{\widetilde{\mathbf{k}}0}$ is the initial value, $\Phi^G_{\widetilde{\mathbf{k}}}$ is the geometrical contribution to the phase, which depends by the physical characteristics of the fluctuations, and $\omega(\widetilde{\mathbf{k}})$ is the perturbations dispersion relation. The explicit expression for the phase and also for the amplitude $\widetilde{g}^0_{i,\widetilde{\mathbf{k}}}(\rho,\theta)$ of the perturbation depends by the type of fluctuation.
Using this general approach, the perturbations of all quantitites related to the magnetic equilibrium can be easily expressed taking into account the contribution of each fluctuation source:

$$\begin{aligned}
\widetilde{n}_\alpha(\rho,\theta,\phi,t) &= \sum_i \sum_{\widetilde{\mathbf{k}}} \widetilde{n}^0_{\alpha,i,\widetilde{\mathbf{k}}}(\rho,\theta)\cos\Phi_{\widetilde{\mathbf{k}}}(\rho,\theta,\phi,t) \\
\widetilde{T}_\alpha(\rho,\theta,\phi,t) &= \sum_i \sum_{\widetilde{\mathbf{k}}} \widetilde{T}^0_{\alpha,i,\widetilde{\mathbf{k}}}(\rho,\theta)\cos\Phi_{\widetilde{\mathbf{k}}}(\rho,\theta,\phi,t) \\
\widetilde{B}_{\rho,s,\phi}(\rho,\theta,\phi,t) &= \sum_i \sum_{\widetilde{\mathbf{k}}} \widetilde{B}^0_{\rho,s,\phi,i,\widetilde{\mathbf{k}}}(\rho,\theta)\cos\Phi_{\widetilde{\mathbf{k}}}(\rho,\theta,\phi,t)
\end{aligned} \tag{2.18}$$

Considering the effects of these perturbations on the ray propagation and the consequences of the equilibrium variations on the current deposition profiles, it is possible to study and to quantify the effects of several types of plasma fluctuations on radiofrequency current drive. It is important to remember that, as just discussed in the first section of the chapter, the time dependence of the perturbations, included in the phase, is referred only to the slow time scales, and should be considered only in the quasilinear evaluation of the current profiles, not in the study of the ray propagation, which evolves at fast waves time scales.

2.4 Ray tracing in a perturbed magnetic equilibrium

Since the fluctuations do not evolve in time scales comparable with the wave period, the term of the phase (2.17) dependent by the time is neglected in the integration of the ray equations, and the equilibrium perturbations introduced in this section for studying the effects of the fluctuations on the ray trajectories are time independent. According to that and assuming the wave frequency ω constant into the plasma, the dispersion relation is independent by the time, and the ray equations have the same general expression introduced in chapter 1:

$$\begin{aligned} \frac{d\mathbf{X}}{dt} &= -\frac{\partial \mathcal{D}}{\partial \mathbf{k}} \Big/ \frac{\partial \mathcal{D}}{\partial \omega} \\ \frac{d\mathbf{k}}{dt} &= \frac{\partial \mathcal{D}}{\partial \mathbf{X}} \Big/ \frac{\partial \mathcal{D}}{\partial \omega} \end{aligned} \tag{2.19}$$

Where $\mathbf{X}$ is the position of the ray and $\mathbf{k}$ is the wave vector. Remembering the discussion about the weak damping limit in chapter 1, the wave propagation can be studied considering only the hermitian part of the dispersion tensor, the dispersion relation, introduced in section 1.2.1, is defined by the following expression:

$$\mathcal{D}(\mathbf{N}, \omega) = \mathcal{D}(N_{\parallel}, N_{\perp r}, \beta_{T\alpha}, \overline{\omega}_{p\alpha}, \overline{\omega}_{c\alpha}) \tag{2.20}$$

And then:

$$\mathcal{D}(N_{\parallel}, N_{\perp r}, \beta_{T\alpha}, \overline{\omega}_{p\alpha}, \overline{\omega}_{c\alpha}) \equiv \det \mathbb{D}^{H}_{\mathbf{k},\omega}(N_{\parallel}, N_{\perp r}, \beta_{T\alpha}, \overline{\omega}_{p\alpha}, \overline{\omega}_{c\alpha}) \tag{2.21}$$

Where $N_{\parallel}$ and $N_{\perp}$ are the components of the refractive index $\mathbf{N} = c\mathbf{k}/\omega$ respect to the magnetic field and and $\overline{\omega}_{c\alpha}$, $\overline{\omega}_{p\alpha}$, $\beta_{T\alpha}$ are the functions of the equilibrium quantities introduced in chapter 1. From here in this section $N_{\perp}$ will refer to the zero-order real solution of the dispersion relation $N_{\perp r} = N_{\perp r0}$ (see subsections 1.2.1 and 1.2.2), and the dispersion relation $\mathcal{D}$ to the hermitian tensor $\mathbb{D}^{H}_{\mathbf{k},\omega}$.

The 8-dimensional vector $\mathbf{Y}$ which represents the generic phase-space is:

$$\mathbf{Y} = \begin{pmatrix} \mathbf{X} \\ \mathbf{k} \\ t \\ \omega \end{pmatrix} \tag{2.22}$$

For solving the ray equations (2.19), it is necessary to evaluate explicitely the derivatives of the dispersion relation (2.21) respect to the components of $\mathbf{Y}$:

$$\frac{\partial N_\parallel}{\partial \mathbf{Y}}; \qquad \frac{\partial N_\perp}{\partial \mathbf{Y}}; \qquad \frac{\partial X_{ij}^\alpha}{\partial \mathbf{Y}}; \tag{2.23}$$

The derivatives of the susceptibility tensor components, since the dispersion relation is assumed to be independent by the time, are given by the general expression:

$$\begin{aligned} \frac{\partial X_{ij}^\alpha}{\partial \mathbf{Y}} &= \frac{\partial X_{ij}^\alpha}{\partial N_\parallel}\frac{\partial N_\parallel}{\partial \mathbf{Y}} + \frac{\partial X_{ij}^\alpha}{\partial N_\perp}\frac{\partial N_\perp}{\partial \mathbf{Y}} + \\ &+ \frac{\partial X_{ij}^\alpha}{\partial \beta_{T\alpha}}\frac{\partial \beta_{T\alpha}}{\partial \mathbf{Y}} + \frac{\partial X_{ij}^\alpha}{\partial \overline{\omega}_{p\alpha}}\frac{\partial \overline{\omega}_{p\alpha}}{\partial \mathbf{Y}} + \frac{\partial X_{ij}^\alpha}{\partial \overline{\omega}_{c\alpha}}\frac{\partial \overline{\omega}_{c\alpha}}{\partial \mathbf{Y}} \end{aligned} \tag{2.24}$$

The explicit form of the tensor $\mathbb{X}_{\mathbf{k},\omega}^\alpha(N_\parallel, N_\perp, \beta_{T\alpha}, \overline{\omega}_{p\alpha}, \overline{\omega}_{c\alpha})$ depends by the plasma dispersion model (cold,warm,hot), but the quantities $N_\parallel, N_\perp, \beta_{T\alpha}, \overline{\omega}_{p\alpha}, \overline{\omega}_{c\alpha}$ and then their derivatives respect to $\mathbf{Y}$ are functions of the magnetic equilibrium and of the coordinates system. As a consequence, in order to study the effects of the fluctuations on the ray propagation, the corrections due to the equilibrium perturbations (2.18) must be included into the expressions for the components of the refractive index and for the derivatives (2.23).

2.4.1 Ray equations

In the canonical flux coordinates system (ρ, θ, ϕ) and (k_ρ, m, n), the ray equations (2.19) becomes [21]:

$$\begin{aligned} \frac{d\rho}{dt} &= -\frac{\partial \mathcal{D}}{\partial k_\rho}\Big/\frac{\partial \mathcal{D}}{\partial \omega} \\ \frac{d\theta}{dt} &= -\frac{\partial \mathcal{D}}{\partial m}\Big/\frac{\partial \mathcal{D}}{\partial \omega} \\ \frac{d\phi}{dt} &= -\frac{\partial \mathcal{D}}{\partial n}\Big/\frac{\partial \mathcal{D}}{\partial \omega} \end{aligned} \tag{2.25}$$

And

$$\begin{aligned} \frac{dk_\rho}{dt} &= \frac{\partial \mathcal{D}}{\partial \rho}\Big/\frac{\partial \mathcal{D}}{\partial \omega} \\ \frac{dm}{dt} &= \frac{\partial \mathcal{D}}{\partial \theta}\Big/\frac{\partial \mathcal{D}}{\partial \omega} \\ \frac{dn}{dt} &= \frac{\partial \mathcal{D}}{\partial \phi}\Big/\frac{\partial \mathcal{D}}{\partial \omega} \end{aligned} \tag{2.26}$$

Without considering fluctuations, the toroidal magnetic configuration is axisymmetric, the dispersion relation is independent by the toroidal angle ϕ and the toroidal component of the wave vector n is constant along the ray trajectory, this axisymmetry is violated introducing the equilibrium parturbations, then taking into account the fluctuations, $\partial\mathcal{D}/\partial\phi \neq 0$ and all the six equations (2.25) and (2.26) must be solved.

2.4.2 Parallel index of refraction

The component of the refractive index parallel to the magnetic field is related to the parallel wave vector of the radiofrequency wave by the relation: $N_\parallel = ck_\parallel/\omega$. $k_\parallel$ is defined by the scalar product:

$$k_\parallel = \mathbf{k}\cdot\mathbf{b} \tag{2.27}$$

The magnetic field versor $\mathbf{b} = \mathbf{B}/B$ must be calculated taking into account the total magnetic field, composed by the equilibrium field for a quiescent plasma and the perturbation generated by the fluctuations, according to the general expression (2.14), and neglecting the temporal dependence of the fluctuating term:

$$\mathbf{B}(\rho,\theta,\phi) = \overline{\mathbf{B}}(\rho,\theta) + \widetilde{\mathbf{B}}(\rho,\theta,\phi) \tag{2.28}$$

The perturbation may be represented in term of components using the set of orthogonal cordinates (ρ, s, ϕ):

$$\widetilde{\mathbf{B}} = \widetilde{B}_\rho\hat{\rho} + \widetilde{B}_s\hat{\mathbf{s}} + \widetilde{B}_\phi\hat{\phi} \tag{2.29}$$

Then the total magnetic field becomes:

$$\mathbf{B} = \widetilde{B}_\rho\hat{\rho} + (\sigma_I B_P + \widetilde{B}_s)\hat{\mathbf{s}} + (\sigma_B B_T + \widetilde{B}_\phi)\hat{\phi} \tag{2.30}$$

And the versor $\mathbf{b}$:

$$\mathbf{b} = \widetilde{R}\hat{\rho} + (P + \widetilde{P})\hat{\mathbf{s}} + (T + \widetilde{T})\hat{\phi} \tag{2.31}$$

Where:

$$P = \sigma_I\frac{B_P}{B}; \qquad T = \sigma_B\frac{B_T}{B}; \tag{2.32}$$

And:

$$\widetilde{R} = \frac{\widetilde{B}_\rho}{B}; \qquad \widetilde{P} = \frac{\widetilde{B}_s}{B}; \qquad \widetilde{T} = \frac{\widetilde{B}_\phi}{B}; \tag{2.33}$$

Using this expression for the magnetic field versor and remembering the expression for the wave vector introduced in section (2.2), the parallel component of the radiofrequency wave vector becomes:

$$k_\parallel = k_\rho\,\|\nabla\rho\|\,\widetilde{R} + \frac{m}{r}[(P+\widetilde{P})\cos\alpha - \widetilde{R}\sin\alpha] + \frac{n}{R}(T+\widetilde{T}) \tag{2.34}$$

Where α is the angle between the versors $\hat{\rho}$ and $\hat{\mathbf{r}}$ (see appendix A). It is important to note that neglecting the perturbations due to the fluctuating magnetic field, this expression is exactly equal to the general expression for $k_\parallel$ in a quiescent plasma [21].

2.4.3 Perpendicular index of refraction

The perpendicular index of refraction of the wave, in total analogy with the parallel, is given by: $N_\perp = ck_\perp/\omega$. The perpendicular component of the wave vector may be calculated, knowing k^2 and $k_\perp$, using the relation:

$$k_\perp^2 = k^2 - k_\parallel^2 \tag{2.35}$$

Where the square modulus of the wave vector in our coordinates system is:

$$k^2 = k_\rho^2 \left\|\nabla\rho\right\|^2 - 2k_\rho \left\|\nabla\rho\right\| \frac{m}{r}\sin\alpha + \frac{m^2}{r^2} + \frac{n^2}{R^2} \tag{2.36}$$

Substituing the expression for $k_\parallel$ into the 2.35, the result is:

$$\begin{aligned} k_\perp^2 &= \left(k_\rho \left\|\nabla\rho\right\| - \frac{m}{r}\sin\alpha\right)^2 + \left(T\frac{m}{r}\cos\alpha - P\frac{n}{R}\right)^2 - \\ &- \left[k_\rho \left\|\nabla\rho\right\| \widetilde{R} + \frac{m}{r}\left(\widetilde{P}\cos\alpha - \widetilde{R}\sin\alpha\right) + \frac{n}{R}\widetilde{T}\right]^2 - \\ &- 2\left(P\frac{m}{r}\cos\alpha + T\frac{n}{R}\right)\left[k_\rho \left\|\nabla\rho\right\| \widetilde{R} + \frac{m}{r}\left(\widetilde{P}\cos\alpha - \widetilde{R}\sin\alpha\right)\frac{n}{R}\widetilde{T}\right] \end{aligned} \tag{2.37}$$

Also in this case, neglecting the contributions associated with the perturbations, the expression for $k_\perp$ in the general axisymmetric geometry [21] is recovered.

2.4.4 Derivatives

Using the explicit expressions (2.34) and (2.37), it is possible to calculate the derivatives of the refractive index $\mathbf{N} = c\mathbf{k}/\omega$ required in the ray equations (see relation (2.24)):

$$\frac{\partial N_\parallel}{\partial \mathbf{Y}}; \frac{\partial N_\perp}{\partial \mathbf{Y}}; \tag{2.38}$$

Using the toroidal conjugate coordinates, the components of the phase-space are: $\mathbf{Y} = (\rho, \theta, \phi, k_\rho, m, n, t, \omega)$. Remembering that the wave frequency is assumed to be constant in time and the equilibrium is independent by t, the derivatives of $N_\parallel$ are:

$$\frac{\partial N_\parallel}{\partial \omega}; \frac{\partial N_\parallel}{\partial \rho}; \frac{\partial N_\parallel}{\partial \theta}; \frac{\partial N_\parallel}{\partial \phi}; \frac{\partial N_\parallel}{\partial k_\rho}; \frac{\partial N_\parallel}{\partial m}; \frac{\partial N_\parallel}{\partial n}; \tag{2.39}$$

While the derivatives of $N_\perp$ are:

$$\frac{\partial N_\perp}{\partial \omega}; \frac{\partial N_\perp}{\partial \rho}; \frac{\partial N_\perp}{\partial \theta}; \frac{\partial N_\perp}{\partial \phi}; \frac{\partial N_\perp}{\partial k_\rho}; \frac{\partial N_\perp}{\partial m}; \frac{\partial N_\perp}{\partial n}; \tag{2.40}$$

It is important to note that if the perturbations are neglected, and as a consequence the equilibrium configuration is axisymmetric, the refractive index is

independent by the toroidal angle, and $\partial N_\parallel/\partial\phi, \partial N_\perp/\partial\phi = 0$. These derivatives are computed explicitely using the expressions (2.34) and (2.36) into the definition $\mathbf{N} = \mathbf{k}c/\omega$ and into the relation:

$$\frac{\partial N_\perp}{\partial \mathbf{Y}} = \frac{1}{N_\perp}\left(\frac{\partial N^2}{\partial \mathbf{Y}} - 2N_\parallel \frac{\partial N_\parallel^2}{\partial \mathbf{Y}}\right) \tag{2.41}$$

For evaluating the derivatives of $\beta_{T\alpha}, \overline{\omega}_{p\alpha}$ and $\overline{\omega}_{c\alpha}$ respect to $\mathbf{Y}$, it is important to remember that these functions are by definition of the equilibrium independent by the wave vector $\mathbf{k}$, such that:

$$\frac{\partial \beta_{T\alpha}}{\partial \mathbf{k}} = \frac{\overline{\omega}_{p\alpha}}{\partial \mathbf{k}} = \frac{\overline{\omega}_{c\alpha}}{\partial \mathbf{k}} = 0 \tag{2.42}$$

Remembering that fluctuations time scales are much slower than the wave time scales and that ω is constant, $\beta_{T\alpha}, \overline{\omega}_{p\alpha}$ and $\overline{\omega}_{c\alpha}$ can be considered independent by t:

$$\frac{\partial \beta_{T\alpha}}{\partial t} = \frac{\overline{\omega}_{p\alpha}}{\partial t} = \frac{\overline{\omega}_{c\alpha}}{\partial t} = 0 \tag{2.43}$$

$\beta_{T\alpha}$ is independent by the frequency, then:

$$\frac{\partial \beta_{T\alpha}}{\partial \omega} = 0 \tag{2.44}$$

Considering the fluctuations effects the species temperature T_α, the species density n_α and the magnetic field $\mathbf{B}$, become:

$$T_\alpha(\rho,\theta,\phi) = \overline{T}_\alpha(\rho) + \widetilde{T}_\alpha(\rho,\theta,\phi) \tag{2.45}$$

$$n_\alpha(\rho,\theta,\phi) = \overline{n}_\alpha(\rho) + \widetilde{n}_\alpha(\rho,\theta,\phi) \tag{2.46}$$

$$\mathbf{B}(\rho,\theta,\phi) = \overline{\mathbf{B}}(\rho,\theta) + \widetilde{\mathbf{B}}(\rho,\theta,\phi) \tag{2.47}$$

Since $\beta_{T\alpha}$ is function of T_α, $\overline{\omega}_{p\alpha}$ of n_α and $\overline{\omega}_{c\alpha}$ of the modulus of the magnetic field, the derivatives which must be calculated are:

$$\frac{\partial \beta_{T\alpha}}{\partial \rho}; \frac{\partial \beta_{T\alpha}}{\partial \theta}; \frac{\partial \beta_{T_\alpha}}{\partial \phi}; \frac{\partial \overline{\omega}_{p\alpha}}{\partial \rho}; \frac{\partial \overline{\omega}_{p\alpha}}{\partial \theta}; \frac{\partial \overline{\omega}_{p\alpha}}{\partial \phi}; \frac{\partial \overline{\omega}_{p\alpha}}{\partial \omega}; \frac{\partial \overline{\omega}_{c\alpha}}{\partial \rho}; \frac{\partial \overline{\omega}_{c\alpha}}{\partial \theta}; \frac{\partial \overline{\omega}_{c\alpha}}{\partial \phi}; \frac{\partial \overline{\omega}_{c\alpha}}{\partial \omega}; \tag{2.48}$$

Explicit expressions for these equilibrium derivatives are reported in appendix B. It is important to remark the fundamental differencies respect to the axisymmetric case without fluctuations, where all derivatives respect to ϕ are zero and the temperature and the density are functions only of the flux coordinate ρ, such that $\partial\beta_{T\alpha}/\partial\theta, \partial\overline{\omega}_{p\alpha}/\partial\theta = 0$.

2.5 Current drive calculations in a perturbed magnetic equilibrium

The modifications associated with the perturbations of the magnetic equilibrium have been introduced into the ray equations (2.25) and (2.26). The radiofrequency wave is described by a set of rays, which trajectories are calculated

accounting the perturbations of the equilibrium generated by the fluctuations, these perturbations can induce refractions of the ray trajectory and variation of the wave vector which can affect strongly the wave damping evolution and spatial localization of the power deposition. The evaluation of the elements of the quasilinear diffusion tensor $\mathbb{D}^{QL}$ is required for the solution of the bounce-averaged kinetic equation and for the calculation of the current induced into the plasma. The elements of $\mathbb{D}^{QL}$ are functions of $\left\|\widetilde{\mathbf{E}}_{\mathbf{k},\omega}\right\|^2$, then they can be calculated in function of the power dissipated by the wave, given by the expression (1.57). The damping along each ray j is estimated solving the single ray power flow equation:

$$\frac{dP_j(\psi)}{dV(\psi)} = P_j^{abs}(\psi) \tag{2.49}$$

Where $dV(\psi)$ is the element of volume crossed by the ray, $P_j(\psi)$ is the power dissipated by the ray and P_j^{abs} is the contribution of the ray j to the total power absorbed by the resonant electrons, the (2.49) is expression of the global convergence condition introduced in section 1.2.1 in term of a balance equation [19]. The power gained by the electrons P_j^{abs}, as it can be observed by the relation (1.57), depends by the antihermitian part of the dispersion tensor $\mathbb{D}_{\mathbf{k},\omega}$, which is function of the equilibrium distribution function $\overline{f}$, solution of the bounce-averaged kinetic equation (1.32). In practice, the evaluation of the quasilinear diffusion tensor requires the solution of the ray power flow equation, but on the other side the power gained by the electrons for effect of the quasilinear diffusion, $P_{j,QL}^{abs}$, is function of $\overline{f}$, which evaluation through the solution of the kinetic equation requires the estimation of $\mathbb{D}^{QL}$. In order to ensure the self-consistency of the scheme, the equation (**??**) is firstly solved assuming $\overline{f} = f_M$ and $P_j^{abs} = P_{j,lin}^{abs}$; starting by the linear damping calculated with the Maxwellian distribution function, the quasilinear diffusion tensor is estimated on each flux surface considering the contribution of each ray:

$$\mathbb{D}^{QL}(\psi, \mathbf{p}) = \sum_j \mathbb{D}_j^{QL}(P_j(\psi), \psi, \mathbf{p}) \tag{2.50}$$

Once this tensor is evaluated, the bounce averaged kinetic equation (1.32) is integrated on the slow timescales of the order of the collisional period τ_c by means of the 3-D Fokker-Planck solver LUKE [22], the equilibrium distribution function and the current J, connected to $\overline{f}$ by the relation (1.19), are calculated. The power damped on the electrons $P_{j,QL}^{abs}$ is estimated using the new $\overline{f}$ and is used in the power flow equation for the successive iteration. The ray power flow equation (2.49) is coupled to the ray equations modified with the equilibrium perturbations generated by the fluctuations, and then also the quasilinear diffusion tensor is calculated considering the perturbed equilibrium. The equilibrium perturbations generated by the fluctuations do not evolve in fast time scales which characterize the wave propagation ($\tau = 2\pi/\omega$), while they changes in the slow timescales comparable with the collisional, as

it is shown by the inequality (2.3). This means that in the calculation of the quasilinear wave damping the evolution in time of the fluctuations processes cannot be neglected as it is in the study of the propagation. Since the time evolution of the fluctuations is relevant only in the wave damping, the term of the perturbations phase (2.17) dependent by the time can be expressed in function of the quasilinear time step $\Delta\tau$ used in the integration of the kinetic equation. This time step is a constant quantity, because in the integration a temporal uniform grid is assumed [22]. The fluctuations phase given by the (2.17) becomes:

$$\Phi_{\widetilde{\mathbf{k}}} = \Phi_{\widetilde{\mathbf{k}}0} + \Phi^{G}_{\widetilde{\mathbf{k}}}(\rho, \theta, \phi) + \widetilde{\omega}(\widetilde{\mathbf{k}})\Delta\tau \tag{2.51}$$

In practice an uniform grid which point are $t_n = n\Delta\tau$ is defined, and at each instant $t_n = n\Delta\tau$ the phase value evolves in time, while remains constant in the intervals between two successive points of the grid. In section 2.1 it has been explained that the frequencies and the period of fluctuations processes considered must satisfy the inequalities:

$$\tau_\omega \ll \tau_b \ll \tau_c, \widetilde{\tau} \tag{2.52}$$

$$\nu_c, \widetilde{\omega}/2\pi \ll \omega_b/2\pi \ll \omega/2\pi \tag{2.53}$$

Consequently, it can be studied fluctuations processes with $\widetilde{\tau}$ and $\widetilde{\omega}$ such that:

$$\tau_\omega \ll \tau_b \ll \widetilde{\tau} \ll \tau_c \tag{2.54}$$

$$\nu_c \ll \widetilde{\omega}/2\pi \ll \omega_b/2\pi \ll \omega/2\pi \tag{2.55}$$

Or, alternatively:

$$\tau_\omega \ll \tau_b \ll \tau_c \ll \widetilde{\tau} \tag{2.56}$$

$$\widetilde{\omega}/2\pi \ll \nu_c \ll \omega_b/2\pi \ll \omega/2\pi \tag{2.57}$$

The equilibrium distribution function varies in the slow time scales of the order of the collisional period τ_c, then the quasilinear integration time step used by the Fokker-Planck solver in the integration of the kinetic equation is major or equal to τ_c. Since some fluctuations processes, as it is shown by relation (2.54), have a time scale shorter than the collisional times, the quasilinear diffusion operator is estimated by means of an averaging procedure of the ray, by launching N rays each one carrying the fraction of the total injected power $P_{ray} = P_{rf}/N$ in the integration time $\Delta\tau/N$, such that the total power is conserved and the spreading of the ray in this time interval is accounted. The effects of perturbations which time scales are slower than the collisional times, satisfying the (2.56), can be easily estimated by choosing an integration time step $\Delta\tau \approx \widetilde{\tau}$ and evolving the value of the fluctuations phase at each $t = t_n = n\Delta\tau$ corresponding to a point of the temporal grid used in the integration of the kinetic equation.

Chapter 3

Fluctuations processes

In this chapter two examples of fluctuations which effects on radiofrequency current drive can be described using the proposed model are introduced: random fluctuations of the electron density and of the magnetic field which wave vector lies on the flux surfaces (in the case of electron density these fluctuations can be considered as a consequence of the Electron Drift Waves), and toroidal magnetic ripple, which is described as a static perturbation of the magnetic equilibrium. The physical characteristics of these processes are illustrated in details, with particular attention to the random properties of the stochastic fluctuations.

3.1 Stochastic fluctuations

Fluctuations of density, temperature, and magnetic field have been relevated and studied experimentally in modern tokamaks experiments with several diagnostic techniques [1, 2, 3, 26, 27, 28]. These fluctuations, generated by drift waves in the case of density, are of stochastical nature and can modify the accessibility conditions of the radio frequency waves and the induced current profiles. The fluctuations frequency $\widetilde{f} = \widetilde{\omega}/2\pi$ belongs to the interval $10\text{KHz} < \widetilde{f} < 200\text{KHz}$ [2], so it satisfies perfectly the condition of applicability of the model (2.2), and these fluctuations can be described as stochastic perturbations of the magnetic equilibrium, using explicit expressions for the perturbed fields (2.18) appropriate to modelize the physical characteristics of these phenomena.

3.1.1 Physical characteristics

The modulus of the fluctuations wave vector $\widetilde{k}$ varies from values of the order of $\widetilde{k} \approx 0.5\text{m}^{-1}$, to values of the order of $\widetilde{k} \approx 10^3\text{m}^{-1}$ [2, 3, 27]. From the experiments it has been verified the relation $\widetilde{\lambda}_{\|} \simeq (0.1-0.3)qR_p$, [26, 28], where q is the safety factor and R_p the plasma major radius, so taking $\widetilde{\lambda}_{\|} \simeq 0.2qR_p$,

we have $\widetilde{k}_{\parallel} \simeq 2\pi/\left(0.2qR_p\right)$. In the table 3.1 are reported the values of $\widetilde{k}_{\parallel}$ and $\widetilde{\lambda}_{\parallel}$ calculated for JET, Tore Supra, FTU and ITER tokamaks assuming $q = q_a$ and using the following parameters:

- for JET $q_a = 4$; $R_p = 2.96$m;
- for Tore Supra $q_a = 5$; $R_p = 2.46$m;
- for FTU $q_a = 7$; $R_p = 0.935$m;
- for ITER $q_a = 7$; $R_p = 6.2$m;

	JET	Tore Supra	FTU	ITER
$\widetilde{k}_{\parallel}$	2.7m^{-1}	2.6m^{-1}	$4.8m^{-1}$	0.7m^{-1}
$\widetilde{\lambda}_{\parallel}$	2.4m	2.5m	1.3m	3.7m

Table 3.1: Values of $\widetilde{k}_{\parallel}$ and $\widetilde{\lambda}_{\parallel}$ calculated using parameters of JET, TORE SUPRA, FTU and ITER tokamaks

The parallel wave length of the radio frequency wave $\lambda_{\parallel}$ is related to the parallel refractive index $N_{\parallel}$ by the relation $\lambda_{\parallel} = c/fN_{\parallel}$. Using typical values corresponding to rf systems used on the Tore Supra and JET tokamaks, $f_{LH} = 3.7$GHz and $N_{\parallel LH} \simeq 2$, $\lambda_{\parallel LH}$ is about $4 \cdot 10^{-2}$m for the LH wave, while it is $\lambda_{\parallel EC} \simeq 1.3 \cdot 10^{-2}$m for the Electron Cyclotron (EC) wave with $f_{EC} = 110$GHz and $N_{\parallel EC} \simeq 0.2$. Considering both LH than EC waves, and comparing the values of the parallel wave length and wave vector with the values reported in the table, the following relation is verified:

$$\widetilde{\lambda}_{\parallel} \gg \lambda_{\parallel} \tag{3.1}$$

And then:

$$\widetilde{k}_{\parallel} \ll k_{\parallel} \tag{3.2}$$

As a consequence, the component $\widetilde{k}_{\parallel}$ can be neglected and $\widetilde{k}$ can be approximated to $\widetilde{k}_{\perp}$:

$$\widetilde{k}_{\parallel} \approx 0; \qquad \widetilde{k} \approx \widetilde{k}_{\perp}; \tag{3.3}$$

Density fluctuations in tokamak plasmas are in general due to drift waves, [9, 11, 10], the drift dynamics lies on the flux surfaces, then the nested flux surface configuration determined by the values of ψ or $\rho(\psi)$ is not modified by these oscillations and the wave vector $\widetilde{\mathbf{k}}$ is also located on the flux surfaces. Since $\widetilde{\mathbf{k}} \approx \widetilde{k}_{\perp}$, the oscillations direction is orthogonal to the magnetic field lines. From here in this thesis, the drift waves are considered as the prototype of stochastic perturbation process, and also fluctuations of the temperature and of the magnetic field are assumed to lie on the flux surfaces.

The general expression for the equilibrium perturbations $\widetilde{g}_i$ associated to this kind of fluctuations is:

$$\widetilde{g}_i(\rho,\theta,\phi,t) = \sum_{\widetilde{k}_\perp} \widetilde{g}^0_{i,\widetilde{k}_\perp}(\rho,\theta)\cos\Phi_{\widetilde{k}_\perp}(\rho,\theta,\phi,t) \tag{3.4}$$

Explicit expressions for the phase $\Phi_{\widetilde{k}_\perp}(\rho,\theta,\phi,t)$ and for the amplitude $\widetilde{g}^0_{i,\widetilde{k}_\perp}(\rho,\theta)$, appropriate for describing the drift waves characteristics and the stochastic nature of the fluctuations, are derived in the next subsection following two different approaches: the first is a non-local description of the perturbation represented by an harmonic Fourier sum which preserves the periodicity of the oscillations, the second consists in a local approximation based on the eikonal expression of the geometrical phase $\Phi^G_{\widetilde{k}_\perp}$, valid for high values of $\widetilde{k}_\perp$.

3.1.2 Non-local description

The fluctuations are generated by several kind of modes which take place into the plasma (in general MHD modes), these modes are non-local phenomena, then the equilibrium perturbations associated are also of non-local type. The perturbations generated by the drift waves are phenomena lying on the flux surfaces, which direction of oscillation is orthogonal to the magnetic field lines. The periodicity in space of these oscillations implies that the fluctuations field lines, perpendicular to the magnetic field lines, are also closed (see Fig.(3.1)). The magnetic field versor, remembering the expression (2.31), is:

$$\mathbf{b} = P\hat{\mathbf{s}} + T\hat{\phi} \tag{3.5}$$

The perturbations are directed along the versor $\mathbf{b}_\perp = \mathbf{B}_\perp/B$, which lies on the flux surfaces and is orthogonal to $\mathbf{b}$:

$$\mathbf{b}_\perp = -T\hat{\mathbf{s}} + P\hat{\phi} \tag{3.6}$$

The infinitesimal lengths $dl_\parallel$ and $dl_\perp$, calculated respectively along the magnetic and the fluctuations field lines are defined as:

$$dl_\parallel = d\mathbf{X}\cdot\mathbf{b} \tag{3.7}$$

$$dl_\perp = d\mathbf{X}\cdot\mathbf{b}_\perp \tag{3.8}$$

In the coordinates system (ρ,θ,ϕ) the position vector $\mathbf{X}$ (see Appendix A) is given by the expression:

$$\mathbf{X} = R_p\hat{R} + Z_p\hat{Z} + r(\rho,\theta)\hat{r} \tag{3.9}$$

The infinitesimal vector $d\mathbf{X}$ is then [22]:

$$\begin{aligned} d\mathbf{X} &= \frac{\partial\mathbf{X}}{\partial\rho}d\rho + \frac{\partial\mathbf{X}}{\partial\theta}d\theta + \frac{\partial\mathbf{X}}{\partial\phi}d\phi \\ &= \frac{\partial r}{\partial\rho}\hat{r}d\rho + \Big(\frac{\partial r}{\partial\theta}\hat{r} + r\hat{\theta}\Big)d\theta + R\hat{\phi}d\phi \end{aligned} \tag{3.10}$$

Evaluating the scalar products, and neglecting the derivatives respect to the radial flux coordinate because the lines are located on the surfaces $\rho = const$, $dl_{\parallel}$ and $dl_{\perp}$ become:

$$dl_{\parallel} = \left(\frac{\partial r}{\partial \theta}\sin\alpha + r\cos\alpha\right) P d\theta + RT d\phi \tag{3.11}$$

$$dl_{\perp} = -\left(\frac{\partial r}{\partial \theta}\sin\alpha + r\cos\alpha\right) T d\theta + RP d\phi \tag{3.12}$$

The infinitesimal length elememts along the poloidal direction $\hat{\theta}$ and the toroidal direction $\hat{\phi}$ are [25]:

$$dl_{\theta} = \frac{r}{\cos\alpha} d\theta \tag{3.13}$$

$$dl_{\phi} = R d\phi \tag{3.14}$$

The ratio between these two infinitesimal distances in direction parallel and perpendicular to the field lines, consistently with the expressions (3.5) and (3.6) is:

$$\left(\frac{dl_{\theta}}{dl_{\phi}}\right)_{\parallel} = \frac{P}{T} \tag{3.15}$$

$$\left(\frac{dl_{\theta}}{dl_{\phi}}\right)_{\perp} = -\frac{T}{P} \tag{3.16}$$

From these expressions it is possible to obtain the relationships between the infinitesimal poloidal angle $d\theta$ and the infinitesimal toroidal angle $d\phi$ along $\mathbf{b}$ and $\mathbf{b}_{\perp}$:

$$\left(\frac{d\phi}{d\theta}\right)_{\parallel} = \frac{T}{P}\frac{r}{R\cos\alpha} \tag{3.17}$$

$$\left(\frac{d\phi}{d\theta}\right)_{\perp} = -\frac{P}{T}\frac{r}{R\cos\alpha} \tag{3.18}$$

Substituing these relations into the expressions for $dl_{\parallel}$ and $dl_{\perp}$ the final result is:

$$dl_{\parallel} = \left(\frac{1}{r}\frac{\partial r}{\partial \theta}\sin\alpha + \frac{P^2\cos^2\alpha + T^2}{P^2\cos^2\alpha}\right) r P d\theta \tag{3.19}$$

$$dl_{\perp} = -\left(\frac{1}{r}\frac{\partial r}{\partial \theta}\sin\alpha + \frac{T^2\cos^2\alpha + P^2}{T^2\cos^2\alpha}\right) r T d\theta \tag{3.20}$$

The length of the magnetic field lines $L_{\parallel}$ and of the fluctuations field lines $L_{\perp}$ are constant on a given flux surface, (all the field lines have the same length at $\rho = const$). Since both magnetic field lines than fluctuations lines are closed,

$L_\parallel$ and $L_\perp$ can be easily calculated by integrating $dl_\parallel$ and $dl_\perp$ between 0 and 2π:

$$L_\parallel = \int_0^{2\pi} dl_\parallel = \int_0^{2\pi} \left(\frac{1}{r}\frac{\partial r}{\partial \theta}\sin\alpha + \frac{P^2\cos^2\alpha + T^2}{P^2\cos^2\alpha} \right) rP d\theta \qquad (3.21)$$

$$L_\perp = \int_0^{2\pi} dl_\perp = -\int_0^{2\pi} \left(\frac{1}{r}\frac{\partial r}{\partial \theta}\sin\alpha + \frac{T^2\cos^2\alpha + P^2}{T^2\cos^2\alpha} \right) rT d\theta \qquad (3.22)$$

The lengths $L_\parallel = L_\parallel(\rho)$ and $L_\parallel = L_\perp(\rho)$ are function only of the radial flux coordinate ρ, and the expression (3.22) makes it possible to evaluate the length of the fluctuations field line on each flux surface. The distance $l_\perp$ between the origin of the fluctuation field lines posted in $\theta = 0$ and the point on the line correspondent to an angle θ, is given by the expression:

$$l_\perp = \int_0^{\theta} dl_\perp = -\int_0^{\theta} \left(\frac{1}{r}\frac{\partial r}{\partial \theta}\sin\alpha + \frac{T^2\cos^2\alpha + P^2}{T^2\cos^2\alpha} \right) rT d\theta' \qquad (3.23)$$

On a given flux surface all the fluctuations field lines have the same length $L_\perp$, and the distance $l_\perp$ can be calculated on each field line: the extremes of $l_\perp$ are the intersections between a determinated fluctuations field line and the two orthogonal magnetic field lines passing from these points, the distance between the intersections of the same two magnetic field lines with another arbitrary fluctuations field line is always equal to $l_\perp$, for each fluctuations line, as it is shown in Fig.(3.1).

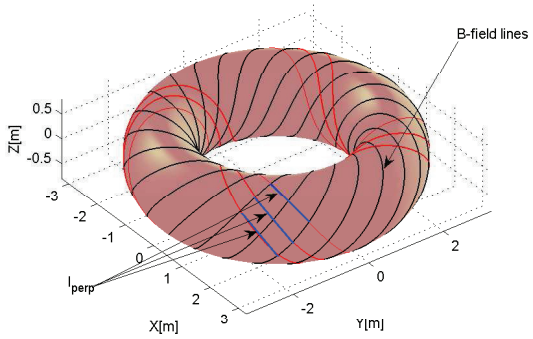

Figure 3.1: Magnetic field lines and fluctuations field lines on a given flux surfaces: The magnetic field lines are reported in black, while the oscillations direction of the fluctuations is given by the red lines orthogonal to **b**. The distance $l_\perp$ between the origin and an arbitrary point on the fluctuations field lines can be calculated on each line, infact all the blue path shown in the figure are equivalent. In the plot it is used a circular and concentric equilibrium representation ($\rho = r/a_p$) with Tore Supra tokamak parameters: plasma minor radius $a_p = 0.8$m, plasma major radius $R_p = 2.46$m, on-axis magnetic field $B_{T0} = 3.9$T. It has been chosen the most extern flux surface correspondent to $\rho = 1$.

Fluctuations phase

The general expression for the equilibrium perturbation due to drift-like processes (3.4) must be specialized in order to describe the random nature of these fluctuations, the illustrated spatial periodic structure based on closed field lines orthogonal to the magnetic field and the non-locality of the perturbations. The perpendicular wave vector of the fluctuations $\widetilde{k}_\perp$ is assumed to be an integer multiple of the quantity $2\pi/L_\perp = 2\pi/\widetilde{\lambda}$ where $L_\perp = \widetilde{\lambda}$ is in practice the perturbations wavelength:

$$\widetilde{k}_\perp = \frac{2\pi j}{L_\perp} \qquad j = 1, 2 \cdots \tag{3.24}$$

This choice for the expression of $\widetilde{k}_\perp$ preserves the periodicity of the oscillation such that the fluctuations are periodic in space with a period equal to $2\pi/L_\perp$ [29]. The geometrical contribution to the phase of a determinate oscillation j is:

$$\Phi_j^G = \beta j = \frac{2\pi j}{L_\perp} l_\perp \tag{3.25}$$

Where β is the angle subtended by the chord of length $l_\perp$ along the fluctuations field line of length $L_\perp$, defined by the relation:

$$\frac{2\pi}{L_\perp} = \frac{\beta}{l_\perp} \Rightarrow \beta = \frac{2\pi}{L_\perp} l_\perp \tag{3.26}$$

It is important to remark that $l_\perp$ and then the angle β must be defined by preserving the possibility of calculating this distance on each equivalent fluctuations field line. Since the fluctuations are processes of stochastic nature, the initial value of the phase of the oscillation corresponding to a determinate value of the index j is a uniformly distributed random variable, $\Phi_{j0} = \widetilde{\varphi}_j$.
The drift waves dispersion relation is given by the relation:

$$\widetilde{\omega}(\widetilde{\mathbf{k}}) = \mathbf{v}_D \cdot \mathbf{k} = v_D \widetilde{k}_\perp \tag{3.27}$$

Where $\mathbf{v}_D$ is the drift wave velocity, which direction is perpendicular to the magnetic field. Substituing $\widetilde{k}_\perp = 2\pi j/L_\perp$ into this equation the result is:

$$\widetilde{\omega}_j = \frac{2\pi j}{L_\perp} v_D \tag{3.28}$$

Remembering that the time variation of the total phase is associated to the slow scales characteristics of the electron distribution function evolution, it is assumed that the time-dependent term of the phase depends by the quasi-linear integration time step $\Delta\tau$. The expression for the total phase of the perturbation becomes:

$$\Phi_j = \left(\frac{2\pi j}{L_\perp} l_\perp + \widetilde{\varphi}_j - \frac{2\pi j}{L_\perp} v_D \Delta\tau \right) \tag{3.29}$$

Using this expression for the phase, the equilibrium perturbation $\widetilde{g}_i$ is finally exprimed in term of Fourier series which preserve both the periodicity than the non-locality of the oscillations [29]:

$$\widetilde{g}_i = \sum_{j=1}^{N} \widetilde{g}^0_{i,j} \cos\left(\frac{2\pi j}{L_\perp} l_\perp + \widetilde{\varphi}_j - \frac{2\pi j}{L_\perp} v_D \Delta\tau\right) \tag{3.30}$$

It is important to note that the value of the geometrical term of the phase is constant along the magnetic field lines, because the length $l_\perp$ does not evolve in direction parallel to the magnetic field (see Fig.(3.1)), the drift wave velocity is also assumed to be constant, as a consequence a perturbation of given amplitude is constant along the magnetic field lines (the magnetic field lines are iso-perturbation contours), and its value is determined by the random component of the phase. In Fig.(3.2) an illustrative example with Tore Supra tokamak parameters is reported: on a given flux surface, the iso-fluctuations lines parallel to the unperturbed magnetic field lines are reported using the blue colormap, each line corresponds to a value of the perturbation determined only by the random phase, the graduation of the color depends by the intensity of the fluctuations, and goes from the darkest lines corresponding to highest values, to the clearest corresponding to lowest. A single fluctuations field line perpendicular to the iso-perturbation lines is reported in red.

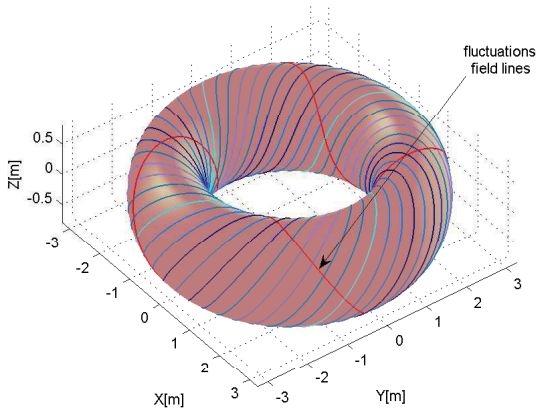

Figure 3.2: Iso-pertubation lines on a given flux surface: the iso-perturbation contours of a generic perturbation of given amplitude, coincident with the magnetic field lines, are plotted using the blu colormap, each line corresponds to a value of the perturbation determined only by the random phase, the graduation of the color depends by the intensity of the fluctuations, and goes from the darkest lines correspond to highest values, to the clearest corresponding to the lowest. A single fluctuations field line perpendicular to the iso-perturbation lines is reported in red. In the plot is used a circular and concentric equilibrium representation ($\rho = r/a_p$) with Tore Supra tokamak parameters: plasma minor radius $a_p = 0.8$m, plasma major radius $R_p = 2.46$m, on-axis magnetic field $B_{T0} = 3.9$T. It has been chosen the most extern flux surface correspondent to $\rho = 1$.

Fluctuations amplitude

The explicit expression for the amplitude of the drift-like fluctuations is directly connected to the autocorrelation of the periodic perturbation represented by the (3.30). The autocorrelation in space of the periodic signal $\widetilde{g}_i$, neglecting the time-dependent term of the phase is calculated as follows:

$$R(l'_\perp) = \frac{1}{L_\perp}\int_{-L_\perp/2}^{L_\perp/2} \widetilde{g}_i(l_\perp)\widetilde{g}_i(l_\perp + l'_\perp)dl_\perp =$$

$$= \frac{1}{L_\perp}\int_{-L_\perp/2}^{L_\perp/2} \left[\sum_{n=1}^{N} \widetilde{g}^0_{i,n}\cos\left(\frac{2\pi n}{L_\perp}l_\perp + \widetilde{\varphi}_n\right)\right]\left[\sum_{j=1}^{N} \widetilde{g}^0_{i,j}\cos\left(\frac{2\pi j}{L_\perp}(l_\perp + l'_\perp) + \widetilde{\varphi}_j\right)\right] dl_\perp =$$

$$= \sum_{j=1}^{N} \frac{(\widetilde{g}^0_{i,j})^2}{2}\cos\left(\frac{2\pi j}{L_\perp}l'_\perp\right) \tag{3.31}$$

The autocorrelation of $\widetilde{g}_i$ can be also defined as the Fourier transform of the spectral distribution $S_g(\widetilde{k}_\perp)$, in this case, there is a descrete set of possible values for the perpendicular wave vector $\widetilde{k}_\perp = 2\pi j/L_\perp$, as a consequence the spectrum can be approximated to the descrete grid of values $S_{g,j}$ and $R(l'_\perp)$ become:

$$R(l'_\perp) = \sum_{j=1}^{N} S_{g,j} e^{i\frac{2\pi j}{L_\perp}l'_\perp} \tag{3.32}$$

Considering only one single oscillation correnspondent to a given value of the index j, $R(l'_\perp)$ is:

$$R(l'_\perp) = \frac{(\widetilde{g}^0_{i,j})^2}{2}\cos\left(\frac{2\pi j}{L_\perp}l'_\perp\right) = S_{g,j}e^{i\frac{2\pi j}{L_\perp}l'_\perp} \tag{3.33}$$

For $l'_\perp = 0$ the following equality is derived:

$$R(0) = \frac{(\widetilde{g}^0_{i,j})^2}{2} = S_{g,j} \tag{3.34}$$

Then the amplitute $\widetilde{g}^0_{i,j}$ of the oscillation corresponding to a certain value of j is given by the expression:

$$\widetilde{g}^0_{i,j} = \sqrt{2S_{g,j}} \tag{3.35}$$

This expression, derived from the definition of autocorrelation of a periodic signal and from the Fourier transform of the spectrum, is absolutely general and it can be used for describing each kind of perturbation of any equilibrium function $(n_\alpha, \mathbf{B}, T_\alpha)$ induced by a drift-like process, without any restriction or condition regarding the fluctuations spectrum S_g.

3.1.3 Local description

The spectrum and the relative fluctuations level $\widetilde{g}/\overline{g}$ have been studied and measured locally in several tokamaks experiments [1, 2, 3, 4, 5]. In order to incorporate into the model the local characteristics of the fluctuations, a local description of the equilibrium perturbations based on the eikonal representation of the phase is presented. Since it is based on the eikonal approach, this local formulation is a good approximation of the general non-local model for high values of the fluctuations wave vector $\widetilde{k}_\perp$. It is important to note that the local description implies the lack of the periodicity in space of the perturbations respect to the global representation.

Fluctuations wave vector

The fluctuations wave vector in the local approximation is expressed using the canonically conjugate coordinates (ρ, θ, ϕ) and (k_ρ, m, n). Introducing the covariant components $(\widetilde{k}_\rho, \widetilde{m}, \widetilde{n})$ and remembering the contravariant basis (2.10), the fluctuations wave vector $\widetilde{\mathbf{k}}$ is given by the general expression:

$$\widetilde{\mathbf{k}} = \widetilde{k}_\rho \left\|\nabla\rho\right\| \hat{\rho} + \frac{\widetilde{m}}{r}\hat{\theta} + \frac{\widetilde{n}}{R}\hat{\phi} \tag{3.36}$$

As just discussed, the wave vector $\widetilde{\mathbf{k}}$ lies on the flux surfaces, then $\widetilde{k}_\rho = 0$ and:

$$\widetilde{\mathbf{k}} = \frac{\widetilde{m}}{r}\hat{\theta} + \frac{\widetilde{n}}{R}\hat{\phi} \tag{3.37}$$

The parallel and the perpendicular components of the fluctuations wave vector become:

$$\widetilde{k}_\parallel = P\frac{\widetilde{m}}{r} + T\frac{\widetilde{n}}{R} \tag{3.38}$$

$$\widetilde{k}_\perp = \pm\sqrt{\frac{\widetilde{m}^2}{r^2}\sin^2\alpha + \left(T\frac{\widetilde{m}}{r}\cos\alpha - P\frac{\widetilde{n}}{R}\right)^2} \tag{3.39}$$

Where it has been assumed that:

$$\widetilde{k}_\parallel = \widetilde{\mathbf{k}}\cdot\mathbf{b} = \widetilde{\mathbf{k}}\cdot\overline{\mathbf{b}} + \widetilde{\mathbf{k}}\cdot\widetilde{\mathbf{b}} \approx \widetilde{\mathbf{k}}\cdot\overline{\mathbf{b}} \tag{3.40}$$

Since the term $\widetilde{\mathbf{k}}\cdot\widetilde{\mathbf{b}}$ is a small correction. Considering that the parallel wave vector is negligible, an expression for $\widetilde{m}$ and $\widetilde{n}$ in function of the perpendicular wave vector can be derived from the (3.38)-(3.39):

$$\widetilde{m} = \pm\frac{r\widetilde{k}_\perp}{\sqrt{1 + \frac{P^2}{T^2}\cos^2\alpha}} \tag{3.41}$$

$$\widetilde{n} = \mp\frac{\frac{P}{T}R\widetilde{k}_\perp\cos\alpha}{\sqrt{1 + \frac{P^2}{T^2}\cos^2\alpha}} \tag{3.42}$$

Fluctuations phase

Also in the local approximation, the initial value $\Phi_{\widetilde{\mathbf{k}}0}$ of the phase associated to a certain $\widetilde{\mathbf{k}}$ is assumed to be an uniformly distributed random variable, $\widetilde{\varphi}_{\widetilde{\mathbf{k}}}$. Since $\widetilde{k}_{\parallel} = 0$, the initial phase is $\Phi_{\widetilde{k}_\perp 0} = \widetilde{\varphi}_{\widetilde{k}_\perp}$.
The geometrical contribution is given by the following path integral calculated along the trajectory of the oscillation:

$$\Phi^G_{\widetilde{\mathbf{k}}} = \int_{\mathbf{X}_0}^{\mathbf{X}} \widetilde{\mathbf{k}}(\mathbf{X}') \cdot d\mathbf{X}' \tag{3.43}$$

The scalar product between $d\mathbf{X}$ (see expression (3.10)) and the fluctuations wave vector is:

$$\widetilde{\mathbf{k}} \cdot d\mathbf{X} = \widetilde{k}_\rho \|\nabla\rho\| \frac{\partial r}{\partial \rho} \cos\alpha d\rho + \Big(\widetilde{k}_\rho \|\nabla\rho\| \frac{\partial r}{\partial \theta} \cos\alpha -$$

$$-\widetilde{k}_\rho \|\nabla\rho\| r \sin\alpha + \widetilde{m}\Big) d\theta + \widetilde{n} d\phi \tag{3.44}$$

Remembering that $\widetilde{k}_\rho = 0$, and $\widetilde{k} = \widetilde{k}_\perp$, it becomes:

$$\widetilde{\mathbf{k}} \cdot d\mathbf{X} = \widetilde{m} d\theta + \widetilde{n} d\phi \tag{3.45}$$

Where $\widetilde{m}$ and $\widetilde{n}$ are given in function of $\widetilde{k}_\perp$ by the expressions (3.41) and (3.42). Substituing these expressions into the (3.45), it is obtained:

$$\widetilde{m} d\theta + \widetilde{n} d\phi = \pm \frac{\frac{P}{T} R \widetilde{k}_\perp \cos\alpha}{\sqrt{1 + \frac{P^2}{T^2}\cos^2\alpha}} \left[\frac{T}{P}\frac{r}{R\cos\alpha} d\theta - d\phi\right] \tag{3.46}$$

Explicit expressions for the ratio between $d\phi$ and $d\theta$ in direction parallel and perpendicular to the magnetic field lines have been introduced in the previous subsection (equations (3.17) and (3.18)), using these expressions the scalar product (3.45) is calculated along the magnetic field lines and along the fluctuations field lines perpendicular to $\mathbf{b}$:

$$\left(\widetilde{m} d\theta + \widetilde{n} d\phi\right)_\parallel = 0 \tag{3.47}$$

$$\left(\widetilde{m} d\theta + \widetilde{n} d\phi\right)_\perp = \frac{r}{R\cos\alpha}\frac{d\theta}{PT} \tag{3.48}$$

The (3.47) implies that also in the local description, as in the non-local model, the geometrical term of the phase has constant value along the magnetic field lines, and the oscillations phase value on these lines is determined by the random contribution and does not evolve in time. This means that, if the perturbations amplitude is dependent only by the radial flux coordinate ρ, also in the local approximation on a given flux surface the fluctuations value on the magnetic field lines is constant.

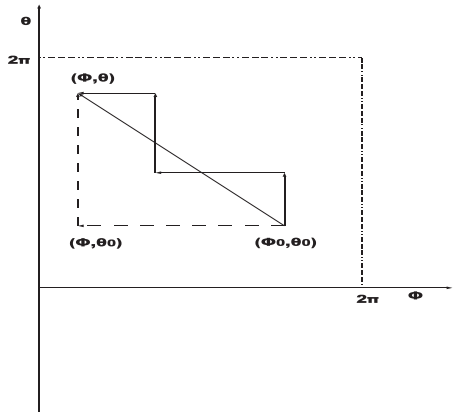

Figure 3.3: Path integral in the $\phi - \theta$ variables to evaluate an explicit expression for the drift wave phase: following the dashed path the integration is performed before in the toroidal angle and in the second step in θ

.

The components $\widetilde{m}$ and $\widetilde{n}$ are function of θ and ϕ, then the path integral (3.43) must be evaluated on the $\phi - \theta$ plane. Starting from the initial coordinates (ϕ_0, θ_0) the integral is calculated along the dashed path reported in the $\phi - \theta$ diagram in Fig(3.3): at the first step it is performed the integration on the toroidal angle, maintaining $\theta = \theta_0$ and remembering that $\widetilde{n}$ does not depend by ϕ, at the second the toroidal angle is fixed and the integral is evaluated between θ_0 and θ. Following this path, the result is:

$$\begin{aligned} \Phi^G_{\widetilde{k}_\perp} &= \int_{\phi_0}^{\phi} d\phi' \widetilde{n}\big(\rho, \theta_0, \widetilde{k}_\perp\big) + \int_{\theta_0}^{\theta} d\theta' \widetilde{m}\big(\rho, \theta, \widetilde{k}_\perp\big) \\ &= \widetilde{n}\big(\rho, \theta_0, \widetilde{k}_\perp\big)\big(\phi - \phi_0\big) + \int_{\theta_0}^{\theta} d\theta' \widetilde{m}\big(\rho, \theta, \widetilde{k}_\perp\big) \end{aligned} \tag{3.49}$$

This is a general expression for the geometrical term of the drift wave phase in the local approximation. The drift waves dispersion relation has just been introduced in the presentation of the global approach, remembering that the direction of the drift velocity $\mathbf{v}_D$ is perpendicular to the magnetic field, it becomes:

$$\widetilde{\omega}(\widetilde{\mathbf{k}}) = \mathbf{v}_D \cdot \mathbf{k} = v_D \widetilde{k}_\perp \tag{3.50}$$

Since the time variation of the phase is associated to the slow scales characteristics of the electron distribution function evolution, the time-dependent term is function of the quasilinear integration time step $\Delta\tau$. The phase of an oscillation with a given $\widetilde{k}_\perp$, in the local approximation is:

$$\Phi_{\widetilde{k}_\perp} = \widetilde{\varphi}_{\widetilde{k}_\perp} + \widetilde{n}\big(\rho, \theta_0, \widetilde{k}_\perp\big)\big(\phi - \phi_0\big) + \int_{\theta_0}^{\theta} d\theta' \widetilde{m}\big(\rho, \theta, \widetilde{k}_\perp\big) - v_D \widetilde{k}_\perp \Delta\tau \tag{3.51}$$

This expression represents a good approximation of the perturbations phase in the general non local approach for great values of $\widetilde{k}_\perp$, but the locality implies the lack of the periodicity in space of the oscillations.

Fluctuations amplitude

The total perturbation associated to drift-like fluctuations is the sum of a great number of single oscillations corresponding to different values of $\widetilde{k}_\perp$, the randomness of the process is due to the contribution $\widetilde{\varphi}_{\widetilde{k}_\perp}$ to the phase (3.51). The mean square relative level of a generic fluctuation can be defined as [9, 11, 12]:

$$\sigma_{gi}^2 = \left\langle \left(\frac{\widetilde{g}_i}{\overline{g}} \right)^2 \right\rangle = \int_{-\infty}^{+\infty} S_{gi}\big(\widetilde{k}_\perp\big) d\widetilde{k}_\perp \tag{3.52}$$

Where σ_{gi} is the spatial profile of the local relative level of fluctuations and $S_{gi}\big(\widetilde{k}_\perp\big)$ is the fluctuations perpendicular wave vector spectrum. Also negative values of $\widetilde{k}_\perp$ are considered. It has been shown experimentally that $S_{gi}(\widetilde{k}_\perp)$ for both density than magnetic field fluctuations is well approximated by a gaussian [4, 5], then the spectral distribution is assumed to be:

$$S_{gi}\big(\widetilde{k}_\perp\big) = \frac{\sigma_{gi}^2}{\sqrt{2\pi} k_{\perp c}} \exp\left(-\frac{\widetilde{k}_\perp^2}{2k_{\perp c}^2} \right) \tag{3.53}$$

Where $k_{\perp c}^{-1}$ is the correlation length of the perturbations. Since the perturbation $\widetilde{g}_i$ is the result of the sum a discrete set of oscillations corresponding to different values of $\widetilde{k}_\perp$, the integral (3.52) can be approximated with a sum over an uniform grid of $\widetilde{k}_\perp$ corresponding to a descrete set of values $S_{gi,\widetilde{k}_\perp}$:

$$S_{gi,\widetilde{k}_\perp} = \frac{\sigma_{gi}^2}{\sqrt{2\pi} k_{\perp c}} \exp\left(-\frac{\widetilde{k}_\perp^2}{2k_{\perp c}^2} \right) \tag{3.54}$$

Substituing the expression (3.53) into the general definition for the perturbations amplitude derived for the general non-local model (3.35), the following expression for $\widetilde{g}_{i,\widetilde{k}_\perp}^{0n}$ is derived:

$$\widetilde{g}_{i,\widetilde{k}_\perp}^{0n} = \sqrt{2 S_{gi,\widetilde{k}_\perp} \Delta\widetilde{k}_\perp} = \sigma_{gi} \cdot \left(\frac{2}{\pi} \right)^{\frac{1}{4}} \cdot \sqrt{\frac{\Delta\widetilde{k}_\perp}{k_{\perp c}}} \cdot \exp\left(-\frac{\widetilde{k}_\perp^2}{4k_{\perp c}^2} \right) \tag{3.55}$$

Where the normalization quantity $\Delta\widetilde{k}_\perp$ is the interval between two consecutive values of the $\widetilde{k}_\perp$ grid that replaces the infinitesimal element $d\widetilde{k}_\perp$ in the passage from the integral to the sum. In toroidal geometry the fluctuations relative level σ_{gi} is assumed to be function of the coordinates ρ and θ, consequently:

$$\widetilde{g}_{i,\widetilde{k}_\perp}^{0n}(\rho,\theta) = \sigma_{gi}(\rho,\theta) \cdot \left(\frac{2}{\pi} \right)^{\frac{1}{4}} \cdot \sqrt{\frac{\Delta\widetilde{k}_\perp}{k_{\perp c}}} \cdot \exp\left(-\frac{\widetilde{k}_\perp^2}{4k_{\perp c}^2} \right) \tag{3.56}$$

This is the general expression for the relative amplitude of the drift-like oscillation corresponding to a determinate value of $\widetilde{k}_\perp$ in the local approximation, the absolute amplitude $\widetilde{g}^0_{i,\widetilde{k}_\perp}$ becomes:

$$\widetilde{g}^0_{i,\widetilde{k}_\perp}(\rho,\theta) = \overline{g}(\rho,\theta)\cdot\sigma_{gi}(\rho,\theta)\cdot\left(\frac{2}{\pi}\right)^{\frac{1}{4}}\cdot\sqrt{\frac{\Delta\widetilde{k}_\perp}{k_{\perp c}}}\cdot\exp\left(-\frac{\widetilde{k}^2_\perp}{4k^2_{\perp c}}\right) \tag{3.57}$$

The following analytical spatial profile for the relative fluctuations level $\sigma_{gi}(\rho,\theta)$ is assumed [12]:

$$\sigma_{gi}(\rho,\theta) = \left\langle\left(\frac{\widetilde{g}_i}{\overline{g}}\right)^2\right\rangle^{\frac{1}{2}} =$$

$$= \sigma_{gimax}\cdot\exp\left[-\frac{1}{2}\frac{(\rho-\rho_0)^2}{(\Delta\rho/\sqrt{2\ln 2})^2}\right]\cdot\left(\frac{1+\lambda\cos\theta}{1+\lambda}\right) \tag{3.58}$$

Where σ_{gimax} is the maximum value of the relative fluctuations level, ρ_0 the radial position of the fluctuations peak, corresponding to $\sigma_{gi} = \sigma_{gimax}$, $\Delta\rho$ is the radial distance between the peak and the position at which the fluctuations relative level is halved ($\sigma_{gi} = \sigma_{gimax}/2$ at $\rho = \rho_0 \pm \Delta\rho$), and λ is an adimensional parameter which represents the dependence of the profile by the poloidal angle (for $\lambda =$ there is no angular dependence and σ_{gi} is only function of ρ). The expressions for the amplitude (3.57) and for the fluctuations mean relative level (3.58), derived in the local approximation, can be easily adapted to describe the local characteristics of any kind of drift-like fluctuations. In the next sections two cases of drift fluctuations are presented and studied using the local eikonal approach: perturbations of the electron density $\widetilde{n}_e$ and of the magnetic field $\widetilde{\mathbf{B}}$. The typical parameters of these fluctuations are used in the expressions for the local amplitude and for the relative spatial profile and the impact of the parameters variation on the statistical properties of the perturbations is investigated by means of a comparative analysis.

3.1.4 Electron density fluctuations

Fluctuations of electronic density generated by electron drift waves have been measured with different diagnostic techniques in several tokamaks [1, 2, 26, 27, 28], expecially in the region near to the plasma edge, and their effects on propagation and non-inductive current generation by LH and EC waves has been estimated to be relevant both in actual current drive experiments [9, 11, 12], than in the future ITER scenarios [13, 14]. The perturbation of n_e generated by a determinated drift-like fluctuations process can be derived by specializing the general expression (3.4):

$$\widetilde{n}_e(\rho,\theta,\phi,t) = \sum_{\widetilde{k}_\perp}\widetilde{n}^0_{e\widetilde{k}_\perp}(\rho,\theta)\cos\Phi_{\widetilde{k}_\perp}(\rho,\theta,\phi,t) \tag{3.59}$$

Using the local representation, the relative amplitude of the electron density oscillation of perpendicolar wave vector $\widetilde{k}_\perp$ is:

$$\widetilde{n}^{0n}_{e\widetilde{k}_\perp}(\rho,\theta) = \sigma_{ne}(\rho,\theta)\cdot\left(\frac{2}{\pi}\right)^{\frac{1}{4}}\cdot\sqrt{\frac{\Delta\widetilde{k}_\perp}{k_{\perp c}}}\cdot\exp\left(-\frac{\widetilde{k}^2_\perp}{4k^2_{\perp c}}\right) \tag{3.60}$$

While the absolute amplitude $\widetilde{n}^0_{e\widetilde{k}_\perp}$ used in the expression (3.59) becomes:

$$\widetilde{n}^0_{e\widetilde{k}_\perp}(\rho,\theta) = \overline{n}_e(\rho)\cdot\widetilde{n}^{0n}_{e\widetilde{k}_\perp}(\rho,\theta) =$$

$$= \overline{n}_e(\rho)\cdot\sigma_{ne}(\rho,\theta)\cdot\left(\frac{2}{\pi}\right)^{\frac{1}{4}}\cdot\sqrt{\frac{\Delta\widetilde{k}_\perp}{k_{\perp c}}}\cdot\exp\left(-\frac{\widetilde{k}^2_\perp}{4k^2_{\perp c}}\right) \tag{3.61}$$

Where $\overline{n}_e(\rho)$ is the unperturbed electronic density. The expressions (3.59) for the perturbation, (3.51) for the phase, and (3.61) for the amplitude are appropriate for describing the local properties of all kinds of fluctuations of the electronic density with $\widetilde{k}_\parallel = 0$ and $\widetilde{k}_\rho = 0$. The specific characteristics of the fluctuations processes determine the value of the correlation length $k_{\perp c}$ and of the parameters σ_{nemax}, $\Delta\rho$ and ρ_0 which influence the local relative level profile:

$$\sigma_{ne}(\rho,\theta) = \left\langle\left(\frac{\widetilde{n}_e}{\overline{n}_e}\right)^2\right\rangle^{\frac{1}{2}} =$$

$$= \sigma_{nemax}\cdot\exp\left[-\frac{1}{2}\frac{(\rho-\rho_0)^2}{(\Delta\rho/\sqrt{2\ln 2})^2}\right]\cdot\left(\frac{1+\lambda\cos\theta}{1+\lambda}\right) \tag{3.62}$$

In several experiments the maximum level of density fluctuations is detected at the edge of the plasma and it is estimated to be between 10% and 30%; the fluctuations peak width is in general thin. This kinds of fluctuations are described by σ_{ne} profiles with $0.1 \le \sigma_{ne} \le 0.3$, $\rho_0 = 1$, and small values of $\Delta\rho$. In Fig.(3.4)/A are compared relative level profiles peaked at the border with $\sigma_{nemax} = 30\%$ and different values of $\Delta\rho = 0.07, 0.14, 0.21$, while in Fig.(3.4)/B are reported profiles with $\rho_0 = 1$, $\Delta\rho = 0.07$, but different maximum relative levels $\sigma_{nemax} = 10\%, 30\%, 50\%$, in both cases it has been assumed the value $\lambda = 0$, then there is no θ-dependence. As it is shown in this figure, major values of $\Delta\rho$ imply broad fluctuation spatial profiles, so the perturbation effects are more distributed into the plasma respect to processes with narrow σ_{ne} trend, which domains is very localized. By choosing large values of $\Delta\rho$, for example $\Delta\rho = 0.5$, and low maximum level of fluctuation, $\sigma_{nemax} = 1\%$ it is also possible to decribe background perturbations, while the very high and localized fluctuations with strong poloidal dependence relevated at the border in the area where the antennas interact with the plasma [1] can be modeled with a profile having $\Delta\rho = 0.01$, $\sigma_{nemax} = 90\%$ and $\lambda \neq 0$. The poloidal dependence of σ_{ne} is due to the factor:

$$\frac{\sigma_{ne}(\rho,\theta)}{(\sigma_{ne}(\rho))_{\lambda=0}} = \left(\frac{1+\lambda\cos\theta}{1+\lambda}\right) \tag{3.63}$$

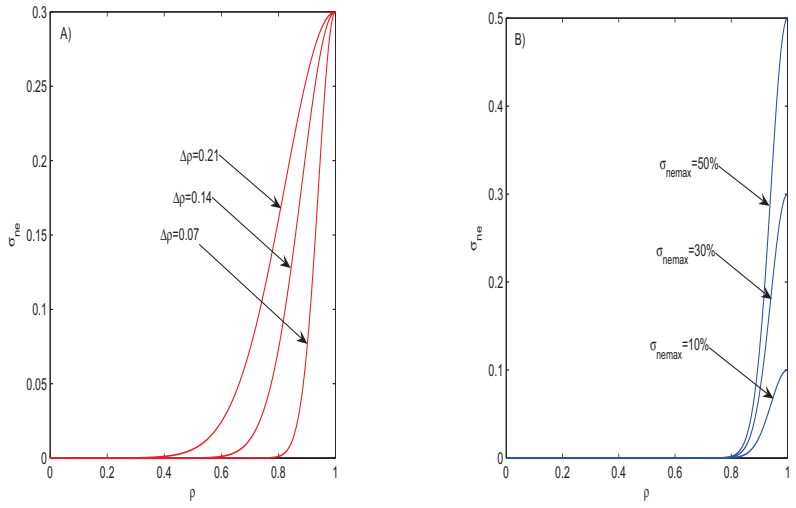

Figure 3.4: A):Comparison between σ_{ne} profiles independent by θ ($\lambda = 0$) peaked at the plasma edge ($\rho_0 = 1$) with the same maximum relative level $\sigma_{nemax} = 30\%$ and different values $\Delta\rho = 0.07, 0.14, 0.21$; B): Comparison between σ_{ne} profiles independent by θ ($\lambda = 0$) peaked at the plasma edge ($\rho_0 = 1$), with the same $\Delta\rho = 0.07$ but different maximum relative levels $\sigma_{nemax} = 10\%, 30\%, 50\%$.

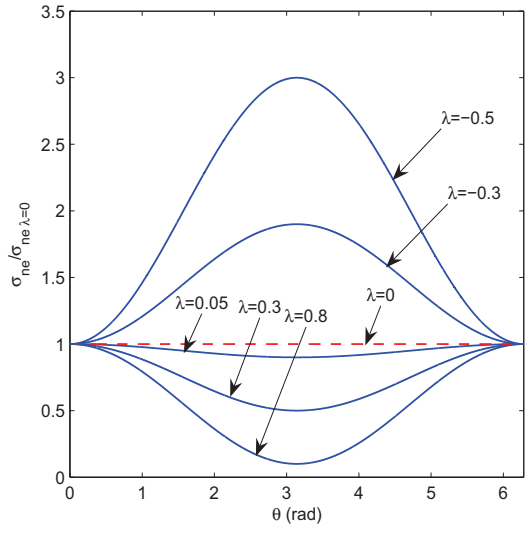

Figure 3.5: Poloidal dependence of σ_{ne} profiles for different values of the parameter $\lambda = -0.5, -0.3, 0.05, 0., 0.8$, the red dashed line corresponds to the case $\lambda = 0$, without poloidal dependence.

This factor is plotted in function of θ for different values on λ in Fig.(3.5). The red dashed line corresponds to the reference case without poloidal dependence, corresponding to $\lambda = 0$, it is important to observe that for $\lambda > 0$ the poloidal dependence factor is always major than 1, while for $\lambda > 0$ it is always minor: in practice for positive values of the parameter λ the poloidal dependence amplifies the local relative level of density fluctuations, for negative values it reduces the same level. In Figs.(3.6) (3.7), (3.8), (3.9) and (3.10) are illustrated the radial and the poloidal dependence of a fluctuations relative level profile peaked at the plasma edge with $\Delta\rho = 0.07$ and maximum value $\sigma_{nemax} = 0.3$ corresponding to the maximum level of $\widetilde{n}_e$ observed in several experiments [1, 12]. This profile is plotted for several values of the parameter λ ($\lambda = -0.5, -0.3, 0.05, 0., 0.8$) in function of ρ for a set of constant $\theta-$values and in function of θ for a set of constant radial positions, in order to study the effects of the poloidal dependence variation and to show the differences respect to the case without poloidal dependence reported in red. In agreement with the previous considerations on the poloidal depencence factor, in these figures it is shown that if $\lambda < 0$, the mean relative level of density fluctuations is minor than the reference case with $\lambda = 0$ in any radial position, while if $\lambda > 0$ it is everywhere major. It is easy to deduce that the effects of the poloidal dependence increase for great values of $|\lambda|$, whereas become low for small values, like $|\lambda| = 0.05$, as it is illustrated in Fig.(3.8).

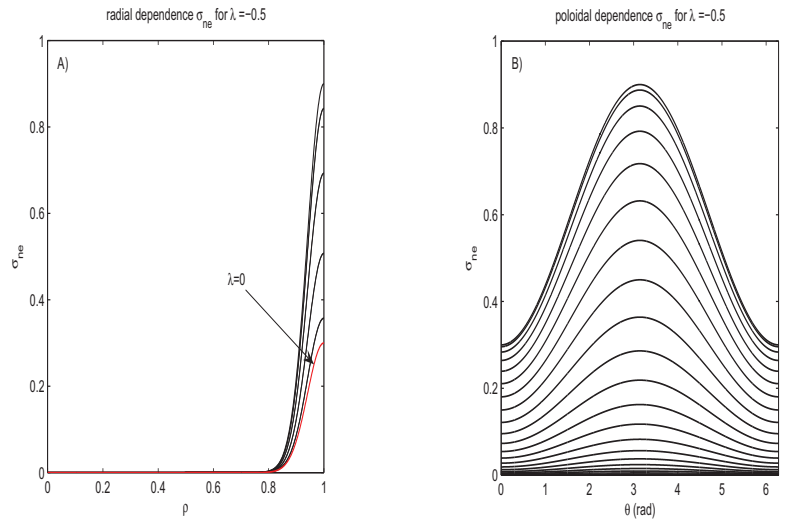

Figure 3.6: A): Radial dependence of σ_{ne} profile with $\sigma_{nemax} = 0.3$, $\rho_0 = 1$, $\Delta\rho = 0.07$ and $\lambda = -0.5$, the profiles are plotted in function of ρ for constant values on θ, the reference case without $\theta-$dependence is reported in red; B): Poloidal dependence of σ_{ne} profile with $\sigma_{nemax} = 0.3$, $\rho_0 = 1$, $\Delta\rho = 0.07$ and $\lambda = -0.5$, the profiles are plotted in function of θ for constant values on ρ.

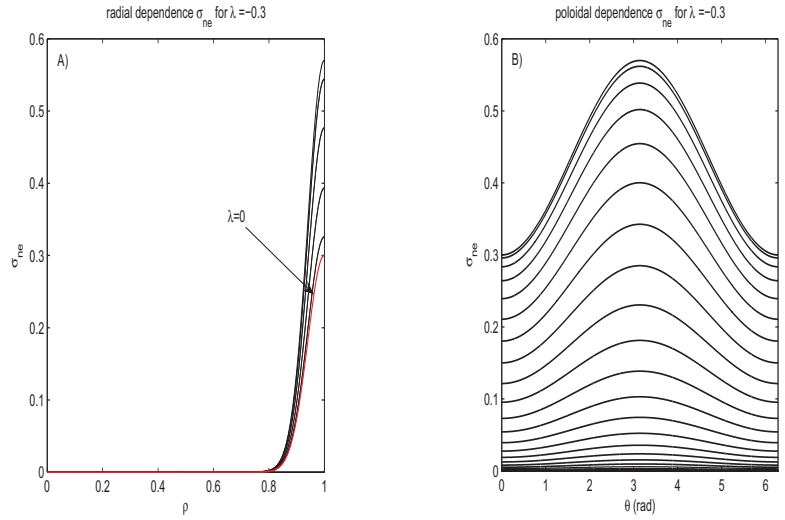

Figure 3.7: A): Radial dependence of σ_{ne} profile with $\sigma_{nemax} = 0.3$, $\rho_0 = 1$, $\Delta\rho = 0.07$ and $\lambda = -0.3$, the profiles are plotted in function of ρ for constant values on θ, the reference case without $\theta-$dependence is reported in red; B): Poloidal dependence of σ_{ne} profile with $\sigma_{nemax} = 0.3$, $\rho_0 = 1$, $\Delta\rho = 0.07$ and $\lambda = -0.3$, the profiles are plotted in function of θ for constant values on ρ.

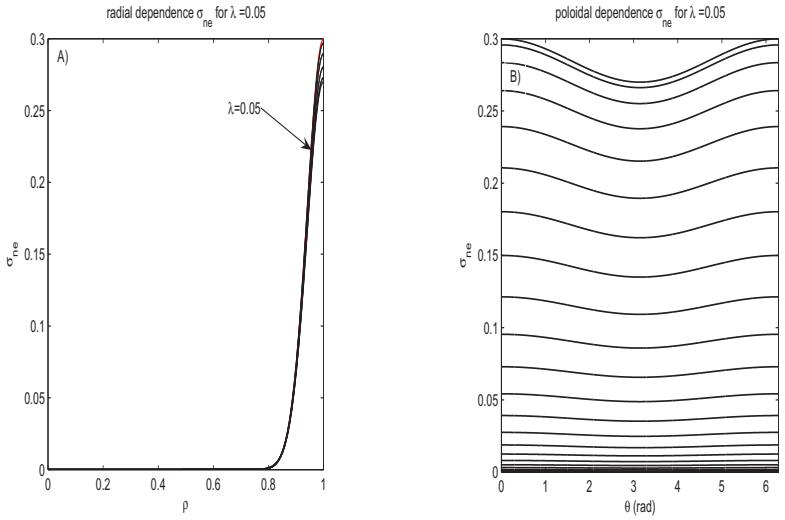

Figure 3.8: A): Radial dependence of σ_{ne} profile with $\sigma_{nemax} = 0.3$, $\rho_0 = 1$, $\Delta\rho = 0.07$ and $\lambda = 0.05$, the profiles are plotted in function of ρ for constant values on θ, the reference case without $\theta-$dependence is reported in red; B): Poloidal dependence of σ_{ne} profile with $\sigma_{nemax} = 0.3$, $\rho_0 = 1$, $\Delta\rho = 0.07$ and $\lambda = 0.05$, the profiles are plotted in function of θ for constant values on ρ.

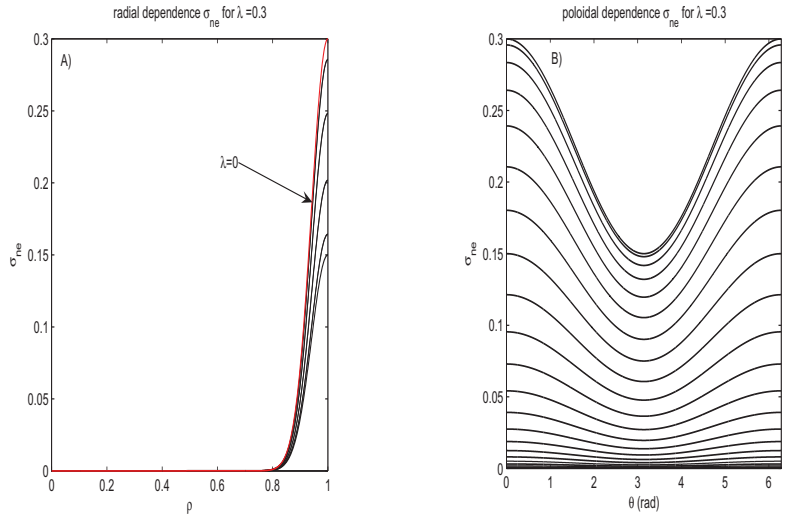

Figure 3.9: A): Radial dependence of σ_{ne} profile with $\sigma_{nemax} = 0.3$, $\rho_0 = 1$, $\Delta\rho = 0.07$ and $\lambda = 0.3$, the profiles are plotted in function of ρ for constant values on θ, the reference case without $\theta-$dependence is reported in red; B): Poloidal dependence of σ_{ne} profile with $\sigma_{nemax} = 0.3$, $\rho_0 = 1$, $\Delta\rho = 0.07$ and $\lambda = 0.3$, the profiles are plotted in function of θ for constant values on ρ.

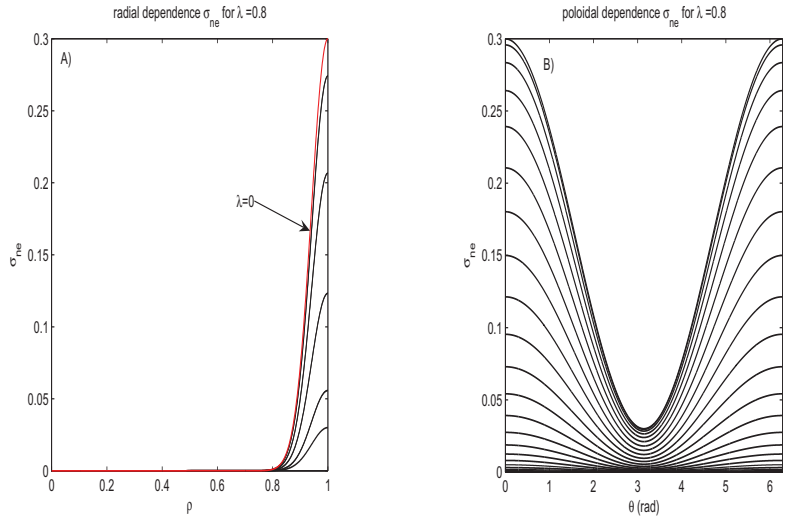

Figure 3.10: A): Radial dependence of σ_{ne} profile with $\sigma_{nemax} = 0.3$, $\rho_0 = 1$, $\Delta\rho = 0.07$ and $\lambda = 0.8$, the profiles are plotted in function of ρ for constant values on θ, the reference case without $\theta-$dependence is reported in red; B): Poloidal dependence of σ_{ne} profile with $\sigma_{nemax} = 0.3$, $\rho_0 = 1$, $\Delta\rho = 0.07$ and $\lambda = 0.8$, the profiles are plotted in function of θ for constant values on ρ.

The effects of the several parameters on the local relative level of density fluctuations have been illustrated using some simple examples. The parameters of the σ_{ne} profiles can be adapted on the basis of the fluctuations local characteristics without restrictions and without conditions on the plasmas features. The statistical properties of the presented expression for the electron density perturbation (3.59) will be discussed in subsection 3.1.6.

3.1.5 Magnetic field fluctuations

Magnetic field fluctuations generated by several magnetohydrodynamic modes have been detected and localized in toroidal plasmas with microwaves scattering diagnostic techniques [2, 7]. The magnetic perturbations, as the density fluctuations induced by the drift waves, lie on the flux surfaces. This implies that the radial components of the wavevector and of the field generated by the fluctuations are zero ($\widetilde{k}_\rho = 0, \widetilde{B}_\rho = 0$). The oscillations are oriented in direction orthogonal to the magnetic field lines, then $\widetilde{B} = \widetilde{B}_\perp$ and the component parallel to the equilibrium field versor $\mathbf{b}$ is zero:

$$\widetilde{B}_\parallel = 0 \tag{3.64}$$

The expression for the perpendicular perturbation $\widetilde{B}_\perp$ in the local representation is:

$$\widetilde{B}_\perp(\rho,\theta,\phi,t) = \sum_{\widetilde{k}_\perp} \widetilde{B}^0_{\perp\widetilde{k}_\perp}(\rho,\theta)\cos\Phi_{\widetilde{k}_\perp}(\rho,\theta,\phi,t) \tag{3.65}$$

Using the local representation, the relative amplitude of the magnetic field oscillation associated to a certain value of the perpendicular wave vector $\widetilde{k}_\perp$ is:

$$\widetilde{B}^{0n}_{\perp\widetilde{k}_\perp}(\rho,\theta) = \sigma_{B_\perp}(\rho,\theta)\cdot\left(\frac{2}{\pi}\right)^{\frac{1}{4}}\cdot\sqrt{\frac{\Delta\widetilde{k}_\perp}{k_{\perp c}}}\cdot\exp\left(-\frac{\widetilde{k}^2_\perp}{4k^2_{\perp c}}\right) \tag{3.66}$$

While the absolute amplitude $\widetilde{B}^0_{\perp\widetilde{k}_\perp}$ becomes:

$$\widetilde{B}^0_{\perp\widetilde{k}_\perp}(\rho,\theta) = \overline{B}(\rho,\theta)\cdot\widetilde{B}^{0n}_{\perp\widetilde{k}_\perp}(\rho,\theta) =$$

$$= \overline{B}(\rho,\theta)\cdot\sigma_{B_\perp}(\rho,\theta)\cdot\left(\frac{2}{\pi}\right)^{\frac{1}{4}}\cdot\sqrt{\frac{\Delta\widetilde{k}_\perp}{k_{\perp c}}}\cdot\exp\left(-\frac{\widetilde{k}^2_\perp}{4k^2_{\perp c}}\right) \tag{3.67}$$

Where $\overline{B}(\rho)$ is the unperturbed magnetic field modulus, $k_{\perp c}$ is the correlation length and $\sigma_{B\perp}$ is the local relative level of magnetic fluctuations, which profile is assumed to have the same form of the density fluctuations [12]:

$$\sigma_{B_\perp}(\rho,\theta) = \left\langle\left(\frac{\widetilde{B}_\perp}{\overline{B}}\right)^2\right\rangle^{\frac{1}{2}} = \sigma_{B_\perp max}\cdot\exp\left[-\frac{1}{2}\frac{(\rho-\rho_0)^2}{(\Delta\rho/\sqrt{2\ln 2})^2}\right]\cdot\left(\frac{1+\lambda\cos\theta}{1+\lambda}\right) \tag{3.68}$$

The maximum relative level of magnetic fluctuations detected in toroidal devices is tipically between the 1% and the 0.01%, and from the experimental observations it has been extrapolated the following relation between the magnetic and density fluctuations relative levels [12, 7]:

$$\frac{\left\langle \widetilde{B}_{\perp}^{2} \right\rangle / \overline{B}^{2}}{\left\langle \widetilde{n}_{e}^{2} \right\rangle / \overline{n}_{e}^{2}} \approx 10^{-4} - 10^{-5} \tag{3.69}$$

The measurements show that the magnetic fluctuations can be more peaked in the plasma interior rather than at plasma edge [7]. In Fig.(3.11)/A), the $\sigma_{B_\perp}$ profiles independent by θ ($\lambda = 0$), peaked at $\rho = 0.6$, having maximum relative level $\sigma_{B_\perp max} = 0.3\%$ and different values of $\Delta\rho = 0.07, 0.14, 0.21$ are illustrated, while in Fig.(3.11)/B) the profiles corresponding to $\rho_0 = 0.6, \Delta\rho = 0.07, \lambda = 0$ with different maximum relative levels $\sigma_{B_\perp max} = 0.3\%, 0.2\%, 0.1\%, 0.03\%, 0.01\%$ are plotted. Since the $\sigma_{B_\perp}$ profile presents the same general analytical form of σ_{ne}, the effect of the poloidal dependence on the mean relative level of magnetic fluctuations is the same of the $\theta-$dependence on the mean relative level of density fluctuations, discussed in details in the previous subsection.

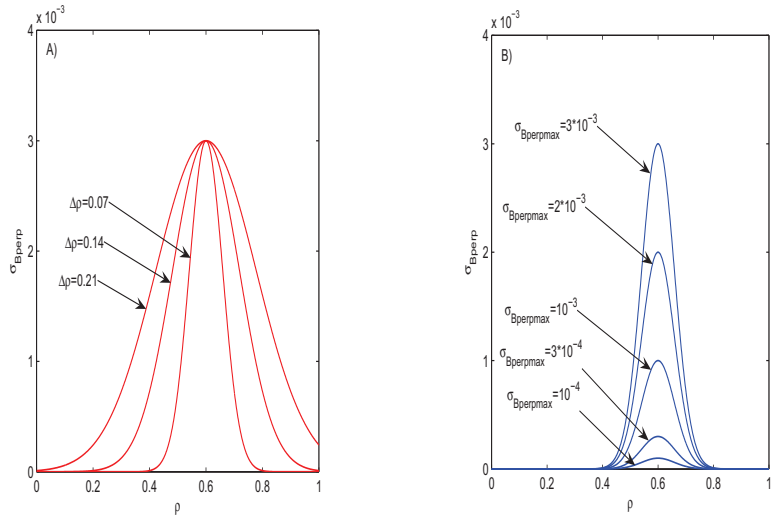

Figure 3.11: A):Comparison between $\sigma_{B_\perp}$ profiles independent by θ ($\lambda = 0$) peaked at the $\rho = 0.6$ with the same maximum relative level $\sigma_{B_\perp max} = 0.3\%$ and different values $\Delta\rho = 0.07, 0.14, 0.21$; B): Comparison between $\sigma_{B_\perp}$ profiles independent by θ ($\lambda = 0$) peaked at $\rho = 0.6$, with the same $\Delta\rho = 0.07$ but different maximum relative levels $\sigma_{B_\perp max} = 0.3\%, 0.2\%, 0.1\%, 0.03\%, 0.01\%$.

The components of magnetic field generated by the fluctuations, $\widetilde{B}_s$ and $\widetilde{B}_\phi$, can be derived in function of $\widetilde{B}_\perp$, given by the explicit expression (3.65).

Remembering that $\widetilde{B}_\rho = 0$ for construction, $\widetilde{\mathbf{B}}$ becomes:

$$\widetilde{\mathbf{B}} = \widetilde{B}_s \hat{\mathbf{s}} + \widetilde{B}_\phi \hat{\phi} \tag{3.70}$$

The components of the perturbation parallel and perpendicular to the equilibrium magnetic field lines are:

$$\widetilde{B}_\parallel = \widetilde{\mathbf{B}} \cdot \mathbf{b} = P\widetilde{B}_s + T\widetilde{B}_\phi \tag{3.71}$$

$$\widetilde{B}_\perp = \widetilde{\mathbf{B}} \cdot \mathbf{b}_\perp = T\widetilde{B}_s - P\widetilde{B}_\phi \tag{3.72}$$

Since $\widetilde{B}_\parallel = 0$, from these two equations the poloidal and the toroidal component of the perturbation can be derived only in function of $\widetilde{B}_\perp$:

$$\widetilde{B}_s = T\widetilde{B}_\perp \tag{3.73}$$

$$\widetilde{B}_\phi = -P\widetilde{B}_\perp \tag{3.74}$$

The component of the fluctuations magnetic field in the alternative coordinates system (r, θ, ϕ) can be evaluated in function of $\widetilde{B}_\perp$ and of the angle α between the versors $\hat{\rho}$ and $\hat{\mathbf{r}}$:

$$\widetilde{B}_r = \widetilde{B}_s \sin\alpha = T\widetilde{B}_\perp \sin\alpha \tag{3.75}$$

$$\widetilde{B}_\theta = \widetilde{B}_s \cos\alpha = T\widetilde{B}_\perp \cos\alpha \tag{3.76}$$

From these expressions it is possible to derive the components of $\widetilde{B}$ in the (R, Z, ϕ) system, which depend directly by the poloidal angle θ:

$$\widetilde{B}_R = \widetilde{B}_r \cos\theta - \widetilde{B}_\theta \sin\theta = -T\widetilde{B}_\perp \sin(\theta - \alpha) \tag{3.77}$$

$$\widetilde{B}_Z = \widetilde{B}_r \sin\theta + \widetilde{B}_\theta \cos\theta = T\widetilde{B}_\perp \cos(\theta - \alpha) \tag{3.78}$$

Starting by the expression for the generic perpendicular magnetic field perturbation (3.65) it is possible to describe locally each kind of magnetic fluctuations which lies on the flux surfaces by choosing the appropriated values for the parameters of the amplitude (3.67) and a sufficient number of oscillations corresponding to a set of $\widetilde{k}_\perp$. The components of the magnetic field generated by the fluctuations in all the three alternatives coordinates systems introduced in section 2.2 can be evaluated in function of $\widetilde{B}_\perp$, then once the perpendicular perturbation is defined, it is immediated to define the associated components in the considered coordinates system.

3.1.6 Statistical analysis

Electron density and magnetic field fluctuations processes introduced in this section present a stochastic nature, described by the random term of the phase both in non-local than in eikonal-like local approach. These stochastic aspects are investigated in the local approximation by means of a statistical analysis.

Since the time evolution of the fluctuations is very slow respect to the wave propagation and does not affect the ray evolution, only statistical behaviour in space is considered. The analysis is performed using as example of fluctuations the electron density perturbations in the eikonal-like representation (3.59), which phase is given by the expression (3.51), amplitude by the (3.61), and mean relative spatial profile by the (3.62). The local expression of the relative electronic density perturbation, $\widetilde{n}_e^r = \widetilde{n}_e/\overline{n}_e$, ignoring the temporal dependence of the phase, is:

$$\widetilde{n}_e^r(\rho,\theta,\phi) = \sum_{\widetilde{k}_\perp} \widetilde{n}^r_{e\widetilde{k}_\perp}(\rho,\theta,\phi) = \sum_{\widetilde{k}_\perp} \widetilde{n}^{0r}_{e\widetilde{k}_\perp}(\rho,\theta)\cos\Phi_{\widetilde{k}_\perp}(\rho,\theta,\phi) \tag{3.79}$$

Where the relative amplitude of the oscillation corresponding to a given $\widetilde{k}_\perp$ is:

$$\widetilde{n}^{0r}_{e\widetilde{k}_\perp}(\rho,\theta) = \sigma_{ne}(\rho,\theta)\cdot\left(\frac{2}{\pi}\right)^{\frac{1}{4}}\cdot\sqrt{\frac{\Delta\widetilde{k}_\perp}{k_{\perp c}}}\cdot\exp\left(-\frac{\widetilde{k}_\perp^2}{4k_{\perp c}^2}\right) \tag{3.80}$$

An expression for the toroidal angle in function of θ is derived from the relation (3.18) for the ratio between $d\phi$ and $d\theta$:

$$\phi(\theta) = -\frac{P}{T}\frac{r\theta}{R\cos\alpha} \tag{3.81}$$

Using the (3.81), the phase $\Phi_{\widetilde{k}_\perp}$ and then also the perturbation can be expressed only in fuction of ρ and θ:

$$\widetilde{n}_e^r(\rho,\theta) = \sum_{\widetilde{k}_\perp} \widetilde{n}^r_{e\widetilde{k}_\perp}(\rho,\theta) = \sum_{\widetilde{k}_\perp} \widetilde{n}^{0r}_{e\widetilde{k}_\perp}(\rho,\theta)\cos\Phi_{\widetilde{k}_\perp}(\rho,\theta) \tag{3.82}$$

This expression makes it possible to study the fluctuations spectrum in function of the poloidal angle θ on a given flux surface corresponding to a determined value of ρ, and to evaluate the statistical distribution of the perturbations process $f(\widetilde{n}_e^r) = f(\widetilde{n}_e/\overline{n}_e)$ on the same surface. Assuming $\rho = const$, the perturbation is given by a sum of a large number of cosinusoidal oscillations dependent by the poloidal angle. Each one of these presents mean value zero (because it is cosinusoidal) and random contribution to the phase $\widetilde{\varphi}_{\widetilde{k}_\perp}$ independent by the others. The total perturbation can be treated as the sum of a large number of statistical variables having mean value zero and distribution independent by the others, for the central limit theorem, the distribution $f(\widetilde{n}_e^r) = f(\widetilde{n}_e/\overline{n}_e)$ of the relative fluctuations amplitude on a given flux surface corresponding to $\rho = const$ must be a gaussian (Maxwellian) with mean value zero (because the mean values of each single oscillation is zero):

$$f\left(\widetilde{n}_e^r\right) = \frac{1}{\sqrt{2\pi}\sigma_{ne}}\exp\left(\frac{(\widetilde{n}_e^r)^2}{2\sigma_{ne}^2}\right) \tag{3.83}$$

Where the variance $\mathrm{Var}\,(\widetilde{n}_e^r)$ is given by the mean square local relative level of density fluctuations σ_{ne}^2:

$$\mathrm{Var}\,(\widetilde{n}_e^r) = \mathrm{Var}\left(\frac{\widetilde{n}_e}{\overline{n}_e}\right) = \left\langle \left(\frac{\widetilde{n}_e}{\overline{n}_e} - \left\langle \frac{\widetilde{n}_e}{\overline{n}_e} \right\rangle\right)^2 \right\rangle = \left\langle \left(\frac{\widetilde{n}_e}{\overline{n}_e}\right)^2 \right\rangle = \sigma_{ne}^2 \qquad (3.84)$$

The spectrum of the relative density perturbations on a given flux surface is now studied in function of the angle θ, and the theoretical distribution (3.83) is compared with the numerical distribution evaluated creating an histogram of the fluctuations process corresponding to each set of parameters.
The fluctuations process (3.82) is evaluated numerically as the sum of a number N of oscillations, each one corresponding to a different value of $\widetilde{k}_\perp$ ($N = N_{\widetilde{k}_\perp}$), and having a different random term of the phase $\widetilde{\varphi}_{\widetilde{k}_\perp}$. An uniform grid of $\widetilde{k}_\perp$ values centered in $\widetilde{k}_\perp = 0$ is generated, and the maximum absolute value $|\widetilde{k}_{\perp max}|$, satisfying the relation $-|\widetilde{k}_{\perp max}| \leq \widetilde{k}_\perp \leq |\widetilde{k}_{\perp max}|$, is chosen in relation to the correlation perpendicular wave vector $k_{\perp c}$ and to the minimum relative oscillation amplitude n_{prec} considered for the numerical interpolation, which is performed with a technique based on the Fourier series expansion. For $\widetilde{k}_\perp = \widetilde{k}_{\perp max}$ the amplitude of the oscillation is equal to the minimum considered for the Fourier expansion:

$$\exp\left(-\frac{\widetilde{k}_{\perp max}^2}{k_{\perp c}^2}\right) = n_{prec} \qquad (3.85)$$

From this relation, remembering that $k_{\perp c}$ is positive, the following expression is derived:

$$|\widetilde{k}_{\perp max}| = \pm 2k_{\perp c}\sqrt{-\ln(n_{prec})} \qquad (3.86)$$

Then the fluctuations perpendicular wave vector values are taken in the interval:

$$-2k_{\perp c}\sqrt{-\ln(n_{prec})} \leq \widetilde{k}_\perp \leq +2k_{\perp c}\sqrt{-\ln(n_{prec})} \qquad (3.87)$$

The correlation wave vector $k_{\perp c}$ is assumed to be a constant parameter tipical of the fluctuations process, and since the grid is uniform, also the normalization interval $\Delta\widetilde{k}_\perp$ present in the expression (3.80) is constant and it is given by the difference between two consecutive values of $\widetilde{k}_\perp$ in the grid:

$$\Delta\widetilde{k}_\perp = |\widetilde{k}_{\perp j+1} - \widetilde{k}_{\perp j}| \qquad (3.88)$$

In the analysis here reported the minimum relative amplitude considered for the Fourier expansion is fixed at a value $n_{prec} = 10^{-2}$; the spectrum and the fluctuations distribution are studied varying the correlation wave vector $k_{\perp c}$, the number of $\widetilde{k}_\perp$ assumed for generating the grid and the poloidal dependence parameter λ of the relative level spatial profile. A numerical equilibrium calculated with the 2-D Grad-Shafranov solver HELENA [30] is considered, and parameters of the Tore Supra tokamak are used:

- plasma minor radius $a_p = 0.8\text{m}$;
- plasma major radius $R_p = 2.46\text{m}$;
- on-axis magnetic field $B_{T0} = 3.9\text{T}$;
- unperturbed electron density at the plasma edge: $\overline{n}_{ea} = 0.05 \cdot 10^{19}\text{m}^{-3}$;
- unperturbed electron density at the plasma core: $\overline{n}_{e0} = 3 \cdot 10^{19}\text{m}^{-3}$;

A spatial profile of the relative fluctuations level σ_{ne} peaked at the plasma edge ($\rho_0 = 1$), independent by the poloidal angle ($\lambda = 0$), with maximum relative fluctuations level $\sigma_{nemax} = 30\%$ and semi-amplitude parameter $\Delta\rho = 0.07$ is initially assumed. This profile, introduced in the ref.[12], is reported in Fig.(3.12).

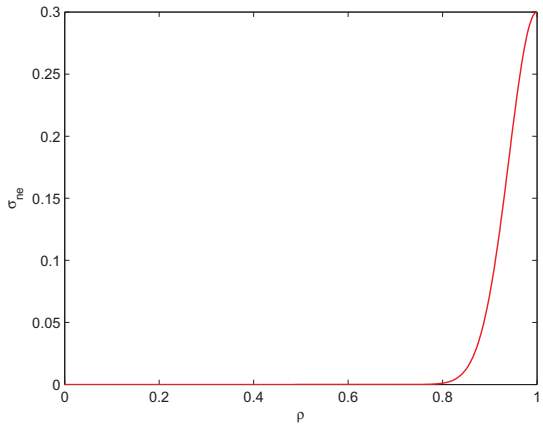

Figure 3.12: σ_{ne} profile used in the statistical analysis: it is independent by the poloidal angle θ ($\lambda = 0$) and peaked at the plasma edge ($\rho_0 = 1$). The maximum relative level of fluctuations is $\sigma_{nemax} = 30\%$ and semi-amplitude parameter is $\Delta\rho = 0.07$

In Fig.(3.13)/A) the spectrum of a density fluctuations process having the σ_{ne} profile shown in Fig.(3.12) is reported in function of the poloidal angle θ: the perturbation is calculated on the flux surface corresponding to $\rho = 1 = \rho_0$, at the plasma edge, where the relative level is maximum, and the normalized correlation wave vector is assumed to be $a_p k_{\perp c} = 300$, corresponding to $k_{\perp c} \simeq 375\text{m}^{-1}$ and to a correlation length $\lambda_{\perp c} \simeq 2 \cdot 10^{-2}\text{m}$ for Tore Supra parameters (in tokamak devices it has been detected $10^{-2}\text{m} \leq \lambda_{\perp c} \leq 10^{-3}\text{m}$ [12]). This perturbation is generated using a number $N_{\widetilde{k}_\perp} = 600$ of $\widetilde{k}_\perp$ and then it is given by the sum of $N = 600$ corresponding oscillations. Since the relative fluctuations level profile is independent by the poloidal angle, the amplitude of this perturbation is independent by θ. The distribution function $f(\widetilde{n}_e/\overline{n}_e)$ on

the flux surface $\rho = 1$ is calculated numerically evaluating the histogram of the perturbation, and it is reported in in Fig.(3.13)/B) (blue line). The numerical distribution is compared with the 1-D gaussian distribution (3.83), reported in the figure (red line), and a good agreement is found. It has been shown both numerically than theoretically that the distribution of relative density fluctuations on a given flux surface is gaussian, this means that the density fluctuations induced by drift waves and in general all the drift-like fluctuations , using the expressions (3.51) for the phase and (3.56) for the amplitude, are represented in the local limit as gaussian stochastic processes. In Fig.(3.14)/A) the spectrums of the same fluctuations process illustrated in Fig.(3.13) calculated on different flux surfaces corresponding to $\rho = \rho_0, \rho_0 + \Delta\rho, \rho_0 + 2\Delta\rho$ are compared. As it can be observed, the perturbations amplitude varies from a flux surface to another, because it depends by the spatial profile σ_{ne}, and obviously it is maximum at $\rho = \rho_0$, where $\sigma_{ne} = \sigma_{nemax}$, while it is halved at $\rho = \rho_0 + \Delta\rho$ and it becomes close to zero at $\rho = \rho_0 + 2\Delta\rho$. Even if the perturbations amplitude changes with ρ, the density fluctuations distribution function on each flux surface remains gaussian, as it is shown in Fig.(3.14)/B). In Fig.(3.15) the effects of the variation of the normalized correlation wave vector $ak_{\perp c}$ on the perturbations spectrum are illustrated: in the figure are reported the spectrums of normalized fluctuations processes $\widetilde{n}_e/\overline{n}_e$ having the relative level spatial profile of Fig.(3.12), calculated on the most extern flux surface corresponding to $\rho = \rho_0 = 1$ using $N_{\widetilde{k}_\perp} = 600$ and considering different values of $a_p k_{\perp c} = 600, 100, 50, 10$. The numerical and theoretical distribution functions corresponding to these fluctuations processes calculated at $\rho = \rho_0$ are reported in Fig.(3.16). As it can be observed in figures, for great values of the normalized correlation wave vector (for example $a_p k_{\perp c} = 600$ reported in Fig.(3.15)/A) or $a_p k_{\perp c} = 300$ reported in Fig.(3.13)/A)), corresponding to small values of the correlation length, the normalized perturbation $\widetilde{n}_e/\overline{n}_e$ varies in function of θ very rapidly such that its values calculated for $0 \leq \theta \leq 2\pi$ represents a good statistical ensemble for evaluating the histogram of the frequencies and estimating the numerical distribution of the process. Infact, as it is shown in Fig.(3.16)/A) and B), for great values of $a_p k_{\perp c}$, the numerical distribution is in good agreement with the theoretical 1-dimensional gaussian distribution. For small values of $a_p k_{\perp c}$, corresponding to great correlation lengths, the perturbation varies more slowly in function of θ and its values calculated for $0 \leq \theta \leq 2\pi$ do not represent a good statistical ensemble: in the Fig.(3.15)/C) and D)), are shown the spectrums corresponding to $a_p k_{\perp c} = 50$ and $a_p k_{\perp c} = 10$, and it can be observed that for these small values of the correlation wave vector the spectrum varies slowly respect to the cases with high $a_p k_{\perp c}$ and becomes essentially a deterministic function. The corresponding numerical distribution functions are no more in good agreement with the 1-D gaussian distribution predicted by the theory. The value $a_p k_{\perp c} = 100$ has been individuated as minimum value to have a gaussian numerical distribution of the process $\widetilde{n}_e/\overline{n}_e$ generated with $N_{\widetilde{k}_\perp} = 600$ in good agreement with the the-

oretical distribution. The spectrums and the numerical distribution functions corresponding to the different values of the normalized correlation wave vector are compared in Fig.(3.17).
The effect of the variation of the number of $\widetilde{k}_\perp$ used in the generation of the fluctuations process is also analized: perturbations with the reference spatial profile of Fig.(3.12) are generated assuming $a_p k_{\perp c} = 300$ and different values of $N_{\widetilde{k}_\perp} = 400, 200, 100, 50$. The spectrums and the distribution functions of these fluctuations calculated on the flux surface $\rho = \rho_0$ are reported in Figs.(3.18) and (3.19). In Fig.(3.18) it is shown that as the number of oscillations used in the generation of the fluctuations decreases, the amplitude of the perturbation presents a modulation in θ. The perturbations created with few number of oscillations, ($N_{\widetilde{k}_\perp} \leq 10$) may become quasiperiodic (not periodic, because the local approximation imples a lack of periodicity). Consequently for processes resulting from the sum of a number of oscillations minor than 100, the numerical distribution function is no more in good agreement with the theoretical one (see Fig.(3.19)/C) and D)).
Finally the fluctuations spectrum and distribution function on a given flux surface are studied varying the poloidal dependence parameter λ of the relative spatial profile σ_{ne}. In Fig.(3.20) the effects of λ variations on the fluctuations spectrum is illustrated: perturbations having a σ_{ne} profile peaked at the plasma edge with $\Delta\rho = 0.07$ and $\lambda = 0.8, 0.3, -0.1, -0.3$, and generated using $N_{\widetilde{k}_\perp} = 600$ with $a_p k_{\perp c} = 300$ are plotted at $\rho = \rho_0$. From this figure it is easy to note that the poloidal dependence of σ_{ne} influences only the amplitude of the perturbation, generating an amplification dependent by θ for $\lambda < 0$ and an attenuation for $\lambda < 0$. This poloidal dependence of the amplitude is summed to the poloidal dependence of the phase which determines the frequency of the oscillations, and it is not accounted in the 1-D gaussian theoretical distribution function, such that the numerical distribution, even it is still gaussian and centered in zero, possesses a different maximum value, major than the theoretical function for $\lambda < 0$, and minor for $\lambda > 0$ (see Fig.3.21).
The statistical characteristics of electronic density fluctuations on a given flux surface and their variations in function of the correlation wave vector, of the number of $\widetilde{k}_\perp$ considered and of the poloidal dependence of σ_{ne} have been studied in the local approximation, the results can be generalized to magnetic field fluctuations, because the expression for the pertubation $\widetilde{B}_\perp$ in the local limit is identical to that for $\widetilde{n}_e$, and consequently the statistical properties of the two processes are the same, the only differences are represented by the values of the $\sigma_{B_\perp}$ profiles assumed for describing magnetic fluctuations according to the experimental observations and by the vectorial nature of these fluctuations: the total perturbation $\widetilde{B}$ is infact the sum of three components, $\widetilde{B}_R, \widetilde{B}_Z$ and $\widetilde{B}_\phi$.

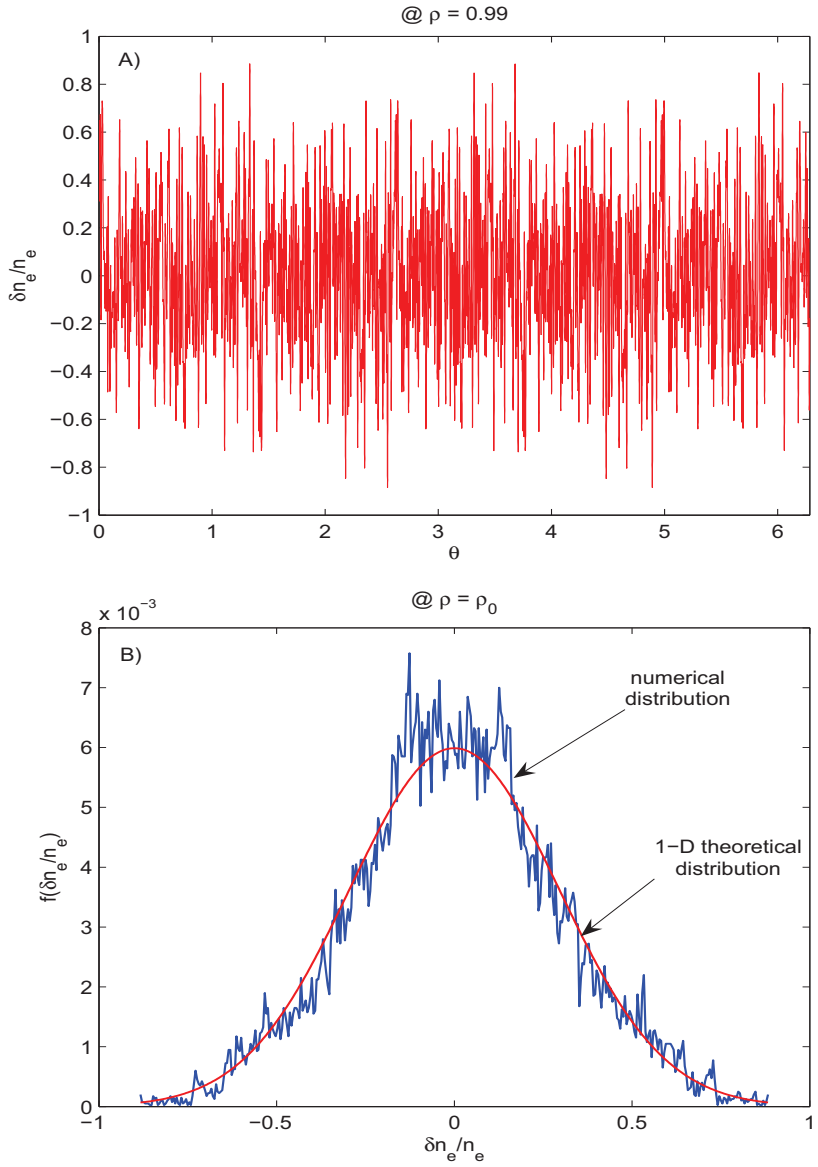

Figure 3.13: A): Spectrum of the perturbation having the spatial profile illustrated in Fig.(3.12) plotted in function of θ on the most extern flux surface $\rho = \rho_0 = 1$, the perturbation is generated by the sum of $N = N_{\tilde{k}_\perp} = 600$ oscillations with $a_p k_{\perp c} = 300$; B): Comparison between the numerical distribution and the 1-D theoretical distribution of the density fluctuations process correspondent to the σ_{ne} profile of Fig.(3.12) and to $N_{\tilde{k}_\perp} = 600$ and $a_p k_{\perp c} = 300$, calculated also at $\rho = \rho_0 = 1$.

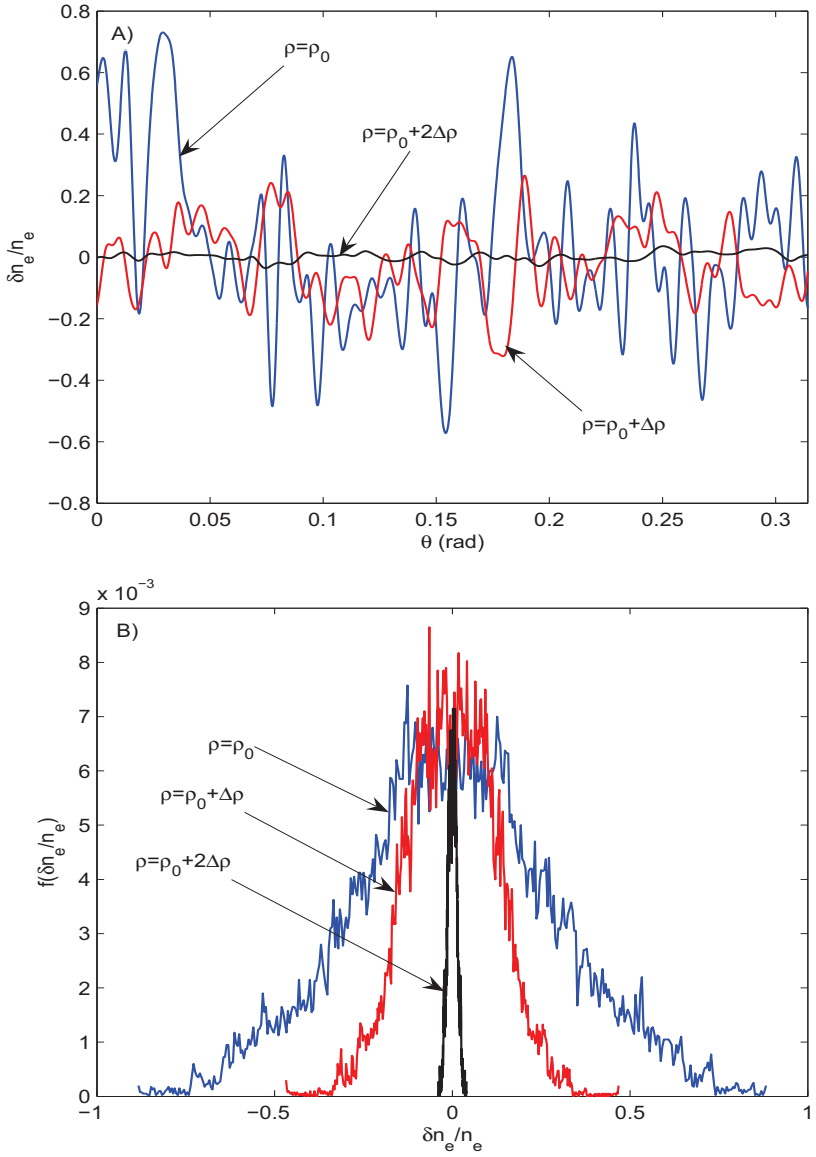

Figure 3.14: A): Spectrum of the perturbation having the spatial profile illustrated in Fig.(3.12) calculated on the flux surfaces $\rho = \rho_0$ (blu line), $\rho_0 + \Delta\rho$ (red line), $\rho_0 + 2\Delta\rho$ (black line), the perturbations are generated by the sum of $N = N_{\tilde{k}_\perp} = 600$ oscillations with $a_p k_{\perp c} = 300$; B): Numerical distributions of the normalzed density fluctuations process correspondent to the σ_{ne} profile of Fig.(3.12) calculated on the flux surfaces $\rho = \rho_0$ (blu line), $\rho_0 + \Delta\rho$ (red line) and $\rho_0 + 2\Delta\rho$ (black line) with $N_{\tilde{k}_\perp} = 600$ and $a_p k_{\perp c} = 300$.

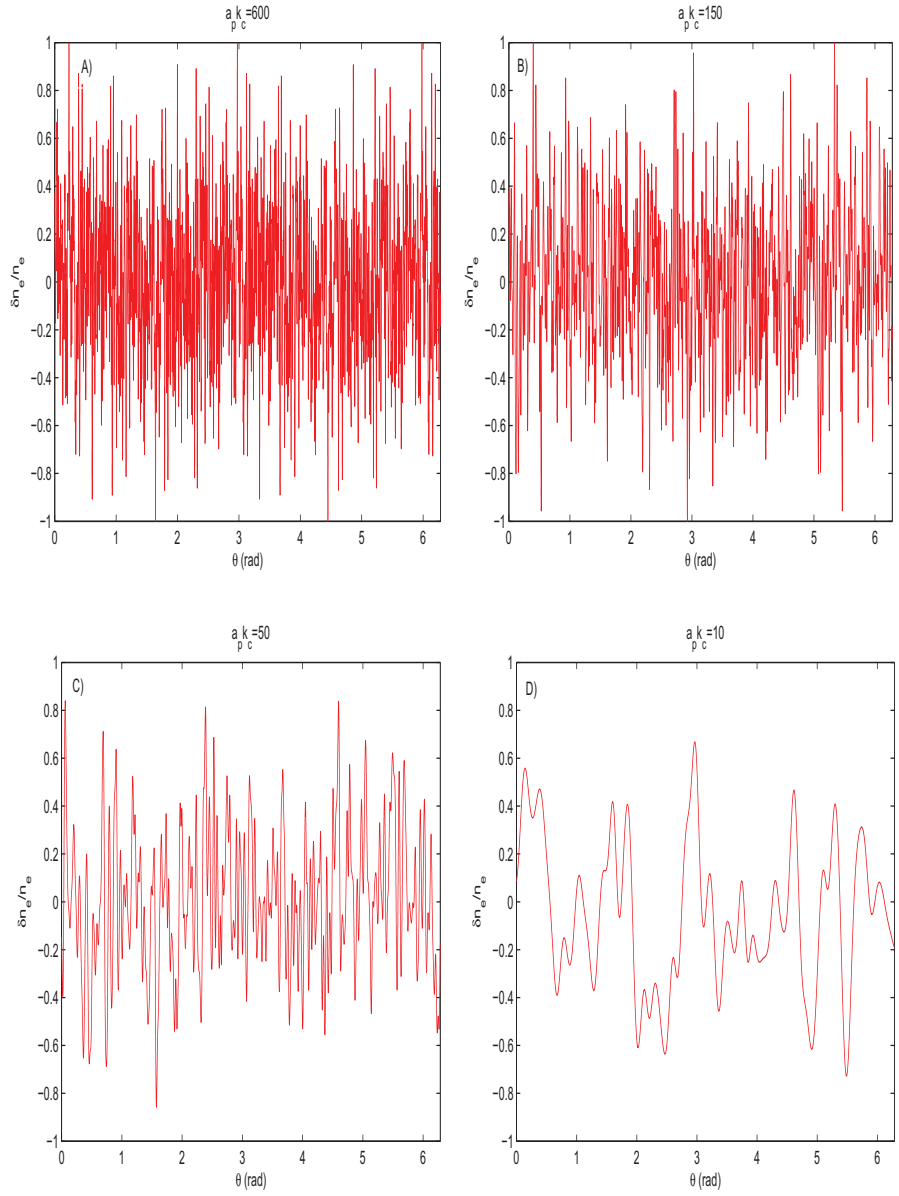

Figure 3.15: Spectrum of the perturbation having the spatial profile illustrated in Fig.(3.12) calculated at $\rho = \rho_0$ with $N_{\tilde{k}_\perp} = 600$ for: A) $a_p k_{\perp c} = 600$, B) $a_p k_{\perp c} = 150$, C) $a_p k_{\perp c} = 50$, D) $a_p k_{\perp c} = 10$;

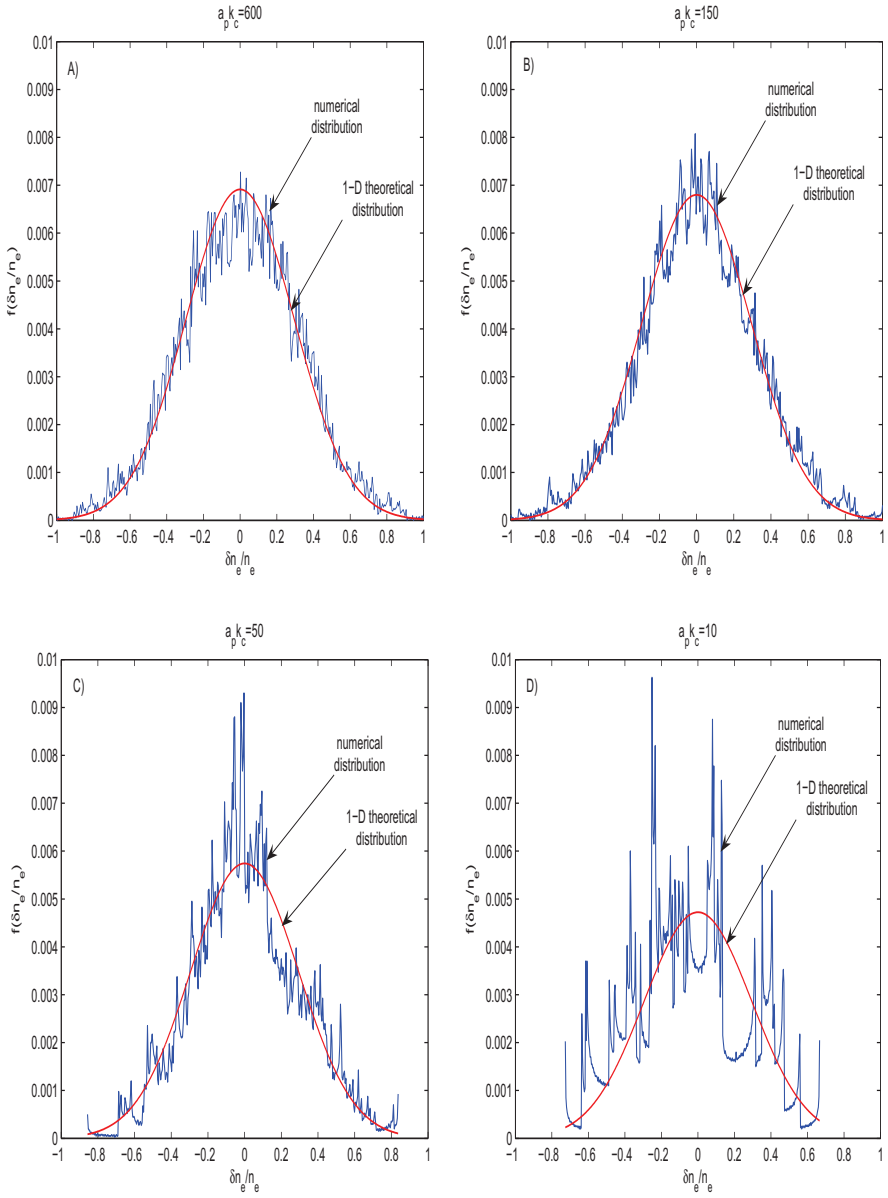

Figure 3.16: Numerical (blu lines) and theoretical (red lines) distribution of the normalized fluctuations process having the spatial profile illustrated in Fig.(3.12) calculated at $\rho = \rho_0$ with $N_{\widetilde{k}_\perp} = 600$ for: A) $a_p k_{\perp c} = 600$, B) $a_p k_{\perp c} = 150$, C) $a_p k_{\perp c} = 50$, D) $a_p k_{\perp c} = 10$;

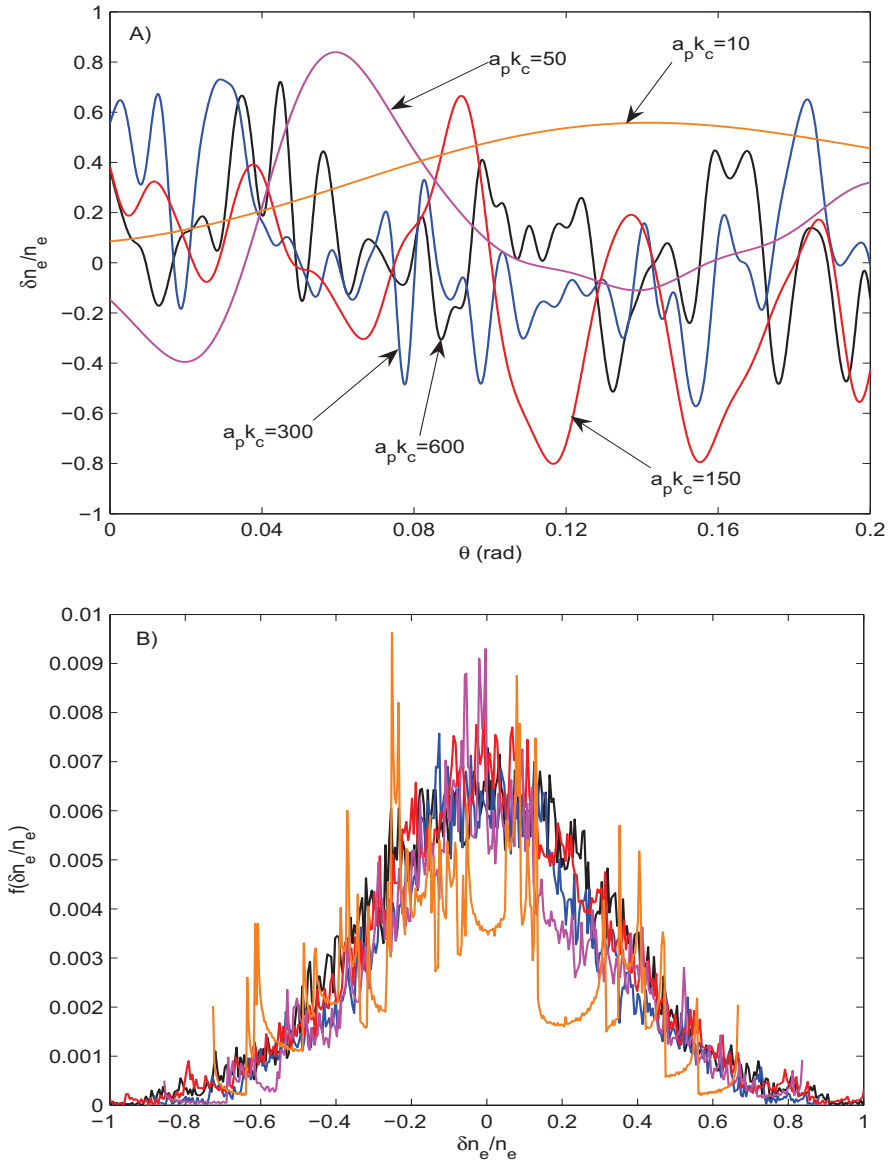

Figure 3.17: A): Comparison between perturbations spectrum having the spatial profile illustrated in Fig.(3.12) calculated at $\rho = \rho_0$ with $N_{\tilde{k}_\perp} = 600$ using different values of the normalized correlation wave vector $ak_c = 600, 300, 150, 50, 10$; B) Comparison between numerical distributions of fluctuations process having the spatial profile illustrated in Fig.(3.12) calculated at $\rho = \rho_0$ with $N_{\tilde{k}_\perp} = 600$ using different values of the normalized correlation wave vector $a_p k_c = 600, 300, 150, 50, 10$, the colors corresponding to each value are the same of A).

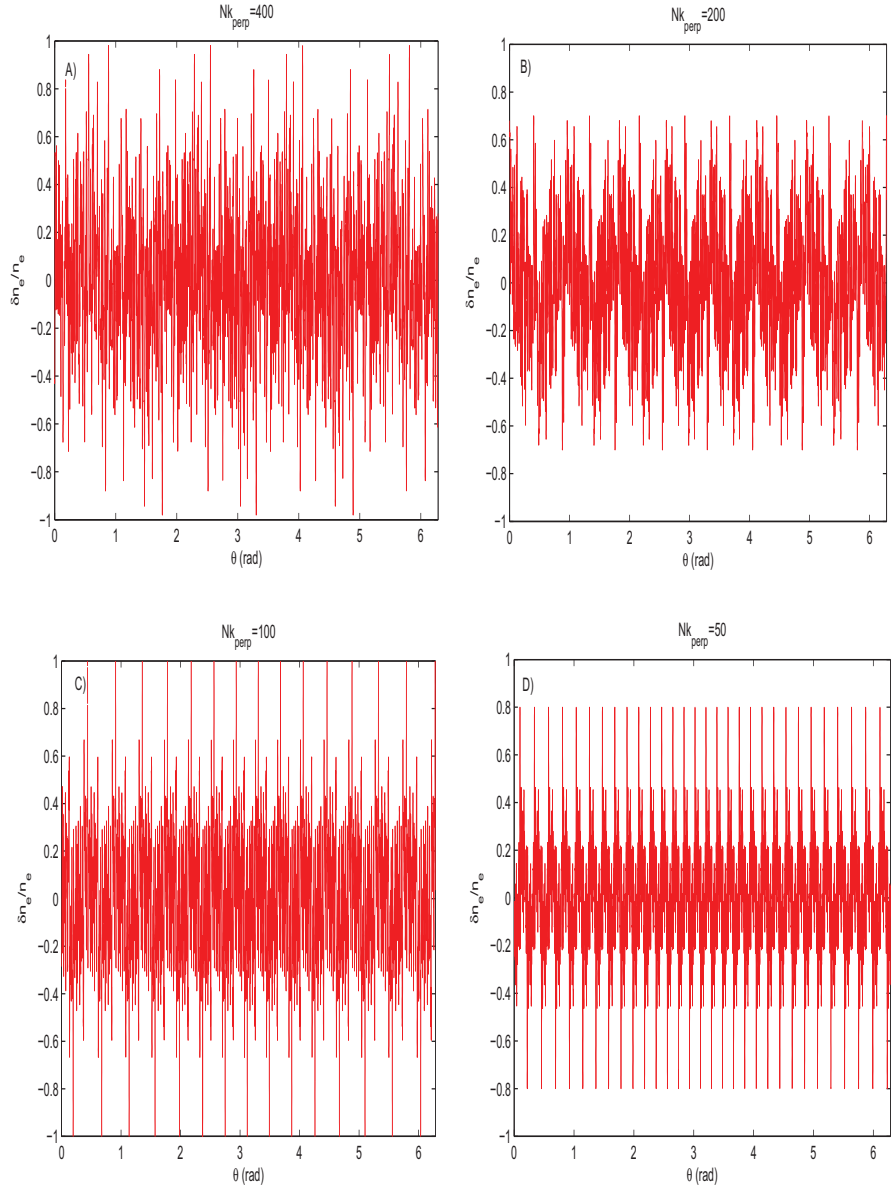

Figure 3.18: Spectrum of the perturbation having the spatial profile illustrated in Fig.(3.12) calculated at $\rho = \rho_0$ with $a_p k_c = 300$ using several numbers of $\widetilde{k}_\perp$: A) $N_{\widetilde{k}_\perp} = 400$, B) $N_{\widetilde{k}_\perp} = 200$, C) $N_{\widetilde{k}_\perp} = 100$, D) $N_{\widetilde{k}_\perp} = 50$;

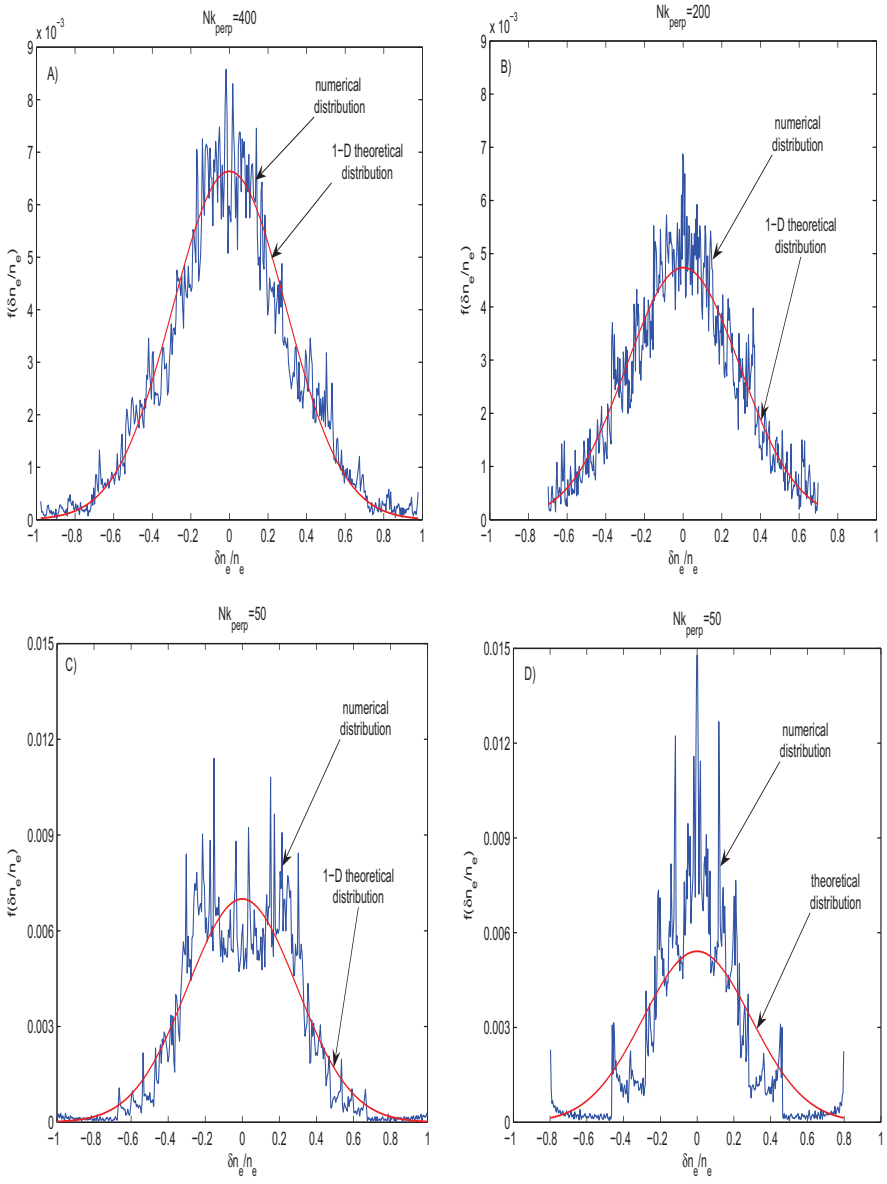

Figure 3.19: Numerical (blu lines) and theoretical (red lines) distribution of the normalized fluctuations process having the spatial profile illustrated in Fig.(3.12) calculated at $\rho = \rho_0$ with $a_p k_c = 300$ using several numbers of $\widetilde{k}_\perp$: A) $N_{\widetilde{k}_\perp} = 400$, B) $N_{\widetilde{k}_\perp} = 200$, C) $N_{\widetilde{k}_\perp} = 100$, D) $N_{\widetilde{k}_\perp} = 50$;

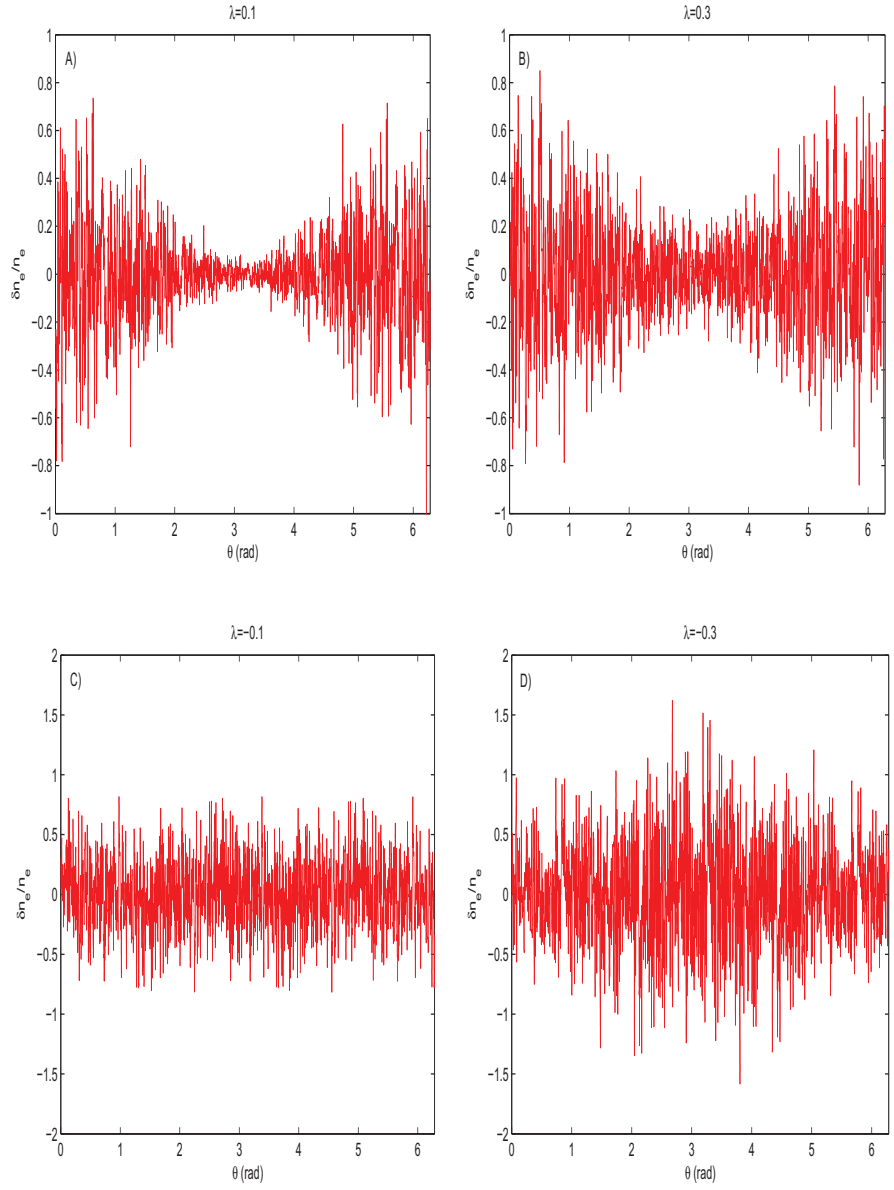

Figure 3.20: Spectrum of a perturbation having σ_{ne} profile with $\rho_0 = 1$ and $\Delta\rho = 0.07$ calculated at $\rho = \rho_0$ using $a_p k_{\perp c} = 300$, $N_{\tilde{k}_\perp} = 600$ and considering different values of the poloidal dependence parameter: A) $\lambda = 0.8$, B) $\lambda = 0.3$, C) $\lambda = -0.1$, D) $\lambda = -0.3$;

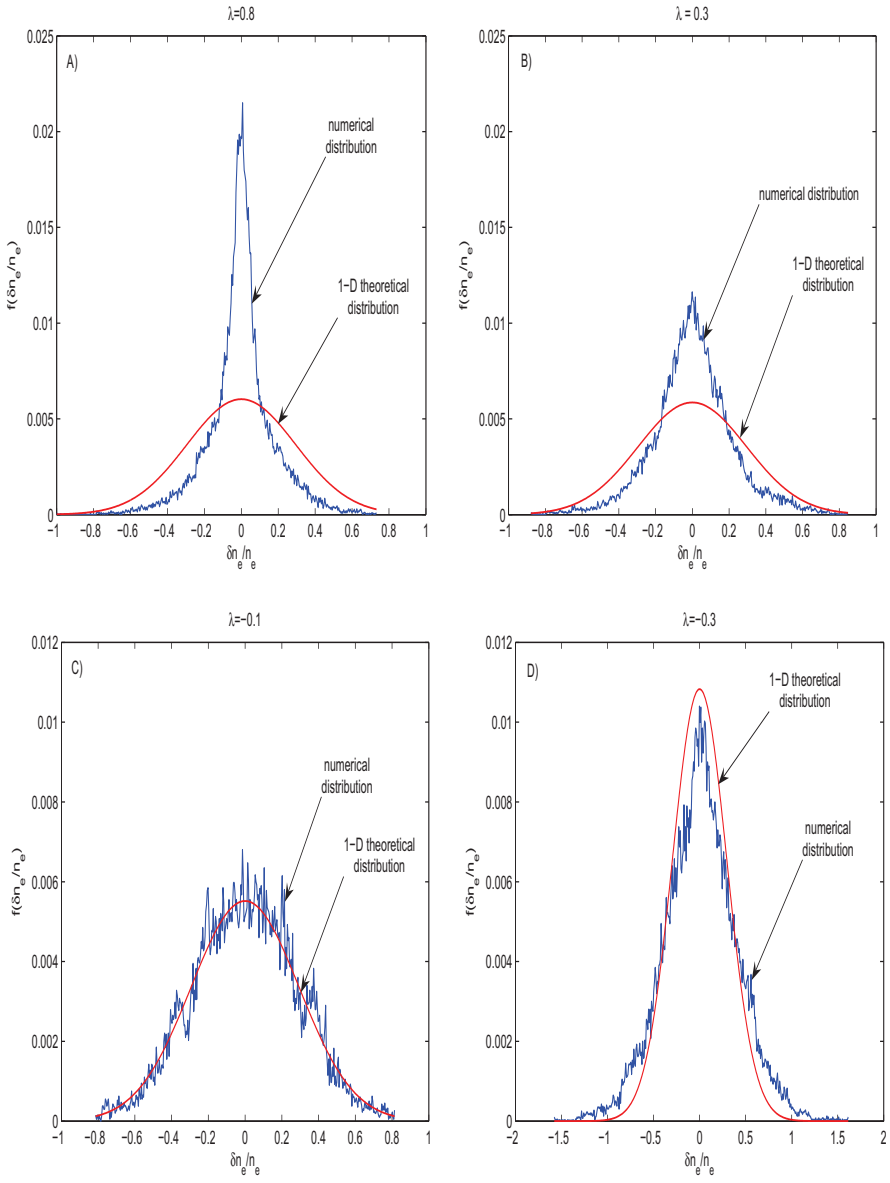

Figure 3.21: Numerical (blu lines) and theoretical (red lines) distribution of a normalized fluctuations process having σ_{ne} profile with $\rho_0 = 1$ and $\Delta\rho = 0.07$ calculated at $\rho = \rho_0$ using $a_p k_{\perp c} = 300$, $N_{\tilde{k}_\perp} = 600$ and considering different values of the poloidal dependence parameter: A) $\lambda = 0.8$, B) $\lambda = 0.3$, C) $\lambda = -0.1$, D) $\lambda = -0.3$;

3.2 Magnetic ripple

In tokamak devices, the toroidal magnetic field is generated by a discrete set of N magnetic coils which wind the torus. The discrete structure of the magnetic system leads to a static modulation of the toroidal field and to a lack of toroidal symmetry which can affect strongly the radial transport [31] and the propagation and the absorption of radio frequency waves into the plasma [32]. This static magnetic field perturbation can be easily described specializing the general expression (2.18) to a case with stationary non random phase related to the number of coils N and amplitude dependent by the geometrical properties of the windings.

3.2.1 Magnetic field ripple in tokamaks

The discreteness of the magnetic coils systems generates a static periodic perturbation of the equilibrium magnetic field, the total field is then:

$$\mathbf{B} = \overline{\mathbf{B}} + \widetilde{\mathbf{B}} \tag{3.89}$$

Where $\overline{\mathbf{B}}$ is the unperturbed field and $\widetilde{\mathbf{B}}$ is the contribution due to the ripple. The perturbation in toroidal direction is generated by the discrete number of windings N, which is constant, consequently the toroidal component of the ripple field is given by the sum of a set of harmonic stationary oscillations having radial mode number $\widetilde{k}_\rho = 0$, poloidal mode number $\widetilde{m} = 0$ and toroidal mode numbers $\widetilde{n} = Nl$ multiples of the number of coils. Specializing the general expression (2.17) to this case, and assuming $\Phi_0 = 0$, the phase of the perturbation becomes:

$$\Phi_l = \Phi_l^G = Nl\phi \tag{3.90}$$

And the toroidal field generated to the perturbation is:

$$\widetilde{B}_\phi(\rho, \theta, \phi) = \sum_l \widetilde{B}^0_{\phi l}(\rho, \theta) \cos(Nl\phi) \tag{3.91}$$

The amplitude of this field is given by the following expression [31]:

$$\widetilde{B}^0_{\phi l} = \overline{B}_\phi(\rho, \theta)\delta_l(\rho, \theta) \tag{3.92}$$

Where $\overline{B}_\phi \equiv B_T$ is the unperturbed toroidal magnetic field and $\delta_l(\rho, \theta)$ is the l-order term of the perturbative expansion of the ripple depth $\delta(\rho, \theta)$, which is defined by the following ratio:

$$\delta(\rho, \theta) = \frac{B_{max} - B_{min}}{B_{max} + B_{min}} \tag{3.93}$$

Where B_{max} is the maximum magnetic field and B_{min} is the minimum at given ρ and θ. Since the magnetic field, accounting the ripple perturbation, depends also by the toroidal angle ϕ, at a given poloidal position its value oscillates

in function of this angle, B_{max} and B_{min} are respectively its maximum and its minimum. The ripple depth depends by the geometrical properties of the coils, and it is in general calculated numerically, in the case of circular coils it is possible to evaluate an analitical expression by solving the equation $\widetilde{\mathbf{B}} = \nabla\widetilde{F}$ with the condition $\nabla^2\widetilde{F} = 0$, satisfied by a static magnetic field in the vacuum, where $\widetilde{F}$ is the perturbed magnetic potential. This procedure is illustrated in details in ref.[31] and the expression for $\delta(\rho,\theta)$ derived, valid for tokamaks with circular magnetic bobine like Tore Supra, is introduced in the next section. In the system (r,θ,ϕ), the radial and poloidal components of the magnetic perturbation are:

$$\widetilde{B}_r(\rho,\theta,\phi) = \sum_l \widetilde{B}^0_{rl}(\rho,\theta)\sin(Nl\phi) = \sum_l \overline{B}_\phi(\rho,\theta)\delta_{rl}(\rho,\theta)\sin(Nl\phi) \tag{3.94}$$

$$\widetilde{B}_\theta(\rho,\theta,\phi) = \sum_l \widetilde{B}^0_{\theta l}(\rho,\theta)\sin(Nl\phi) = \sum_l \overline{B}_\phi(\rho,\theta)\delta_{\theta l}(\rho,\theta)\sin(Nl\phi) \tag{3.95}$$

Where:

$$\widetilde{B}^0_{rl} = \overline{B}_\phi(\rho,\theta)\delta_{rl} \qquad \widetilde{B}^0_{\theta l} = \overline{B}_\phi(\rho,\theta)\delta_{\theta l} \tag{3.96}$$

For coils of arbitrary shape, δ_{rl} and $\delta_{\theta l}$ are determined numerically, but in the circular case they can be expressed in term of the analytical profile of $\delta(\rho,\theta)$. The component $\widetilde{B}_\rho$ and $\widetilde{B}_s$ respectively perpendicular and tangent to the flux surfaces can be computed in function of $\widetilde{B}_r$, $\widetilde{B}_\theta$ and of the angle α between $\hat{\mathbf{r}}$ and $\hat{\rho}$:

$$\widetilde{B}_\rho(\rho,\theta,\phi) = \widetilde{B}_r(\rho,\theta,\phi)\cos\alpha - \widetilde{B}_\theta(\rho,\theta,\phi)\sin\alpha \tag{3.97}$$

$$\widetilde{B}_s(\rho,\theta,\phi) = \widetilde{B}_r(\rho,\theta,\phi)\sin\alpha + \widetilde{B}_\theta(\rho,\theta,\phi)\cos\alpha \tag{3.98}$$

The ripple magnetic field, as we can observe by these expressions, presents a component $\widetilde{B}_\rho$ orthogonal to the flux surfaces, this implies that the equilibrium flux surfaces are modified by the ripple modulation. This is a fundamental difference between the ripple perturbations and the random drift-like magnetic field fluctuations illustrated in the previous section, which present $\widetilde{k}_\rho = 0$ and $\widetilde{B}_\rho = 0$ and then do not affect the surfaces of constant ψ. The radial component of the perturbation leads to a shift of the poloidal section of the flux surfaces, but the shape is conserved and the perturbed equilibrium, as the unperturbed, presents a nested surfaces structure, the only difference is in the values of ψ correspondent to the surfaces. The perturbed flux surfaces must satisfy the relation [25]:

$$\nabla\psi\cdot\mathbf{B} = 0 \tag{3.99}$$

Then the radial flux coordinates, dependent only by ψ, satisfies:

$$\nabla\rho\cdot\mathbf{B} = 0 \tag{3.100}$$

Including the deviation from the unperturbed equilibrium, ρ is given by:

$$\rho(\overline{\rho},\theta,\phi) = \overline{\rho} + \widetilde{\rho}(\overline{\rho},\theta,\phi) \tag{3.101}$$

The relation (3.100), remembering that $\nabla\overline{\rho}\cdot\overline{\mathbf{B}}=0$, becomes:

$$\nabla\overline{\rho}\cdot\widetilde{\mathbf{B}}+\nabla\widetilde{\rho}\cdot\overline{\mathbf{B}}=0 \tag{3.102}$$

Where the small second order term $\nabla\widetilde{\rho}\cdot\widetilde{\mathbf{B}}$ is neglected. Using the explicit form for the magnetic field and the gradient operator in the (ρ,θ,ϕ) system of coordinates:

$$\widetilde{B}_\rho\,\|\nabla\rho\|+\left(\widetilde{B}_s\,\|\nabla\rho\|+\frac{\overline{B}_s}{r}\frac{\partial\widetilde{\rho}}{\partial\theta}\right)\cos\alpha+\frac{\overline{B}_\phi}{R}\frac{\partial\widetilde{\rho}}{\partial\phi}=0 \tag{3.103}$$

The solution of this general equation gives the correction to the radial flux coordinate calculated consistently with the definition of magnetic equilibrium, for the case with circular coils it is possible to evaluate an analytical approximated expression [32].

3.2.2 Circular magnetic field coils

As just anticipated, in the case of circular coils it is possible to evaluate an analytical expression for the ripple depth (3.104). This expression is derived by the perturbative solution of the equation $\widetilde{\mathbf{B}}=\nabla\widetilde{F}$ with the condition $\nabla^2\widetilde{F}=0$, satisfied by a static magnetic field in the vacuum, where $\widetilde{F}$ is the perturbed magnetic potential, illustrated in details in ref.[31]. The calculations are performed using the toroidal coordinate system (r,θ,ϕ), particularly suitable for describing the circular simmetry of the windings, the flux coordinate $\rho=\rho(r,\theta,\phi)$ can be easily expressed in function of these variables. If the toroidal ripple field is generated by a set of uniformly distributed identical coils, only the lowest harmonic correspondent to $l=1$ gives an important contribution to the perturbation, [31, 32], as a consequence $\delta\approx\delta_1$. The circular simmetry makes it possible to evaluate the iso-ripple poloidal contours, where the vale of δ is constant, these contours are circle of radius $a(r,\theta)$ which centers are located at a distance L from the center of the coils, and the expression for the ripple depth is:

$$\delta(r,\theta)\approx\delta_1(r,\theta)=\delta_n I_0\left(\frac{a}{R_0-L_0}N\right) \tag{3.104}$$

Where δ_n is a parameter depending by the geometry. I_0 is the 0-order modified Bessel function of first kind, R_0 is the tokamak vacuum major radius, L_0 is $L(a=0)$, N is the number of coils. The expressions for the iso-ripple radius a and for the shift L, in good approximation, are:

$$a^2 = L^2+r^2+2rL\cos\theta \tag{3.105}$$

$$L = L_0-\frac{1}{2}\frac{a^2}{R_0-L_0} \tag{3.106}$$

From these relations it is possible to derive an expression for the iso-ripple contours radius in function of the coordinates (r, θ):

$$\begin{aligned} a(r,\theta) &= \left[2(R_0 - L_0)\left((R_0 + r\cos\theta) - \sqrt{(R_0 + r\cos\theta)^2 - r^2 - L_0^2 - 2rL_0\cos\theta}\right)\right]^{\frac{1}{2}} \\ &\approx [(r^2 + L_0^2 + 2rL_0)(R_0 - L_0)/(R_0 + r\cos\theta)] \end{aligned} \tag{3.107}$$

Approximated expressions for δ_n and L_0 are derived from the condition $\delta = 1$ and $L = 0$ for $a = (r_n + r_x)/2$, where r_n is the inner and r_x is the outer radius of the toroidal windings:

$$L_0 \approx \frac{(r_n + r_x)^2}{8R_0}; \qquad \delta_n \approx \left[I_0\left(\frac{N}{2}\frac{r_n + r_x}{R_0 - L_0}\right)\right]^{-1}; \tag{3.108}$$

Remembering the asymptotic expression of the modified Bessel function of first kind, the ripple depth varies following the law:

$$\delta \propto \exp\left(\frac{a}{R_0 - L_0}N\right) \tag{3.109}$$

From this relation it is easy to deduce that only the lowest harmonic gives a non negligible contribution to the ripple field: the higher harmonics contributions, are associated with the exponents $aNl/(R_0 - L_0)$ with $l > 1$, for tokamak parameters, $aNl/(R_0 - L_0) >> 1$, such that correspondent terms fall off with the distance from the coils center much faster than the first harmonic contribution.
Injecting the expression (3.104) into the (3.91) and (3.92), and considering only the first harmonic, the following expression for the toroidal ripple field is derived:

$$\widetilde{B}_\phi(r,\theta,\phi) = \overline{B}_\phi\delta(r,\theta)\cos(N\phi) = \overline{B}_\phi\delta_n I_0\left(\frac{a}{R_0 - L_0}N\right)\cos(N\phi) \tag{3.110}$$

The expressions for $\delta_r(r,\theta)$ and $\delta_\theta(r,\theta)$ in the limit of circular coils are [31]:

$$\delta_r(r,\theta) = \delta_n\frac{r + L_0\cos\theta}{a}I_1\left(\frac{a}{R_0 - L_0}N\right) \tag{3.111}$$

$$\delta_\theta(r,\theta) = \frac{L_0\sin\theta}{a}I_1\left(\frac{a}{R_0 - L_0}N\right) \tag{3.112}$$

Using these expressions, the poloidal and the radial components of the perturbation become:

$$\widetilde{B}_r(r,\theta,\phi) = \overline{B}_\phi\delta_n\frac{r + L_0\cos\theta}{a}I_1\left(\frac{a}{R_0 - L_0}N\right)\sin(N\phi) \tag{3.113}$$

$$\widetilde{B}_\theta(r,\theta,\phi) = \overline{B}_\phi\delta_n\frac{L_0\sin\theta}{a}I_1\left(\frac{a}{R_0 - L_0}N\right)\sin(N\phi) \tag{3.114}$$

Where I_1 is the 1-order Bessel modified function of first kind. The explicit expressions for the components of the ripple magnetic field illustrated are valid for all tokamaks which present a number N of identical circular coils uniformly distributed around the toroidal chamber (an example is Tore Supra), by means of the coordinates trasformations, from $\widetilde{B}_r$ and $\widetilde{B}_\theta$ it is possible to derive $\widetilde{B}_\rho$ and $\widetilde{B}_s$, which are the components of the perturbation respectively orthogonal and parallel to the flux surfaces:

$$\widetilde{B}_\rho = \widetilde{B}^0_\rho \sin(N\phi) \tag{3.115}$$
$$\widetilde{B}_s = \widetilde{B}^0_s \sin(N\phi) \tag{3.116}$$

Where the amplitudes are:

$$\widetilde{B}^0_\rho = \overline{B}_\phi(\delta_r \cos\alpha - \delta_\theta \sin\alpha) \tag{3.117}$$
$$\widetilde{B}^0_s = \overline{B}_\phi(\delta_r \sin\alpha + \delta_\theta \cos\alpha) \tag{3.118}$$

Also the cartesian components $\widetilde{B}_R$ and $\widetilde{B}_Z$ can be expressed in the form:

$$\widetilde{B}_R = \widetilde{B}^0_R \sin(N\phi) \tag{3.119}$$
$$\widetilde{B}_Z = \widetilde{B}^0_Z \sin(N\phi) \tag{3.120}$$

Where:

$$\widetilde{B}^0_R = \overline{B}_\phi(\delta_r \cos\theta - \delta_\theta \sin\theta) \tag{3.121}$$
$$\widetilde{B}^0_Z = \overline{B}_\phi(\delta_r \sin\theta + \delta_\theta \cos\theta) \tag{3.122}$$

In this section have been reported the explicit expressions for the components of the ripple magnetic perturbation generated by a set of circular coils in all the three alternative coordinates systems introduced in section 2.2, in the next chapter the effects of this perturbation on ray trajectories will be discussed presenting the results of some examples with parameters typical of a JET-like scenario.

Chapter 4

Current drive simulations in presence of fluctuations

The general model for decribing the effects of the fluctuations on radiofrequency current drive presented in the previous chapters is applied in some examples of lower hybrid and electron cyclotron current drive simulations. The two kinds of magnetic equilibrium perturbations considered are the same discussed in details in chapter 2: drift-like density and magnetic field fluctuations and magnetic ripple. In the first section the cold plasma dispersion model, used in the study of LH and EC waves propagation, is introduced. The fundamental characteristics of lower hybrid and electron cyclotron waves are illustrated in sections 4.2 and 4.3. In section 4.4 the effects of drift-like fluctuations and magnetic ripple on lower hybrid ray trajectories are studied using a simple analytical equilibrium with parameters typical of JET tokamak (JET-like plasma [21, 23]) introduced just to test the perturbations effort on the propagation. In the last two sections some examples of Lower Hybrid and Electron Cyclotron current drive simulations in presence of fluctuations in ITER tokamak scenarios are illustrated.

4.1 Cold plasma dispersion model

The conditions for the applicability of the cold plasma limit are [17]:

$$\frac{k_\perp^2 v_{T\alpha}^2}{\omega_{c\alpha}^2} \ll 1 \tag{4.1}$$

$$\left| \frac{\omega - n\omega_{c\alpha}}{k_\parallel v_{T\alpha}} \right|^2 \gg 1 \tag{4.2}$$

Where $k_\perp$ and $k_\parallel$ are the component of the wave vector perpendicular and parallel to the magnetic field, $v_{T\alpha}$ and $\omega_{c\alpha}$ are the thermal velocity and the cyclotronic frequency of the species, ω is the rf wave frequency and n the

harmonic number. The relation (4.1) implies that the perpendicular wavelength $\lambda_\perp = 2\pi/k_\perp$ must be much larger than the thermal Larmor radius $\rho_{T\alpha} = v_{T\alpha}/\omega_{c\alpha}$. Since $\rho_{T\alpha}$ is the measure of the space explorated by the thermal motion of a particle which at a given instant t is situated on a magnetic field line, this condition implies that in the cold plasma limit the spatial dispersion can be neglected in direction perpendicular to the magnetic field. The relation (4.2) for $n = 0$ states that the parallel phase velocity of the wave $v_{f\|} = \omega/k_\|$ must be much larger than the thermal velocity of species, while for $n \geq 1$ it is satisfied far from the cyclotron resonances. When (4.2) holds, the number of particles in resonance with the wave is small, as a consequence the exchange of energy between the wave and the particles is negligible. In substance, the two conditions of validity of the cold plasma limit imply that spatial dispersion and dissipation through the resonant particles are negligible, then the cold plasma approximation does not decribe the damping on the resonant particles, and it is appropriate only to study the rf wave propagation.

4.1.1 Dielectric tensor

Since the spatial dispersion is neglected, the cold plasma susceptibility tensor $\mathbb{X}_{\mathbf{k},\omega}$ and dielectric tensor $\mathbb{K}_{\mathbf{k},\omega}$ are only functions of the frequency, $\mathbb{X}^C_{\mathbf{k},\omega} \equiv \mathbb{X}(\omega)$ and $\mathbb{K}^C_{\mathbf{k},\omega} \equiv \mathbb{K}(\omega)$, independent by $\mathbf{k}$. The dielectric tensor presents an hermitian form, because the antihermitian part $\mathbb{K}^A_{\mathbf{k},\omega}$, associated to the damping on resonant particles, can be ignored [17, 18]. The elements of $\mathbb{K}(\omega)$ can be easily evaluated by the solution of the linearized particle motion equation [18], or calculating the limit for $T_\alpha \to 0$ of the general hot plasma dielectric tensor derived by the integration of the linearized Vlasov equation introduced in chapter 1 [17]. Assuming a coordinates system (x, y, z) with the static magnetic field $\mathbf{B}_0$ directed along the z-axis (Fig.(4.1)), $\mathbb{K}$ becomes:

$$\mathbb{K}(\omega) = \begin{pmatrix} K_\perp(\omega) & -iK_\times(\omega) & 0 \\ iK_\times(\omega) & K_\perp(\omega) & 0 \\ 0 & 0 & K_\|(\omega) \end{pmatrix} \tag{4.3}$$

The explicit expressions for the components are:

$$\begin{aligned} K_\perp(\omega) &= 1 - \sum_\alpha \frac{\omega^2_{p\alpha}}{\omega^2 - \omega^2_{c\alpha}} = 1 - \sum_\alpha \frac{\overline{\omega}^2_{p\alpha}}{1 - \overline{\omega}^2_{c\alpha}} \\ K_\|(\omega) &= 1 - \sum_\alpha \frac{\omega^2_{p\alpha}}{\omega^2} = 1 - \sum_\alpha \overline{\omega}^2_{p\alpha} \\ K_\times(\omega) &= -\sum_\alpha \frac{\omega^2_{p\alpha}\omega_{c\alpha}}{\omega(\omega^2 - \omega^2_{c\alpha})} = -\sum_\alpha \frac{\overline{\omega}^2_{p\alpha}\overline{\omega}_{c\alpha}}{1 - \overline{\omega}^2_{c\alpha}} \end{aligned} \tag{4.4}$$

Where $\overline{\omega}_{p\alpha} = \omega_{p\alpha}/\omega$ and $\overline{\omega}_{c\alpha} = \omega_{c\alpha}/\omega$ are respectively the normalized plasma and cyclotronic frequencies introduced in the previous chapter. The cold

plasma permittivity tensor can be easily derived by the relation:

$$\mathbb{X}(\omega) = \mathbb{I} + \mathbb{K}(\omega) \tag{4.5}$$

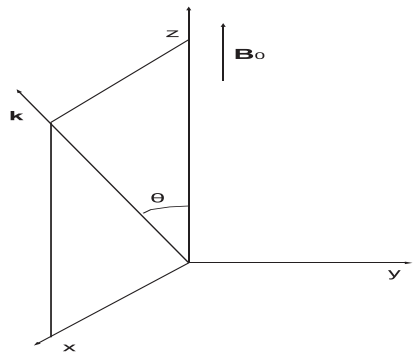

Figure 4.1: System of coordinates (x, y, z) used for the dielectric tensor $\mathbb{K}$ and for the dispersion tensor $\mathbb{D}$.

4.1.2 Dispersion relation

Assuming that the wave vector lies on the $x - z$ plane (see Fig.(4.1)), in the cold plasma limit, the dispersion tensor $\mathbb{D}^C_{\mathbf{k},\omega} \equiv \mathbb{D}(N^2, \vartheta, \omega)$ is given by the hermitian matrix:

$$\mathbb{D}(N^2, \vartheta, \omega) = \begin{pmatrix} K_\perp(\omega) - N^2\cos^2\vartheta & -iK_\times(\omega) & N^2\sin\vartheta\cos\vartheta \\ iK_\times(\omega) & K_\perp(\omega) - N^2 & 0 \\ N^2\sin\vartheta\cos\vartheta & 0 & K_\parallel(\omega) - N^2\sin^2\vartheta \end{pmatrix} \tag{4.6}$$

Where $N = ck/\omega$ is the refractive index. The corresponding dispersion relation is a quadratic equation in N^2:

$$\mathcal{D}(N^2, \vartheta, \omega) = \det\mathbb{D}(N^2, \vartheta, \omega) = A(\omega, \vartheta)N^4 + B(\omega, \vartheta)N^2 + C(\omega) = 0 \tag{4.7}$$

Where:

$$A(\omega, \vartheta) = K_\perp \sin^2\vartheta + K_\parallel \cos^2\vartheta \tag{4.8}$$

$$B(\omega, \vartheta) = (K_\times^2 - K_\perp^2)\sin^2\vartheta - K_\parallel K_\perp(1 + \cos^2\vartheta) \tag{4.9}$$

$$C(\omega) = K_\parallel(K_\perp^2 - K_\times^2) \tag{4.10}$$

Taking the parallel component $N_\parallel$ and the frequency ω as given, and considering $N_\perp$ as the dependent variable, the dispersion relation becomes:

$$A'(\omega)N_\perp^4 + B'(\omega, N_\parallel)N_\perp^2 + C(\omega, N_\parallel) = 0 \tag{4.11}$$

With:

$$A'(\omega) = K_\perp \tag{4.12}$$
$$B'(\omega, N_\parallel) = (N_\parallel^2 - K_\perp)(K_\perp + K_\parallel) + K_\times^2 \tag{4.13}$$
$$C'(\omega, N_\parallel) = K_\parallel[(N_\parallel^2 - K_\perp) - K_\times^2] \tag{4.14}$$

Or in alternative:

$$A'(\omega) = K_\perp \tag{4.15}$$
$$B'(\omega, N_\parallel) = (K_\perp + K_\parallel)N_\parallel^2 - (K_R K_L + K_\perp K_\parallel) \tag{4.16}$$
$$C'(\omega, N_\parallel) = K_\parallel(N_\parallel^2 - K_R)(N_\parallel^2 - K_L) \tag{4.17}$$

Where K_R and K_L are:

$$K_R = K_\perp + K_\times \tag{4.18}$$
$$K_L = K_\perp - K_\times \tag{4.19}$$

The solution of the dispersion relation (4.11) gives $N_\perp^2$ in function of $N_\parallel^2$ and ω:

$$N_\perp^2 = \frac{-B' \pm \sqrt{B'^2 - 4A'C'}}{2A'} \tag{4.20}$$

From these expression it is immediate to see that the wave cut-off, where $N_\perp^2 = 0$, occurs for $C' = 0$, this condition can be satisfied for:

$$K_R = N_\parallel^2 \tag{4.21}$$
$$K_L = N_\parallel^2 \tag{4.22}$$
$$K_\parallel = 0 \tag{4.23}$$

The resonances, where $N_\perp^2 \to \infty$, instead occur for $A' = 0$, which implies:

$$K_\perp = 0 \tag{4.24}$$

4.1.3 Electrostatic approximation

In the electrostatic approximation, the component of the waves electric field trasversal to the refractive index $\mathbf{N}$ is considered negligible, and $\widetilde{\mathbf{E}}$ is assumed to have only a longitudinal component, in practice it is parallel to the wave vector, $\widetilde{\mathbf{E}} = \widetilde{E}\hat{\mathbf{k}}$. In order to find the conditions for the validity of this approximation and to derive the dispersion relation in the electrostatic limit, the waves electric field in the Fourier space, $\widetilde{\mathbf{E}}_{\mathbf{k},\omega}$, is separated into its longitudinal and transverse components with respect to $\mathbf{N}$:

$$\widetilde{\mathbf{E}}_{\mathbf{k},\omega} = \widetilde{\mathbf{E}}^l_{\mathbf{k},\omega} + \widetilde{\mathbf{E}}^t_{\mathbf{k},\omega} \tag{4.25}$$

Introducing this representation, the wave equation presented in first chapter becomes:

$$(N^2 - \mathbb{K}_{\mathbf{k},\omega})\widetilde{\mathbf{E}}^t_{\mathbf{k},\omega} - \mathbb{K}_{\mathbf{k},\omega} \cdot \widetilde{\mathbf{E}}^l_{\mathbf{k},\omega} = 0 \tag{4.26}$$

The transverse component is negligible with respect to the longitudinal when:

$$N^2 \gg |\mathbb{K}_{ij}| \tag{4.27}$$

Where $\mathbb{K}_{ij}$ are the elements of the dielectric tensor $K_{\mathbf{k},\omega}$. If this condition is satisfied, the (4.26) can be reduced to:

$$N^2 \widetilde{\mathbf{E}}^t_{\mathbf{k},\omega} - \mathbb{K}_{\mathbf{k},\omega} \cdot \widetilde{\mathbf{E}}^l_{\mathbf{k},\omega} \simeq 0 \tag{4.28}$$

Then the transverse electric field is given by:

$$\widetilde{\mathbf{E}}^t_{\mathbf{k},\omega} = \frac{1}{N^2} \mathbb{K}_{\mathbf{k},\omega} \cdot \widetilde{\mathbf{E}}^l_{\mathbf{k},\omega} \tag{4.29}$$

The (4.27) and the (4.29) imply that $\widetilde{E}^t_{\mathbf{k},\omega} \ll \widetilde{E}^g_{\mathbf{k},\omega}$, then the electric field direction is quasi-longitudinal and the assumption $\widetilde{\mathbf{E}} = \widetilde{E}\hat{\mathbf{k}}$ is justified. Dot-multiplying by $\mathbf{N}/N$ the expression (4.28), the dispersion relation in the electrostatic limit is derived:

$$\mathcal{D}^{ES} = \frac{\mathbf{N} \cdot \mathbb{K}_{\mathbf{k},\omega} \cdot \mathbf{N}}{N^2} = 0 \tag{4.30}$$

The electrostatic dispersion relation in a cold plasma is then:

$$\mathcal{D}^{ES} = N^2_\perp K_\perp + N^2_\parallel K_\parallel = 0 \tag{4.31}$$

The electrostatic limit is of physical relevance for several radiofrequency waves, as for example lower hybrid waves, which are quasi-electrostatic waves, and for great values of $N_\parallel$, the dispersion relation (4.31) is a good approximation of the full electromagnetic expression (4.11).

4.2 Lower Hybrid waves

In an electron-ion plasma, the lower hybrid range of frequencies satisfies the inequality (for tokamak plasmas the lower hybrid frequency typically belongs to the interval 500MHz $\ll \omega/2\pi \ll$ 8GHz):

$$\omega_{ci} \ll \omega \ll \omega_{ce} \tag{4.32}$$

Assuming also that:

$$\omega \ll \omega_{pe} \tag{4.33}$$

The components of the cold plasma dielectric tensor can be reduced to the following approximated expressions:

$$\begin{aligned} K_\perp &\simeq 1 + \frac{\omega^2_{pe}}{\omega^2_{ce}} - \frac{\omega^2_{pi}}{\omega^2} \\ K_\parallel &\simeq 1 - \frac{\omega^2_{pe}}{\omega^2} \\ K_\times &\simeq \frac{\omega^2_{pe}}{\omega|\omega_{ce}|} \end{aligned} \tag{4.34}$$

Where the component $K_\perp$ can be rewritten as:

$$\begin{aligned} K_\perp &= \left(1+\frac{\omega_{pe}^2}{\omega_{ce}^2}\right)\left(1-\frac{\omega_{pi}^2/\omega^2}{1+\omega_{pe}^2/\omega_{ce}^2}\right) \\ &= \left(1+\frac{\omega_{pe}^2}{\omega_{ce}^2}\right)\left(1-\frac{\omega_{LH}^2}{\omega^2}\right) \\ &= \frac{\omega_{pi}^2}{\omega^2}\left(\frac{\omega^2}{\omega_{LH}^2}-1\right) \end{aligned} \tag{4.35}$$

The lower hybrid frequency ω_{LH} is defined as:

$$\omega_{LH}^2 = \frac{\omega_{pi}^2}{1+\omega_{pe}^2/\omega_{ce}^2} \tag{4.36}$$

From the (4.35) it is easy to observe that when the wave frequency is equal to the lower hybrid frequency, $\omega = \omega_{LH}$, $K_\perp = 0$ and the resonance condition (4.24) is satisfied, then $N_\perp \to \infty$. Near the resonance, mode conversions occur, and the lower hybrid waves can be converted to ion Bernstein waves (IBW), which cannot be described by the cold plasma dispersion model. In oreder to avoid this mode conversion, in most lower hybrid current drive experiments the frequencies are taken higher than ω_{LH}, typically such that $\omega/\omega_{LH} \approx 2$ or 3. An important characteristic of lower hybrid waves consists in the fact that these modes are quasi-electrostatic, then the component of the electric field transverse with respect to the wavevector $\mathbf{k}$ is small compared to the longitudinal component ($\widetilde{E}^t_{\mathbf{k},\omega} \ll \widetilde{E}^g_{\mathbf{k},\omega}$), and for great values of $N_\parallel$ the electrostatic description represents a good approximation of the electromagnetic case.

4.2.1 Accessibility condition

Lower hybrid waves must satisfy an accessibility condition to propagate far enough inside the plasma to reach the wave absorption layers without being reflected or converted into other modes. The electromagnetic dispersion relation (4.11) possesses two different solutions:

$$N_\perp^2 = \frac{-B' \pm \sqrt{B'^2 - 4A'C'}}{2A'} \tag{4.37}$$

The slow wave corresponds to the upper sign, while the fast wave corresponds to the lower sign (the term slow and fast are referred to the magnitude of the phase velocity component perpendicular to the magnetic field $v_{f\perp} = c/N_\perp$ [17]). When the discriminant $B'^2 - 4A'C'$ of the (4.37) is zero, the slow wave merges with the fast wave, and a linear mode conversion occurs. In order to avoid a mode conversion between the wave launching point and the wave absorption layer, the following accessibility criterion must be fulfilled [17, 18]:

$$N_\parallel > N_{\parallel acc} = \sqrt{1+\frac{\omega_{pe}^2}{\omega_{ce}^2}-\frac{\omega_{pi}^2}{\omega^2}} + \sqrt{\frac{\omega_{pe}^2}{\omega_{ce}^2}} \tag{4.38}$$

This condition is obtained from $B'^2 - 4A'C' = 0$ and using the approximated expressions for the components of the diectric tensor (4.34). This accessibility criterion depends on both the magnetic field and the density of the species, and represents a severe limitation of the lower hybrid waves penetration capability into the plasma: it is a lower limit on the parallel index of refraction and an upper limit on the parallel phase velocity of the wave which can reach the plasma core. In tokamak plasmas, the effects of the toroidal curvature and the magnetic field helicity lead to strong upshifts of the parallel index of refration $N_\parallel$ and then to strong downshifts of the parallel phase velocity, and the relation between the launched $N_\parallel$ spectrum and the lower hybrid waves penetration capability into the plasma core requires detailed calculations, performed, in general, by means of raytracing techniques [15].

4.2.2 Lower Hybrid Current Drive

Lower hybrid waves are absorbed by the resonant electrons and transfer energy and momentum to these particles by means of the parallel electron Landau damping [17]. The resonance condition corresponding to this process is derived specializing the general Doppler resonance condition (1.1) for harmonic number $n = 0$:

$$\omega - k_\parallel v_\parallel = 0 \tag{4.39}$$

This relation means that the wave is damped on the electrons having the parallel component of the velocity equal to its parallel phase velocity:

$$v_\parallel = v_{\parallel res} = \frac{\omega}{k_\parallel} \tag{4.40}$$

The energy and the momentum gained by the resonant electrons go entirely to the parallel degree of freedom, and the unidirectional change of the electron velocity generates an asymmetry in the distribution function, assumed to be initially Maxwellian, with resulting current flow. The steady state is given by the balance between the accelleration effects of the waves on the resonant electrons and the collisional relaxation which tends to re-establish the initial Maxwellian distribution [17, 33]. As a consequence, the steady state distribution function is the solution of the steady state version of the bounce-averaged kinetic equation (1.32), which neglecting the effects of the Ohmic electric field is reduced to the following expression:

$$\left\{C(\overline{f})\right\} + \left\{Q(\overline{f})\right\} = 0 \tag{4.41}$$

This equation is in practice a balance between the modification of $\overline{f}_0$ generated by the accelleration of the electrons for effects of the wave, described by the quasilinear operator $\left\{Q(\overline{f})\right\}$, and the collisional friction described by $\left\{C(\overline{f})\right\}$. Observing the (4.40), it is straightforward to deduce that for great values of $k_\parallel$ or alternatively of $N_\parallel$ the phase velocity becomes small and the wave is in resonance with slow electrons (with $v \approx v_{Te}$), while for small values of $k_\parallel$ the

wave is damped on the fast sovrathermal electrons. The slow electrons can be easily pushed by the increment of momentum in parallel direction due to the wave, but are more affected by the collisional friction and lose the gained energy for effects of the collisions more rapidly than sovrathermal electrons, for this reason lower hybrid waves are in general used to drive populations of fast electrons on which the collisional effets are small [17, 33]. The current drive local efficiency is defined as the ratio of the driven current density J and the power density deposited into the plasma for generating the current:

$$\eta_{CD} = \frac{J}{P} \tag{4.42}$$

Lower hybrid current drive experiments on fast electrons populations, using waves with high parallel phase velocity, have been realized in several tokamak devices with very high efficiency performances in agreement with the theoretical predictions [16, 34, 35], but the driven current and the deposited power relevated are orders of magnitude greater than the values expected by the theoretical models and which a very small population of resonant electrons implies [33, 35]. It seems that a fraction of the imposed low parallel refractive index spectrum $N_{\parallel}$ is upshifted into the plasma and the high parallel phase velocity values are downshifted, such that the waves become sufficiently slow to interact with a major number of electrons. Several physical explanations for this paradox have been proposed [36, 37], nevertheless an exaustive solution of the problem (the so-called spectral gap problem) has not been reached yet and the mechanisms responsible for filling the spectral gap has still not been individuated. This unsolved question makes very difficult the analysis and the physical interpretation of data from Lower hybrid current drive experiments.

4.3 Electron Cyclotron waves

The term electron cyclotron waves is in general referred to electromagnetic waves with a frequency in the range of the electron cyclotron frequency. For a given magnetic field the electron cyclotron frequency is $f_{ce} = 28B(\mathrm{T})\mathrm{GHz}$, then for $B = 4\mathrm{T}$, typical on-axis value in tokamak devices, it becomes $f_{ce} = 112\mathrm{GHz}$, in general electron cyclotron resonance heating and current drive systems work at frequencies of the order of 100GHz ($f_{EC} = 110\mathrm{GHz}$ in Tore Supra EC system). At frequencies of this order, the response of the ions to electromagnetic waves can be neglected because of their large inertia, and considering an electron-ion plasma, with an accuracy of order m_e/m_i, the

elements of the cold plasma dielectric tensor can be simplified to [17]:

$$\begin{aligned} K_\perp &\simeq 1 - \frac{\omega_{pe}^2}{\omega^2 - \omega_{ce}^2} \\ K_\parallel &\simeq 1 - \frac{\omega_{pe}^2}{\omega^2} \\ K_\times &\simeq -\frac{\omega_{pe}^2 \omega_{ce}}{\omega(\omega^2 - \omega_{ce}^2)} \end{aligned} \tag{4.43}$$

Since in electron cyclotron resonance heating and current drive experiments the wave are excited with small values of the parallel refractive index, $|N_\parallel| \ll 1$ (for example in Tore Supra experiments $N_{\parallel EC} \simeq 0.2$), the propagation is assumed to be perpendicular to magnetic field, and two different modes exist: the ordinary (O-mode) and the extraordinary (X-mode). This two modes are characterized by the wave polarization: the electric field induced by the O-mode is linearly polarized in direction parallel to the static magnetic field $\mathbf{B}_0$, while the electric field of the X-mode is mostly circularly right-hand polarized in a plane perpendicular to $\mathbf{B}_0$ [17, 18]. The O-mode can propagate only at frequencies higher than the cutoff $K_\parallel = 0$, which using the approximated expressions (4.43) corresponds to $\omega = \omega_{pe}$, then the O-mode has only a propagative branch for $\omega > \omega_{pe}$. On the contrary, the X-mode experiences cutoffs $K_R = N_\parallel^2$ and $K_L = N_\parallel^2$, and the upper hybrid resonance [17]. The R and L cutoff correspond to the frequencies:

$$\omega_{R,L} = \pm\frac{\omega_{pe}}{2} + \sqrt{\left(\frac{\omega_{ce}}{2}\right)^2 + \frac{\omega_{ce}^2}{1 - N_\parallel^2}} \tag{4.44}$$

The upper hybrid resonance frequency is:

$$\omega_{UH} = \sqrt{\omega_{ce}^2 + \omega_{pe}^2} \tag{4.45}$$

The X-mode presents two branches of propagation separated by an evanescent region: the first corresponds to frequencies $\omega > \omega_R$ (the so-called fast X-mode branch), the second to $\omega_L < \omega < \omega_{UH}$. For $\omega = \omega_{UH}$ a mode conversion occurs, and the electron cyclotron waves become electron Bernstein waves (EBW), electrostatic modes which propagation cannot be described using the cold plasma dispersion model.

4.3.1 Electron Cyclotron Current Drive

Electron cyclotron waves transfer energy to the resonant fast electrons satisfying the cyclotronic damping condition:

$$\omega - k_\parallel v_\parallel = \frac{\omega_{ce}}{\gamma} \tag{4.46}$$

The X-mode is circularly right-hand polarized in a plane perpendicular to $\mathbf{B}_0$, thus leads to a transfer of energy in direction perpendicular to the static magnetic field. The O-mode is linearly polarized in direction parallel to $\mathbf{B}_0$, but when the resonant electrons are accellerated by the electric field, the magnetic field induced by the same wave rotates the momentum vector in such a way that also in this case the net energy gain is finally oriented in perpendicular direction. In both cases, electron cyclotron waves absorption leads to an increase in the perpendicular energy of the resonant electrons, and there is no direct momentum transfer from these modes to the plasma. The parallel velocity of the resonant electrons is:

$$v_{\parallel} = v_{\parallel res} = \frac{\omega - \omega_{ce}/\gamma}{k_{\parallel}} \tag{4.47}$$

These electrons usually lose their parallel momentum $p_{\parallel} = \gamma v_{\parallel}$ on a time scale defined by the collision frequency, $\tau \sim \nu_c$, after the resonant interaction their perpendicular momentum increases and they become less collisional than the corresponding electrons with opposite parallel velocity $v_{\parallel} = -v_{\parallel res}$, therefore the resonant electrons collide less with the other plasma species and relax more slowly to $v_{\parallel} = 0$. The asymmetry in the electron collisionality generates and asymmetry in the parallel velocities electron distribution which leads to a steady state current [33, 38]. This mechanism makes possible to drive non-inductive current into the plasma without injecting parallel momentum by using electron cyclotron waves. Electron cyclotron current drive experiments (ECCD) are performed using also second order harmonic resonant interaction, corresponding to a Doppler resonance condition with harmonic number $n = 2$. It is important to note that the electron cyclotron frequency ω_{ce} is function of the space, this restricts power deposition to a region localized around the resonance surface corresponding to $\omega = \omega_{ce}$ for first harmonic excitation, and to $\omega = 2\omega_{ce}$ for second harmonic excitations. As a consequence, the resonant velocity $v_{\parallel res}$ has a continuum of values into the plasma, passing through zero at resonant surfaces, then resonant velocity and driven current are of opposite sign on either side of these surfaces, with resulting current cancellation. For this reason an efficient electron cyclotron current drive requires strongly asymmetric wave absorption about the resonant layer and in ECCD experiments waves launching positions and polarization are chosen such that most of the power is absorbed before reaching the exact cyclotron resonance. The precise spatial localization of the wave absorption around the surface $\omega = \omega_{ce}$ (or $\omega = 2\omega_{ce}$), primarily depending by the frequency and by the value of the static magnetic field [17], makes electron cyclotron current drive a particularly suitable task for controling the details of the current profiles in tokamaks in order to lower the confinement degradation caused by MHD instabilities [39](magnetic islands, sawteeth, neoclassical tearing modes, edge localized modes, etc.).

4.3.2 Accessibility of the electron cyclotron resonance

An important feature of electron cyclotron current drive and heating is the accesibility of the electron cyclotron resonance surface defined by $\omega = \omega_{ce}, 2\omega_{ce}$. The accessibility to the resonance layer for the O-mode is restricted only by the $K_\parallel = 0$ cutoff: when it occurs, $N_\perp = 0$, and the wave is reflected, and this cutoff condition defines a surface of constant density that is the separatrix between the domain of propagation of the wave and the evanescent region. The wave must be excited in such a way that the resonance surface is outside this region, which is individuated in the centre of the plasma, and which extension depends by the plasma characteristics [17]. For the X-mode at the first harmonic two evanescent regions are individuated: the first is between the $K_R = N_\parallel^2$ cutoff and the upper hybrid resonance surfaces individuated respectively by $\omega = \omega_R$ and by $\omega = \omega_{UH}$, the second is defined by the $K_L = N_\parallel^2$ cutoff. The first harmonic electron cyclotron resonance layer must be outside these two regions, while for second harmonic X-mode exists only an evanescent portion of the domain in the center of the plasma, delimited by $\omega = 2\omega_{pe}$ and the resonance layer can be reached as long as it is not inside this cutoff region.

4.4 Effects of equilibrium perturbations on rays trajectories

In this section the effects of the equilibrium perturbations generated by drift-like fluctuations and magnetic ripple on lower hybrid waves rays trajectories are illustrated. The simple analytical equilibrium with parameters tipical of JET tokamak introduced in ref.[21, 23] is assumed.

4.4.1 JET-like plasma

The equilibrium used for testing the perturbations effects on the trajectories presents circular and concentric flux surfaces, such that:

$$\rho = \frac{r}{a_p} \tag{4.48}$$

The unperturbed electronic density, electronic temperature and current density profiles are:

$$\overline{n}_e(\rho) = (\overline{n}_{e0} - \overline{n}_{ea})\left(1-\rho^2\right) + \overline{n}_{ea} \tag{4.49}$$

$$\overline{T}_e(\rho) = \overline{T}_{e0}\left(1-\rho^2\right)^\gamma + \overline{T}_{ea} \tag{4.50}$$

$$J(\rho) = J_0\left(1-\rho^2\right) \tag{4.51}$$

The total current is then:

$$I_P = 2\pi \int_0^{a_p} Jrdr = \pi J_0 \frac{a_p^2}{2} \tag{4.52}$$

Such that:

$$J_0 = \frac{2I_P}{\pi a_p^2} \tag{4.53}$$

The toroidal and poloidal component of the unperturbed magnetic field are respectively:

$$\overline{B}_T = \hat{B}_T \frac{R_p}{R} \tag{4.54}$$

$$\overline{B}_P = \hat{B}_P \frac{R_p}{R} \tag{4.55}$$

Where $\hat{B}_T = B_{T0}$ is the value of the magnetic field on axis and the expression for $\hat{B}_P$, derived from the Ampere's law in the small aspect ratio limit [21], is:

$$\hat{B}_P = \frac{\mu_0 I_P}{2\pi a_p} \frac{1}{\rho} \left[1 - \left(1-\rho^2\right)^2\right] \tag{4.56}$$

The poloidal flux coordinate is then:

$$\psi = R_p \int_0^\rho B_P d\rho = R_p \frac{\mu_0 I_P}{2\pi} \rho^2 \left(1 - \frac{1}{4}\rho^2\right) \tag{4.57}$$

The safety factor profile in the small aspect ratio limit can be easily derived:

$$q \simeq \frac{r}{R_p} \frac{B_T}{B_P} \simeq q_{max} \frac{\rho^2}{1-(1-\rho^2)^2} \tag{4.58}$$

Where:

$$q_{max} = \frac{\hat{B}_T}{\hat{B}_{Pa}} \frac{a_p}{R_p} \tag{4.59}$$

The parameters of the JET-like plasma used in the calculations of the perturbed trajectories are reported in table (4.1).

plasma minor radius a_p	0.95m
plasma major radius R_p	3.05m
on-axis magnetic field B_{T0}	3.2T
plasma current I_P	3.5MA
central electron density $\overline{n}_{e0}$	$5 \times 10^{19}\mathrm{m}^{-3}$
edge electron density $\overline{n}_{ea}$	$0.01 \times 10^{19}\mathrm{m}^{-3}$
central electron temperature $\overline{T}_{e0}$	6KeV
edge electron temperature $\overline{T}_{ea}$	0.1KeV
exponent of the electron temperature profile γ	1.5

Table 4.1: JET-like plasma parameters

In the analysis the ray are launched in the slow mode [23] from the position:

$$\begin{aligned} \rho_0 &= 0.968 \\ \theta_0 &= 0 \\ \phi_0 &= 0 \end{aligned} \tag{4.60}$$

The spectral quantities are assumed to have the following values:

$$\begin{aligned} \omega/(2\pi) &= 3.7\text{GHz} \\ m_0 &= 0 \\ N_{\phi 0} &= -2.0 \end{aligned} \tag{4.61}$$

Where $N_{\phi 0}$ is the initial value of the toroidal component of the refractive index, $N_\phi = ck_\phi/\omega$. The inital value of the covariant component n of the wave vector can be determined in function of $N_{\phi 0}$:

$$n_0 = k_{\phi 0} R_0 = \frac{\omega R_0}{c} N_\phi \tag{4.62}$$

Then the initial value of the parallel index of refraction $N_{\|0}$ can be calculated using this expression and remembering that $m_0 = 0$:

$$N_{\|0} = \frac{c}{\omega}\left(P\frac{m_0}{r_0}\cos\alpha + T\frac{n_0}{R_0}\right) = TN_{\phi 0} \tag{4.63}$$

Where $P = \sigma_I B_P/B$ and $T = \sigma_B B_T/B$ are the component of the magnetic field versor evaluated initially neglecting the perturbations. Using the plasma parameters reported in table (4.1), this value becomes: $N_{\|0} \approx -1.95$. The initial value of the perpendicular refractive index $N_{\perp 0}$ is calculated solving the dispersion relation (4.11) for $N_\| = N_{\|0}$, and thus the initial value of the radial wave number $k_{\rho 0}$ can be evaluated using the expression (2.36).

4.4.2 Ray trajectories in presence of fluctuations

The local eikonal-like description of electron density and magnetic field fluctuations is used to illustrate the effects of the equilibrium magnetic field on ray trajectories in the lower hybrid frequency range. The electron density and the magnetic field are:

$$n_e(\rho,\theta,\phi) = \overline{n}_e(\rho) + \widetilde{n}_e(\rho,\theta,\phi) \tag{4.64}$$

$$\mathbf{B}(\rho,\theta,\phi) = \overline{\mathbf{B}}(\rho,\theta) + \widetilde{\mathbf{B}}(\rho,\theta,\phi) \tag{4.65}$$

The time dependence of the perturbations is not considered in the study of the propagation, because its time scales are very slow compared to the ray evolution. The unperturbed electron density profile is given by the expression (4.49) and the component of the unperturbed magnetic field by the (4.54) and

(4.55), while the perturbations generated by the fluctuations in the local approximation are represented respectively by the (3.59) for the density and by the (3.65), (3.77) and (3.78) for the magnetic field components. The uniform grid of $\widetilde{k}_\perp$ introduced in details in previous chapter is used in the calculation of $\widetilde{n}_e$ and $\widetilde{B}_\perp$, a number $N_{\widetilde{k}_\perp} = 600$ of oscillations each one corresponding to a different value of $\widetilde{k}_\perp$ is considered and the value of the normalized correlation wave vector is assumed to be $a_p k_{\perp c} = 300$. The relative fluctuations spatial profiles σ_{ne} and $\sigma_{B_\perp}$ used in the analysis are reported in function of the radial coordinate in Fig.(4.2): no poloidal dependence ($\lambda = 0$) and half-width parameter $\Delta\rho = 0.07$ are assumed for both electron density than magnetic fluctuations, density perturbations have a maximum relative level $\sigma_{nemax} = 30\%$ and are peaked at the plasma edge ($\rho_0 = 1$), while magnetic perturbations have $\sigma_{B_\perp max} = 0.3\%$ and are peaked at $\rho = \rho_0 = 0.6$. These profiles are used in ref.[12], and describes the characteristics of fluctuations measured in several experiments [1, 2], the effects of equilibrium perturbations on the trajectories are tested launching the ray from the same position indicated by the coordinates (4.60), introducing before density and magnetic fluctuations separately, and after considering both the processes.

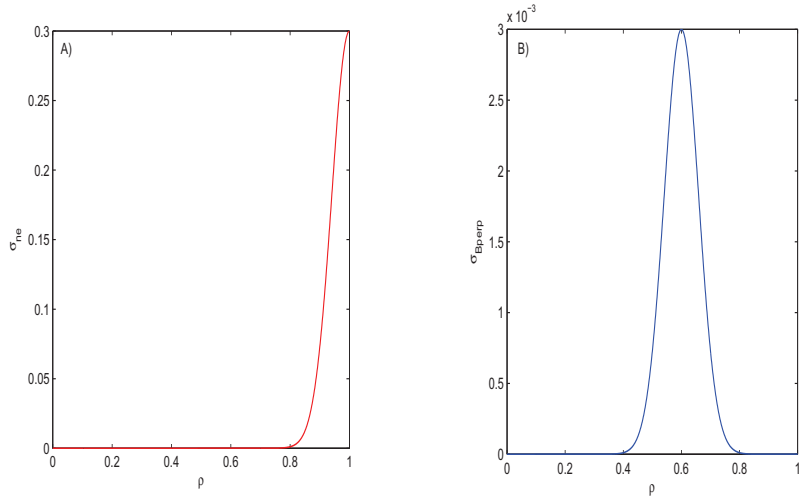

Figure 4.2: A):σ_{ne} profile used for testing fluctuations effects on ray trajectories, no poloidal dependence is assumed ($\lambda = 0$), the peak is assumed to be at the plasma edge ($\rho_0 = 1$) and corresponds to a maximum relative level $\sigma_{nemax} = 30\%$, the half-width value is $\Delta\rho = 0.7$; B):$\sigma_{B_\perp}$ profile used for testing fluctuations effects on ray trajectories, no poloidal dependence is assumed ($\lambda = 0$), the peak is assumed to be at $\rho = \rho_0 = 0.6$ and corresponds to a maximum relative level $\sigma_{B_\perp max} = 0.3\%$, the half-width value is $\Delta\rho = 0.7$;

The evolution of the radial and poloidal ray position and of the components of the refractive index along the trajectory in presence of electron density fluctuations corresponding to the spatial profile illustrated in Fig.(4.2)/A) is

reported in function of the toroidal normalized angle $\phi/2\pi$ and compared with the case without fluctuations in Figs.(4.3) and (4.4). The rays are launched from the initial position (4.60) with the inital values of the spectral quantities (4.61). From the evolution of the radial and poloidal position it can be observed that the ray trajectory, after a brief initial segment where it is identical to the case without fluctuations, can be strongly modified by perturbations generated by density fluctuations peaked at the plasma edge. The relevance of these trajectory modifications in current drive calculations depends by the characteristics of the considered scenario, in ITER-like scenarios, for example, the power trasported by the ray is rapidly damped, near the plasma edge, before than the trajectories start varying for effects of the fluctuations. Also the spectral quantities of the ray are strongly affected by the perturbations: since fluctuations have the maximum at the plasma edge, the trend of the parallel and of the perpendicular index of refraction becomes different by the case without fluctuations from the beginning of the trajectory, and the effects of the fluctuations on $N_\perp$ can modify the damping of the ray. However, it is very important to remember that the random nature of the density fluctuations generated by drift waves makes the ray trajectories stochastic, thus the evolution of the position and of the refractive index along rays launched with identical initial conditions can become very different, and the effects of the perturbation on the absorption cannot be deduced and quantified from the behaviour of one single ray. Since fluctuations induce a breaking in axisymmetry of the system, the toroidal mode number n is no longer a constant of the ray evolution, as it can be observed in Fig.(4.4). The behaviour of n is very sensitive to equilibrium parturbations: as the ray start propagating into the plasma, it covers immediately the area with maximum level of fluctuations, and the toroidal wave number varies strongly respect to the constant value correspondent to the case without fluctuations, when the ray penetrates into the plasma core, where fluctuations amplitude is zero (see the spatial profile in Fig.(4.2)/A)), n remains constant, and it restarts oscillating in ϕ when the ray returns at the plasma edge, where fluctuations level is again high. In Figs.(4.6) and (4.6) the evolution of the ray position and of the components of the refractive index in presence of magnetic field fluctuations having the spatial profile of Fig.(4.2)/B) is compared with the case without fluctuations. The initial conditions are the same used for density fluctuations ((4.60) and (4.61)). Unlike the case with density perturbations, the ray trajectory is not significantly affected by magnetic field fluctuations, as it can be observed in the figures, and also the parallel and perpendicular refractive index behaviour varies minimally respect to the evolution without fluctuations. The only component of the refractive index strongly affected by magnetic fluctuations is the toroidal one n, which remains constant when the ray goes through the zones of the plasma where the perturbations amplitude is negligible as for example at the edge (the fluctuations spatial profile considered is peaked at $\rho = 0.6$), and oscillates when the ray crosses the zones where fluctuations level is high.

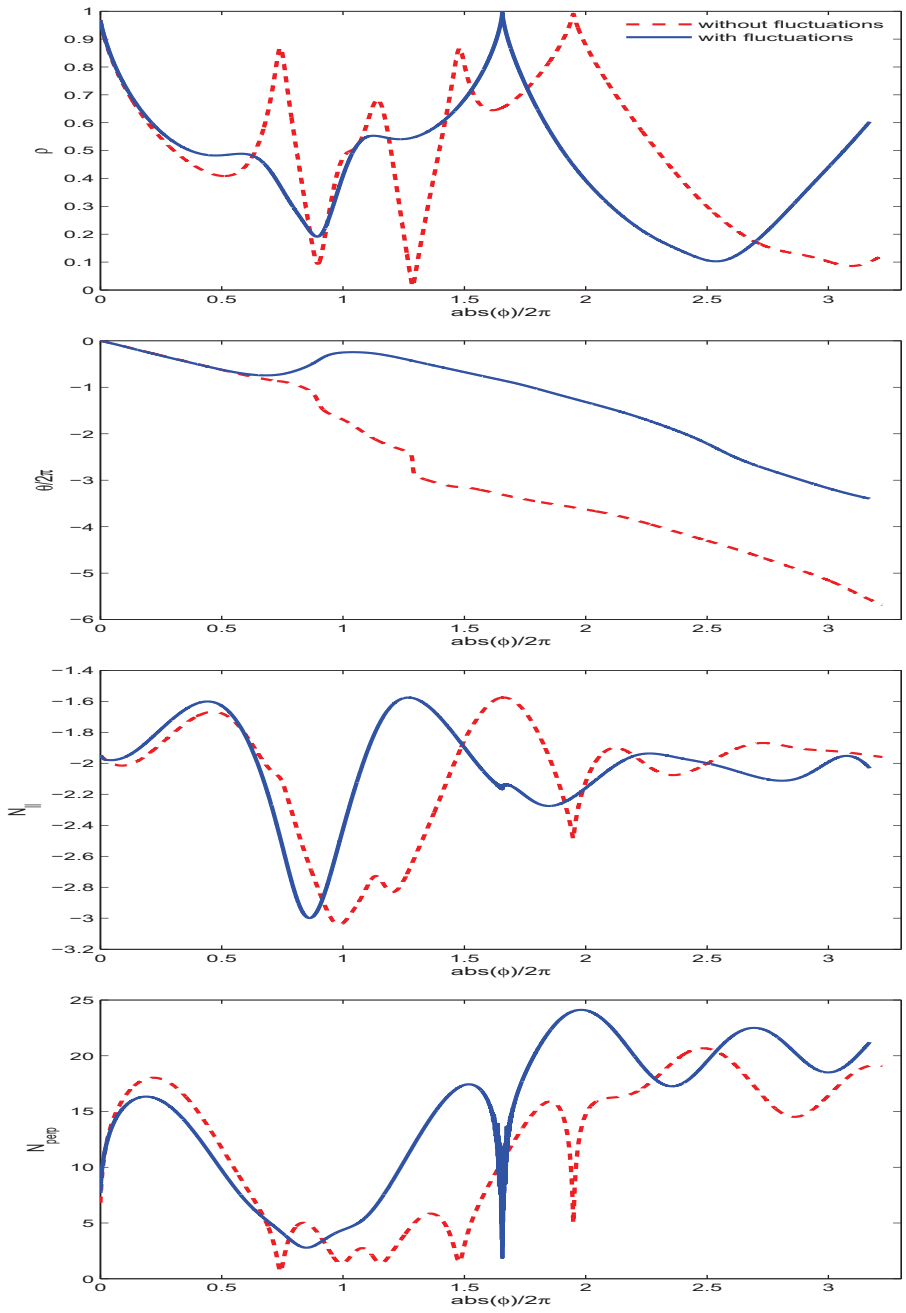

Figure 4.3: Comparison between the ray behaviour in presence of density fluctuations $\widetilde{n}_e$ (blue solid lines) and the ray behaviour without fluctuations (dashed red lines): the radial position ρ, the normalized poloidal angle $\theta/2\pi$, the parallel index of refraction $N_\parallel$ and the perpendicular index of refraction $N_\perp$ are plotted in function of the toroidal angle $\phi/2\pi$.

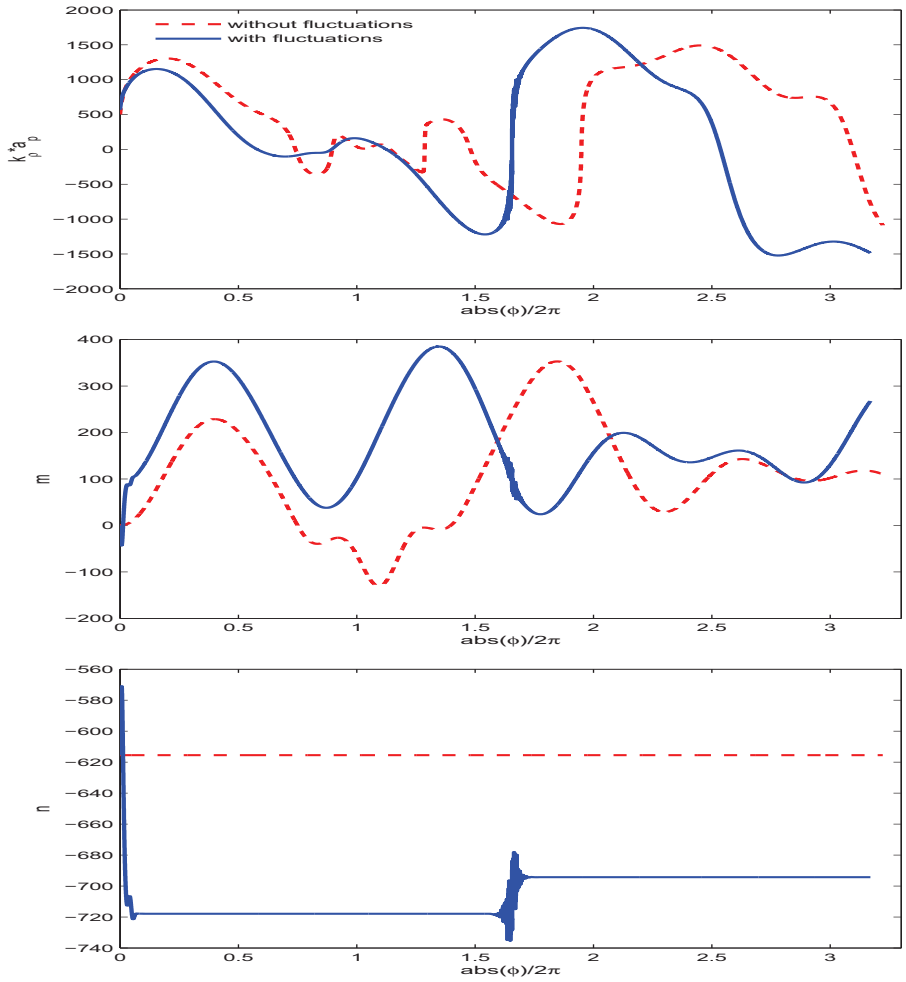

Figure 4.4: Comparison between the ray behaviour in presence of density fluctuations $\widetilde{n}_e$ (blue solid lines) and the ray behaviour without fluctuations (dashed red lines): the normalized radial wave number $k_\rho a_p$, the poloidal wave number m and the toroidal wave number n are plotted in function of the toroidal angle $\phi/2\pi$.

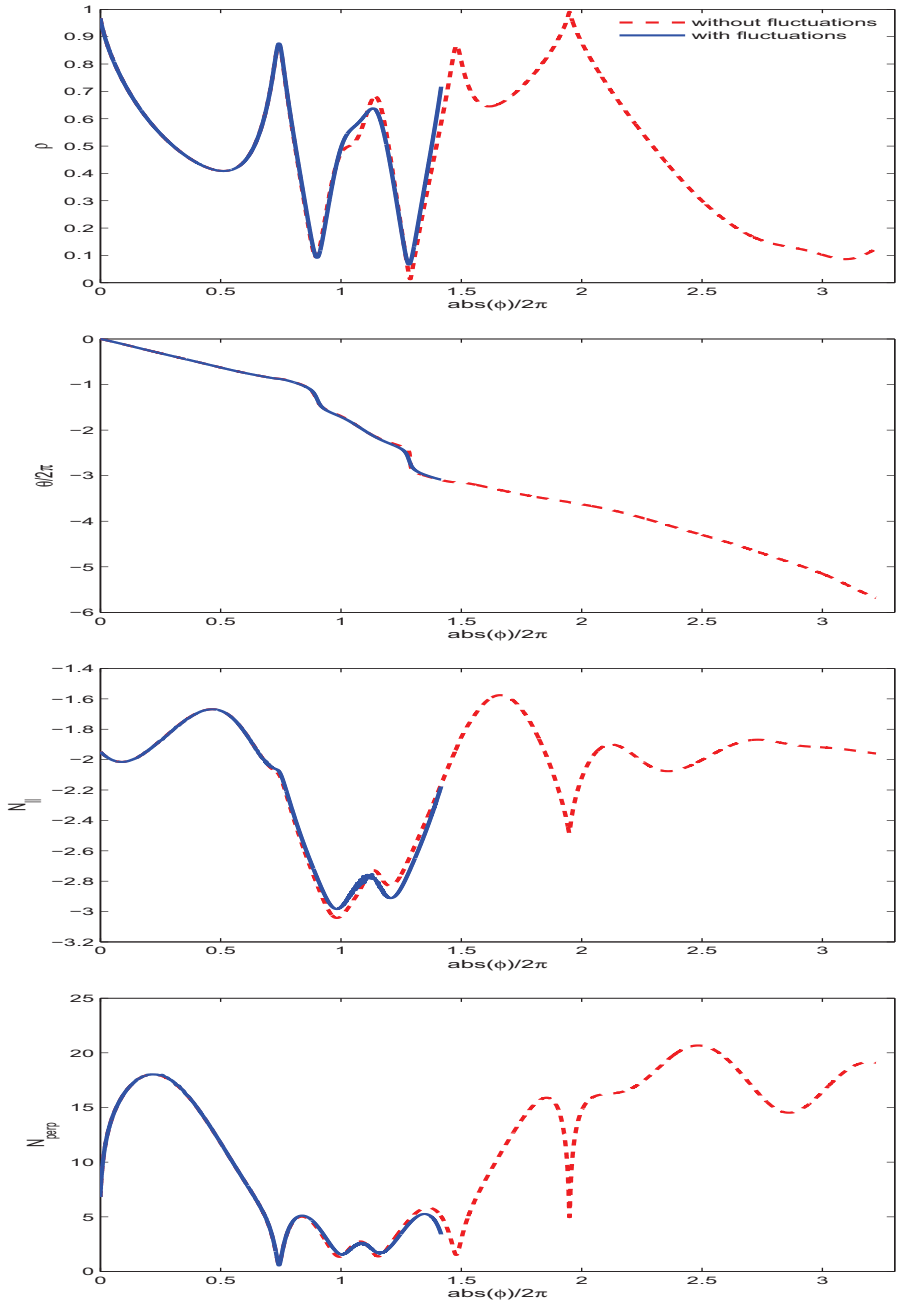

Figure 4.5: Comparison between the ray behaviour in presence of magnetic field fluctuations $\widetilde{\mathbf{B}}$ (blue solid lines) and the ray behaviour without fluctuations (dashed red lines): the radial position ρ, the normalized poloidal angle $\theta/2\pi$, the parallel index of refraction $N_{\parallel}$ and the perpendicular index of refraction $N_{\perp}$ are plotted in function of the toroidal angle $\phi/2\pi$.

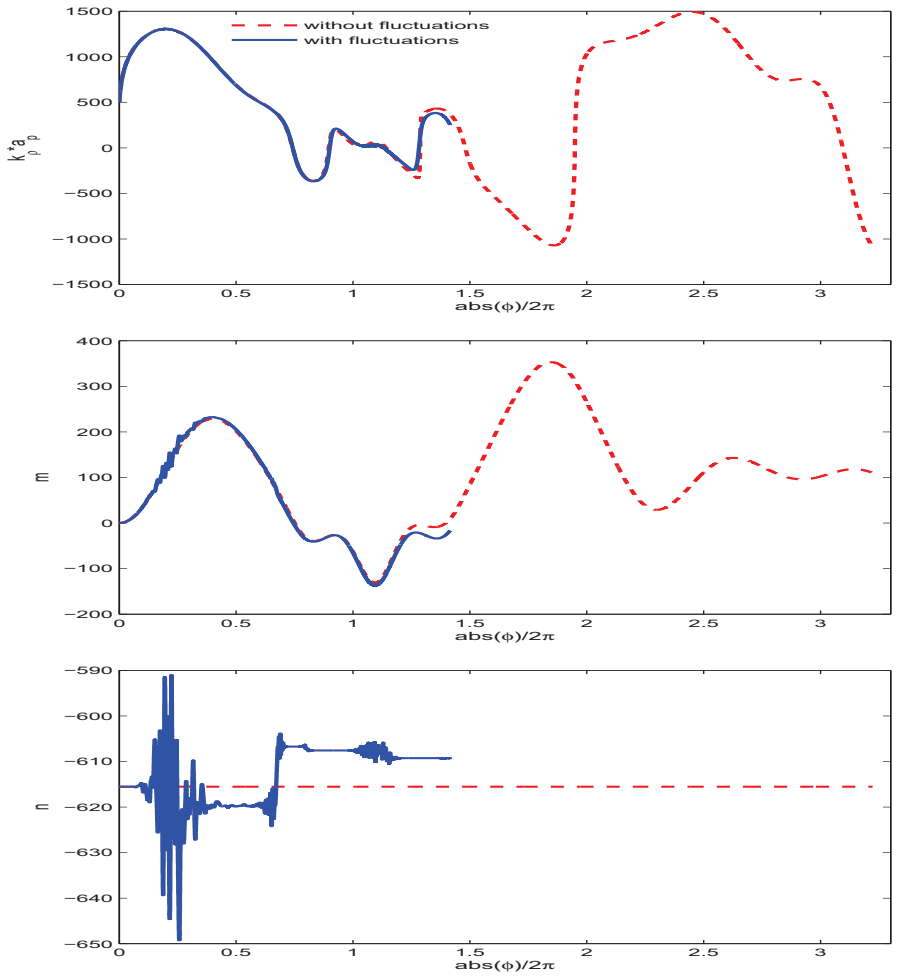

Figure 4.6: Comparison between the ray behaviour in presence of magnetic field fluctuations $\widetilde{\mathbf{B}}$ (blue solid lines) and the ray behaviour without fluctuations (dashed red lines): the normalized radial wave number $k_\rho a_p$, the poloidal wave number m and the toroidal wave number n are plotted in function of the toroidal angle $\phi/2\pi$.

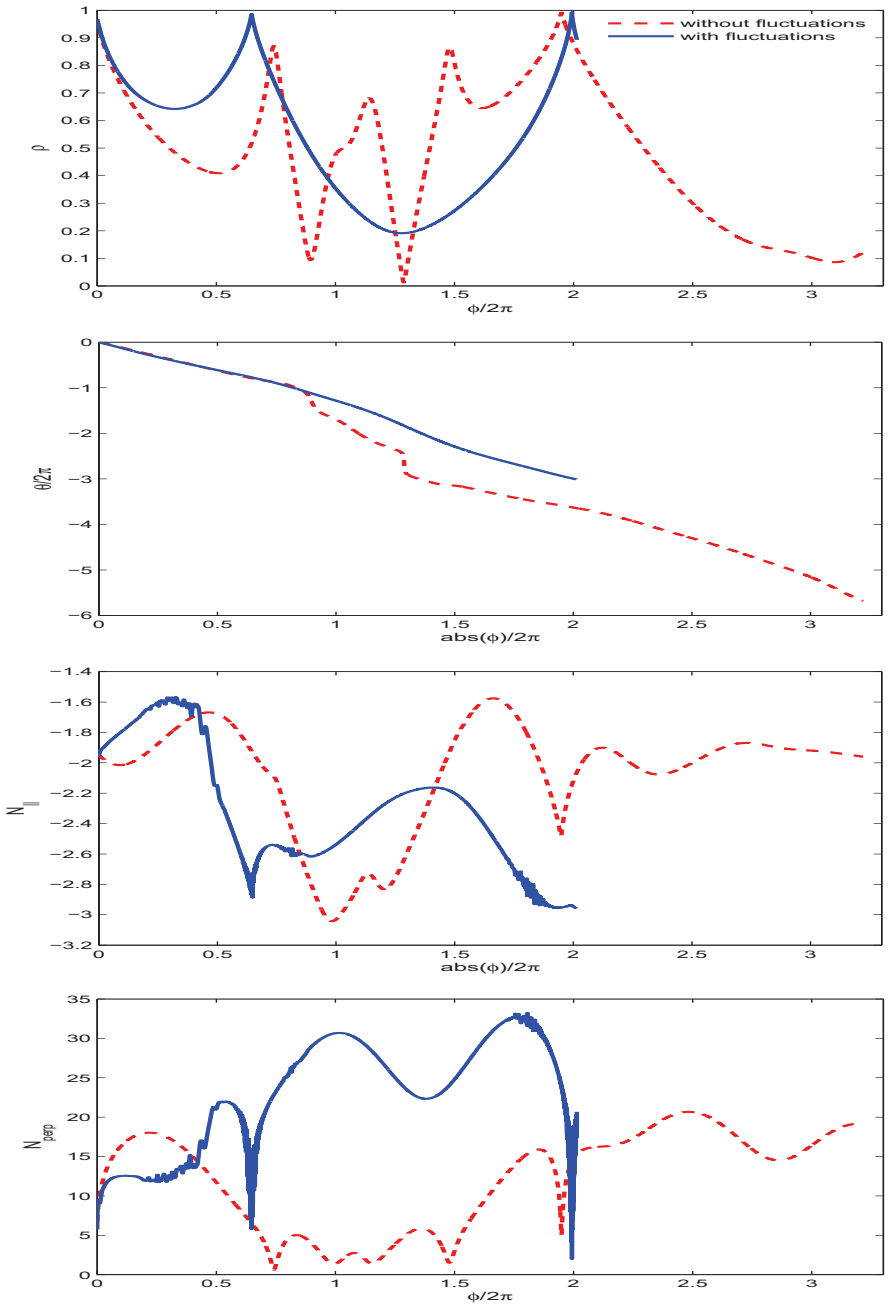

Figure 4.7: Comparison between the ray behaviour in presence of both electron density and magnetic field fluctuations, $\widetilde{n}_e$ and $\widetilde{\mathbf{B}}$ (blue solid lines), and the ray behaviour without fluctuations (dashed red lines): the radial position ρ, the normalized poloidal angle $\theta/2\pi$, the parallel index of refraction $N_\parallel$ and the perpendicular index of refraction $N_\perp$ are plotted in function of the toroidal angle $\phi/2\pi$.

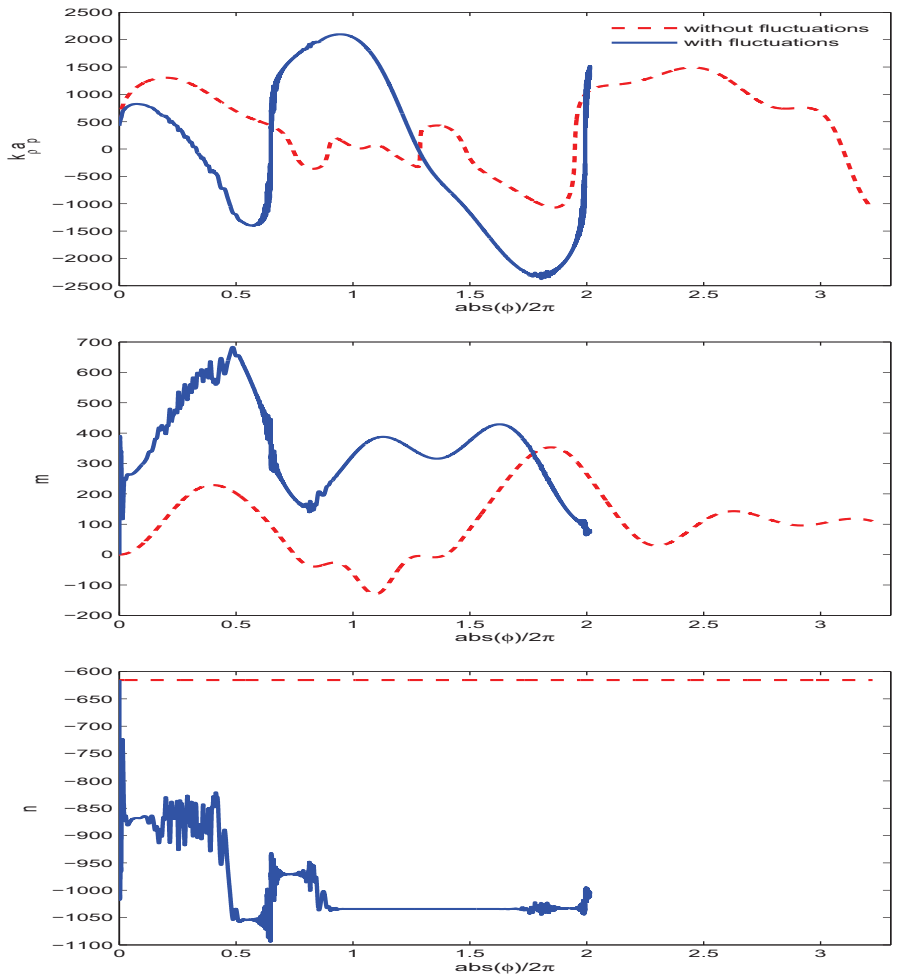

Figure 4.8: Comparison between the ray behaviour in presence of both electron density and magnetic field fluctuations, $\widetilde{n}_e$ and $\widetilde{\mathbf{B}}$, (blue solid lines) and the ray behaviour without fluctuations (dashed red lines): the normalized radial wave number $k_\rho a_p$, the poloidal wave number m and the toroidal wave number n are plotted in function of the toroidal angle $\phi/2\pi$.

As it is clearly shown in figures, the effects of electron density fluctuations on the trajectories and on refractive index evolution are much more significant respect to magnetic field fluctuations, and then consequences of equilibrium density perturbations generated by drift waves on the propagation are dominant respect to the effects of magnetic field fluctuatons. In Figs.(4.7) and (4.8) the ray behaviour in presence of both density and magnetic fluctuations having relative level profiles reported in Fig.(4.2) is illustrated. The rays are launched with the same initial conditions of the previous cases. It is important to note the differencies between the behaviour of the ray reported in Figs.(4.3) and (4.4) and the ray illustrated in Figs.(4.7) and (4.8): since magnetic fluctuations effects on propagation are negligibles, the variations of the trajectories respect to the case without perturbations are associated essentially to density fluctuations, the two rays are launched with the same initial conditions, but the evolution of the ray coordinates and of the components of the refractive index presents visible differencies. This differencies are due to the random nature of the drift-like fluctuations, and demonstrate that for effects of these processes the trajectory of the ray becomes essentially stochastic.

4.4.3 Ray trajectories in presence of magnetic ripple

The ripple field in JET-like scenario is assumed to be generated by a set of N uniformly distributed circular coils, then the perturbation of the equilibrium magnetic field can be expressed using the analytical expressions derived in Ref.[31] and introduced in section 3.2.2. The toroidal ripple field is given by the expression (3.110) and it is here reported:

$$\widetilde{B}_\phi = \overline{B}_\phi \delta_n I_0\left(\frac{a}{R_0 - L_0}N\right)\cos(N\phi) \tag{4.66}$$

Where $\overline{B}_\phi$ is the unperturbed toroidal magnetic field, represented in this case by the expression (4.54), N is the number of coils, $a(r,\theta)$ is the radius of the iso-ripple contours given by the (3.107), R_0 is the vacuum vessel major radius, L_0 is the distance between the center of the coils and the iso-ripple contour corresponding to $a = 0$ and δ_n is an adimensional parameter depending by the geometry of the coils.The radial and poloidal component of the perturbation generated by the set of coils are:

$$\widetilde{B}_r(r,\theta,\phi) = \overline{B}_\phi \delta_n \frac{r + L_0\cos\theta}{a} I_1\left(\frac{a}{R_0 - L_0}N\right)\sin(N\phi) \tag{4.67}$$

$$\widetilde{B}_\theta(r,\theta,\phi) = \overline{B}_\phi \delta_n \frac{L_0\sin\theta}{a} I_1\left(\frac{a}{R_0 - L_0}N\right)\sin(N\phi) \tag{4.68}$$

Explicit expressions for the components $\widetilde{B}_\rho, \widetilde{B}_s$ and $\widetilde{B}_R, \widetilde{B}_Z$ in function of $\widetilde{B}_r$ and $\widetilde{B}_\theta$ have been also introduced and discussed in details in the previous chapter (see relations (3.115),(3.116),(3.119),(3.120)). In the case of circular coils,

the parameters L_0 and δ_n are given in function of the inner and outer radius of the windings, r_n and r_x, by the expressions (3.108). Consequently, the perturbation of the magnetic field depends only by a few number of parameters which values is connected to the design of the different tokamak devices: the vacuum vessel major radius R_0, the number of coils N, the inner and outer radius of the windings, r_n and r_x. The values of these parameters used for testing ripple effects on lower hybrid waves propagation in the JET-like scenario introduced in subsection 4.4.1 are reported in table (4.2).

vacuum major radius R_0	3.05m
number of coils N	18
inner windings radius r_n	1.00m
outer windings radius r_x	1.50m

Table 4.2: Parameters used for testing magnetic ripple effects on ray trajectories in a JET-like plasma.

The behaviour of the radial and poloidal ray position and of the components of the refractive index along the trajectory in presence of ripple magnetic field is reported in function of the toroidal normalized angle $\phi/2\pi$ in Figs.(4.9) and (4.10) and compared with the evolution of the same quantities in an unperturbed axisymmetric equilibrium, without fluctuations and ripple. The rays initial position and the starting values of the spectral quantities are the same used for testing the fluctuations effects ((4.60) and (4.61)). Both the ray trajectory and the components of the refractive index are strongly affected by the ripple field. An high frequency modulation of the toroidal wave number n can be observed, the amplitude of this modulation is great when the ray propagates into the zones close to the plasma edge, where the ripple corrections to the magnetic field are high, and becomes negligible when the ray crosses the plasma core, where the value of the ripple field vanishes [31, 32]. This behaviour can be noted also in the component of the refractive index parallel and perpendicular to the magnetic field, $N_\parallel$ and $N_\perp$, and in the poloidal and radial components m and $k_\rho a_p$: in the well localized zones in proximity of the edge, these quantities oscillate at high frequencies around a medium trend, while when the ray penetrates into the plasma, the oscillations amplitude decreases and the evolution becomes regular, but remains different respect to the case without any perturbation. The perturbation induced by magnetic ripple is stationary, then independent by the time, and unlike the perturbations generated by stochastic fluctuations, it does not have a random term in the phase. Consequently the modifications to the ray trajectory and to the evolution of the refracive index in this case are not of random nature, and rays launched with identical initial conditions in a rippled magnetic equilibrium have the same trajectory.

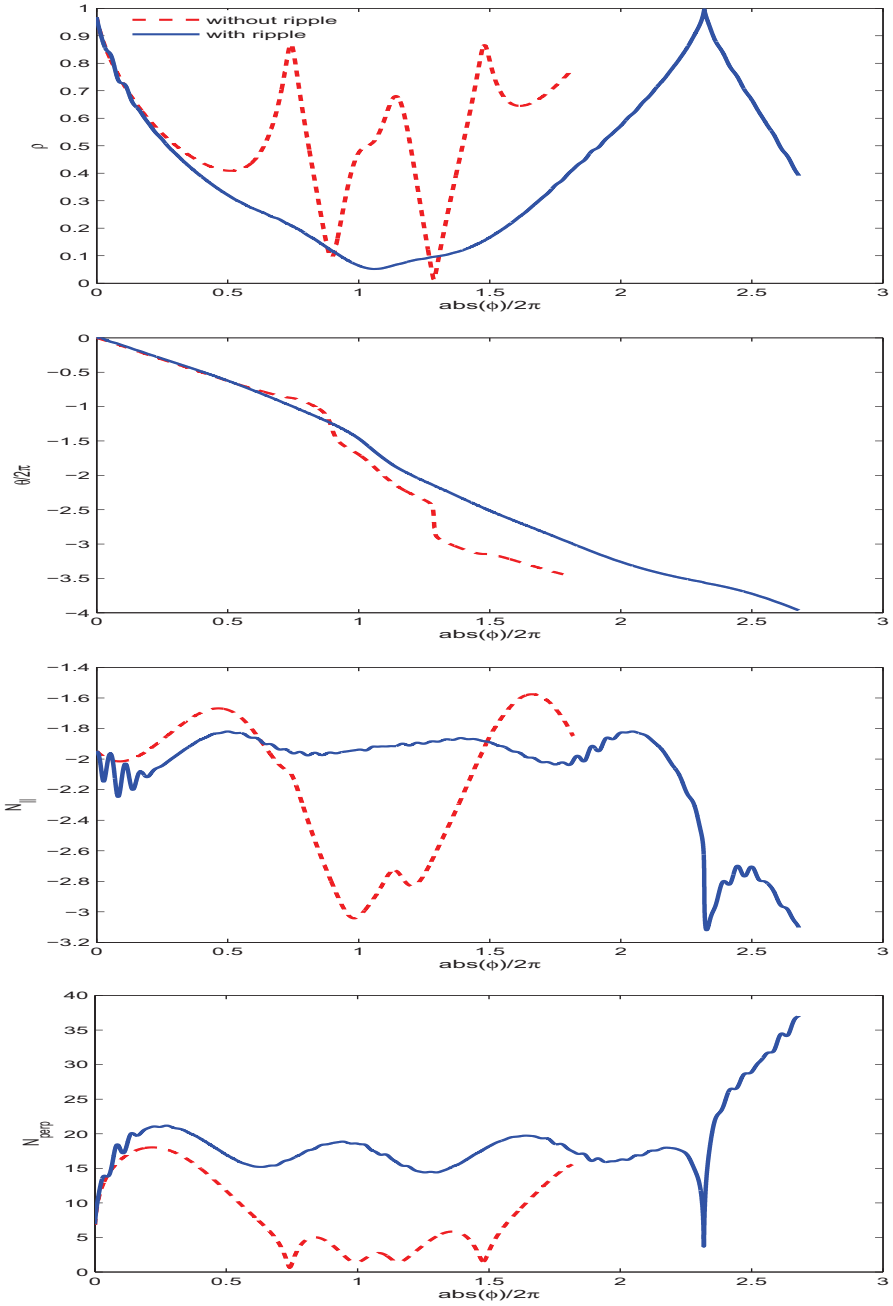

Figure 4.9: Comparison between the ray behaviour in presence of ripple magnetic field $\tilde{\mathbf{B}}$ (blue solid lines) and the ray behaviour in an unperturbed axisymmetric equilibrium (dashed red lines): the radial position ρ, the normalized poloidal angle $\theta/2\pi$, the parallel index of refraction $N_{\parallel}$ and the perpendicular index of refraction $N_{\perp}$ are plotted in function of the toroidal angle $\phi/2\pi$.

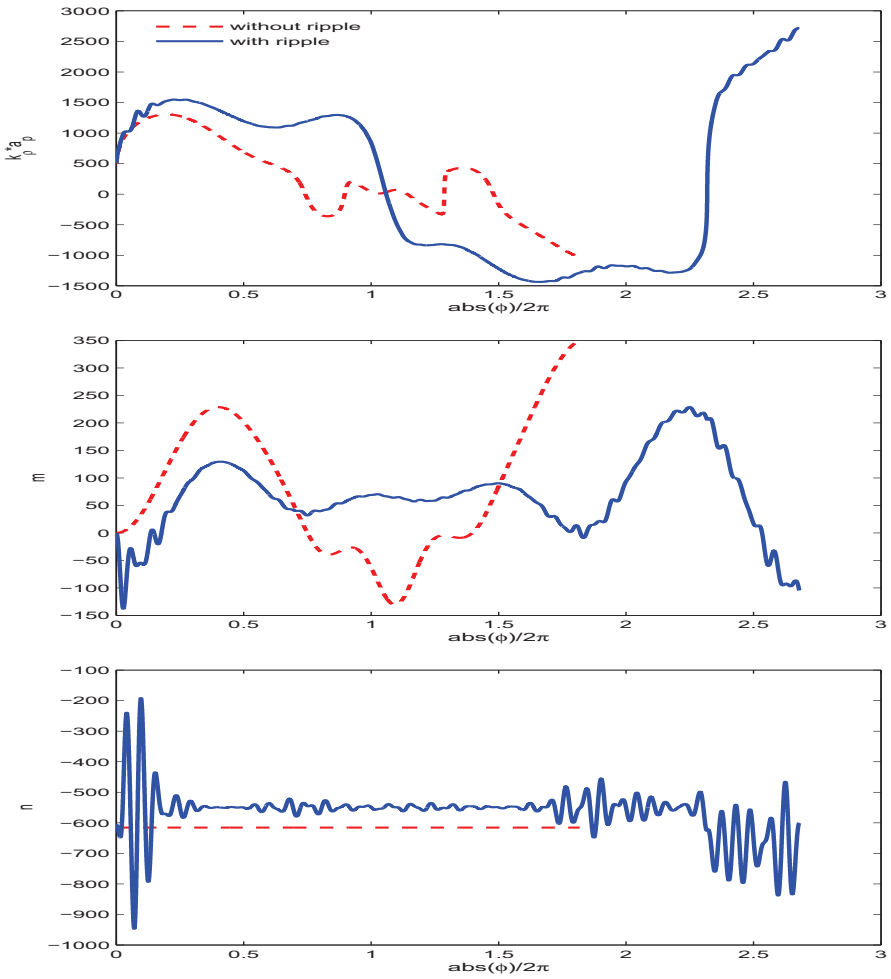

Figure 4.10: Comparison between the ray behaviour in presence of ripple magnetic field $\widetilde{\mathbf{B}}$ (blue solid lines) and the ray behaviour in an unperturbed axisymmetric equilibrium (dashed red lines): the normalized radial wave number $k_\rho a_p$, the poloidal wave number m and the toroidal wave number n are plotted in function of the toroidal angle $\phi/2\pi$.

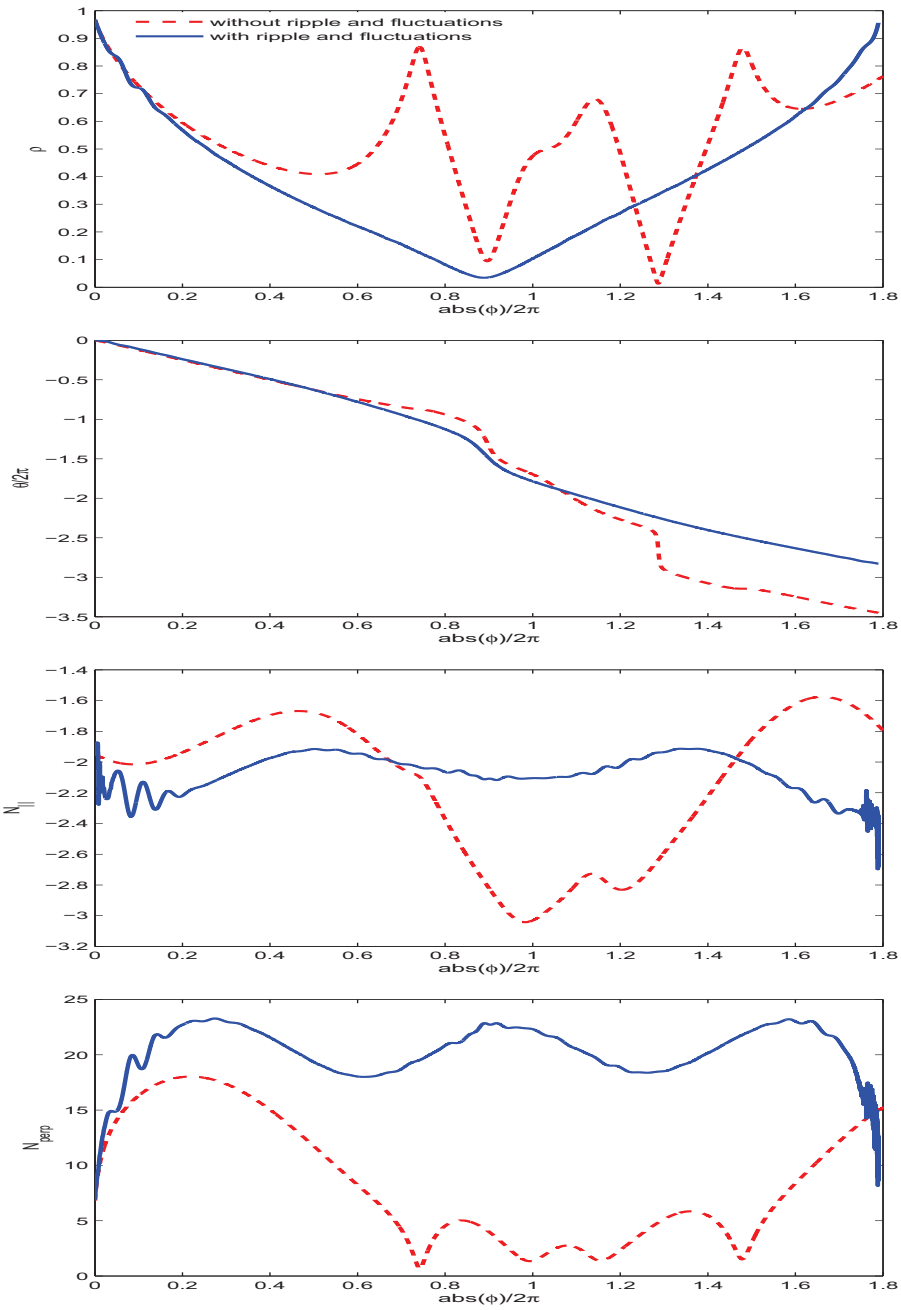

Figure 4.11: Comparison between the ray behaviour in presence of ripple magnetic field $\widetilde{\mathbf{B}}$ and drift-like density fluctuations $\widetilde{n}_e$ (blue solid lines), and the ray behaviour in an unperturbed axisymmetric equilibrium (dashed red lines): the radial position ρ, the normalized poloidal angle $\theta/2\pi$, the parallel index of refraction $N_\parallel$ and the perpendicular index of refraction $N_\perp$ are plotted in function of the toroidal angle $\phi/2\pi$.

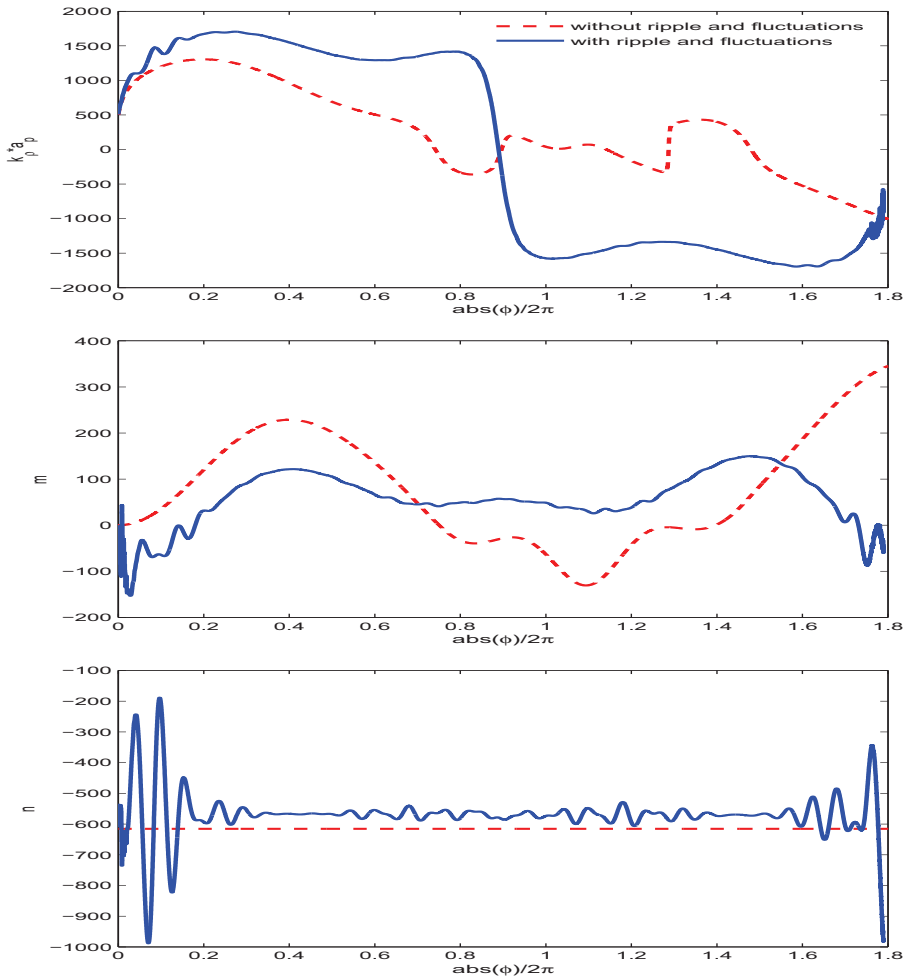

Figure 4.12: Comparison between the ray behaviour in presence of ripple magnetic field $\widetilde{\mathbf{B}}$ and drift-like density fluctuations $\widetilde{n}_e$ (blue solid lines) and the ray behaviour in an unperturbed axisymmetric equilibrium (dashed red lines): the normalized radial wave number $k_\rho a_p$, the poloidal wave number m and the toroidal wave number n are plotted in function of the toroidal angle $\phi/2\pi$.

In Figs.(4.11) and (4.12) the behaviour of the ray in presence of both magnetic ripple and drift-like density fluctuations having the spatial profile of Fig.(4.2)/A) is illustrated. Also in these figures, as in (4.9) and the (4.10), where the evolution of a ray launched with the same initial conditions considering only the ripple perturbation is shown, when the ray propagates near the plasma edge, an high frequency modulation of the refractive index components is observed, expecially in the toroidal component n. This means that when the ripple field is accounted, in proximity of the edge, where the ripple correction is high, its effects on the propagation are dominant respect to the fluctuations, and especially the modulation of the toroidal wave number n from a quantitative point of view is more relevant than the stochastic oscillations generated by the fluctuations.

4.5 LHCD in an ITER scenario with perturbed equilibrium

In this section some examples of lower hybrid current drive (LHCD) simulations performed considering fluctuations effects are presented. The equilibrium perturbations generated by the fluctuations are expressed in the local form, and applications of the model to the up/down symmetric ITER scenario 4 [40, 41] are illustrated and discussed in details. In this scenario current drive calculations are faster than in Tore Supra and FTU cases, because for effects of the plasma characteristics (densities and temperatures profiles), the power carried by the rays is in general fully damped near the edge, before than the rays reach for the first time the plasma core and return at the border. This makes ITER scenario 4 particularly suitable for testing fluctuations effects on lower hybrid current drive. Plasma parameters characteristics of ITER scenario 4 are reported in table (4.3).

plasma minor radius a_p	1.85m
plasma major radius R_p	6.35m
on-axis magnetic field B_{T0}	5.3T
central electron density $\overline{n}_{e0}$	$7.25 \times 10^{19}\mathrm{m}^{-3}$
edge electron density $\overline{n}_{ea}$	$2.3 \times 10^{19}\mathrm{m}^{-3}$
central electron temperature $\overline{T}_{e0}$	24KeV
edge electron temperature $\overline{T}_{ea}$	0.18KeV
effective charge Z_{eff}	2.23

Table 4.3: Parameters of ITER scenario 4

The poloidal section of the flux surfaces correspondent to ITER scenario 4 equilibrium, evaluated with HELENA code [30], and the radial profiles of the unperturbed equilibrium quantities are illustrated in Figs.(4.13) and (4.14).

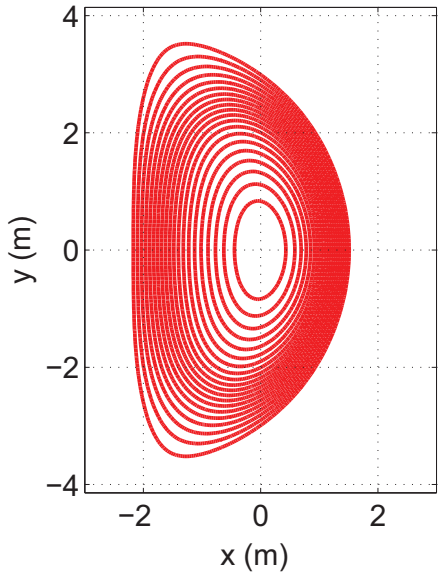

Figure 4.13: Poloidal section of the magnetic flux surfaces correspondent to $\psi = const$ for the ITER scenario 4 equilibrium.

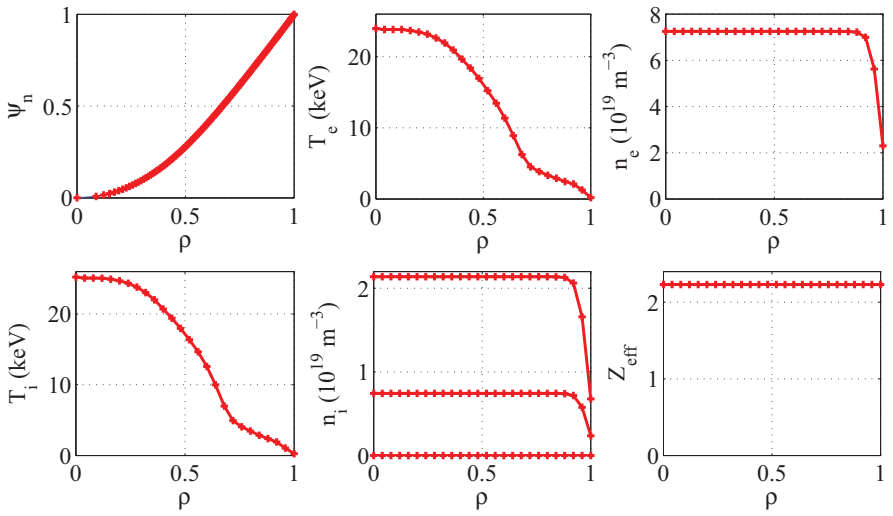

Figure 4.14: Radial profiles of normalized poloidal magnetic flux, electron temperature, electron density, ion temperatures, ion densities, and effective charge for the ITER scenario 4 equilibrium.

The lower hybrid waves frequency is $f_{LH} = \omega_{LH}/2\pi = 5.0$GHz and the total power injected into the plasma is $P_{LH} = 20$MW. Four rays are launched into the plasma from the vertical positions $Z = 0.15, 1.15$m, two correspond to the positive lobe of the antenna and have initial value of the refractive index $N_{\|0} = 4$, while the other two represent the negative lobe and have $N_{\|0} = -2$. The trajectories are stopped when the fraction of power carried by the rays is fully absorbed.
Two different electron density fluctuations processes are considered, and the associated perturbations $\widetilde{n}_{e1}$ and $\widetilde{n}_{e2}$ are both calculated in the local approximation assuming a number of oscillations $N_{\widetilde{k}_\perp} = 900$ with normalized correlation wave vector $a_p k_{\perp c} = 300$. The first process $\widetilde{n}_{e1}$ is a background perturbation having maximum level $\sigma_{ne1max} = 3\%$ at $\rho = \rho_0 = 0.5$, semi-amplitude parameter $\Delta\rho = 0.5$ and no poloidal dependence ($\lambda = 0$), while the second σ_{ne2} presents a very thin spatial profile peaked at the plasma edge ($\rho_0 = 1$) with a maximum relative level $\sigma_{ne2max} = 30\%$, semi-amplitude parameter $\Delta\rho = 0.02$ and a strong poloidal dependence ($\lambda = 0.54$). The radial evolution of $\widetilde{n}_{e1}$ and $\widetilde{n}_{e2}$ and the poloidal dependence of $\widetilde{n}_{e2}$ are reported in Fig.(4.15).

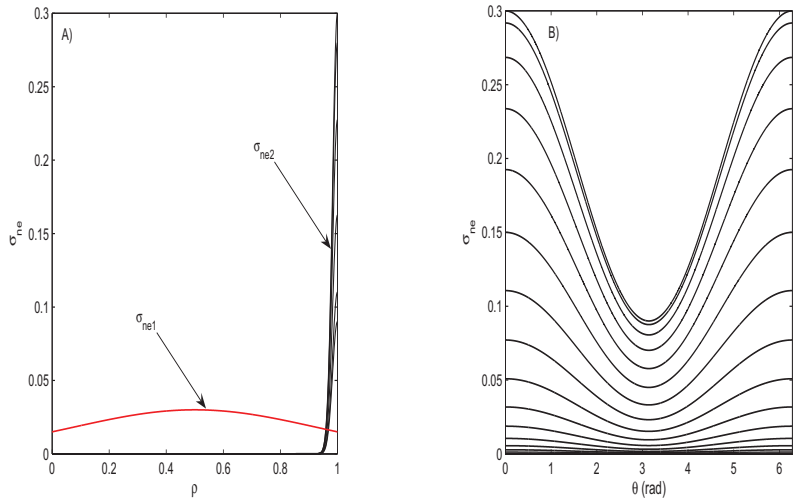

Figure 4.15: A) Radial dependence of the spatial profiles associated with the two fluctuations processes considered in LHCD simulations in ITER scenario 4: the red line corresponds to $\widetilde{n}_{e1}$, peaked at $\rho = \rho_0 = 0.5$ and having $\sigma_{ne1max} = 3\%, \lambda = 0, \Delta\rho = 0.5$, while the black line corresponds to $\widetilde{n}_{e2}$, peaked at the edge and having $\sigma_{ne2max} = 30\%, \lambda = 0.54, \Delta\rho = 0.02$; B) Poloidal depencence of the spatial profile σ_{ne2} correspondent to the perturbation $\widetilde{n}_{e2}$;

In Figs.(4.16) and (4.17) the evolutions of the parallel refractive index of the rays used for the calculation of the quasilinear diffusion operator considering only the background process (Fig.(4.16)), and both the perturbations (Fig.(4.17)) are plotted in function of the ray length (blue solid lines).

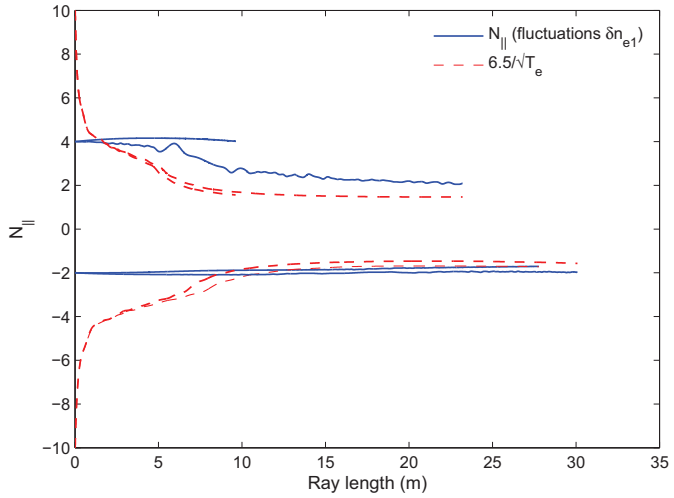

Figure 4.16: Parallel refractive index along the ray: the evolution of $N_{\parallel}$ along the trajectories of the rays used for LHCD calculations considering only the background density perturbation $\widetilde{n}_{e1}$ is reported in function of the ray length (blue solid lines); the parallel refractive index threshold given by the condition $N_{\parallel} \geq 6.5/\sqrt{T_e(\mathrm{KeV})}$ above which a strong Landau damping occurs is plotted for each ray launched into the plasma (red dashed lines).

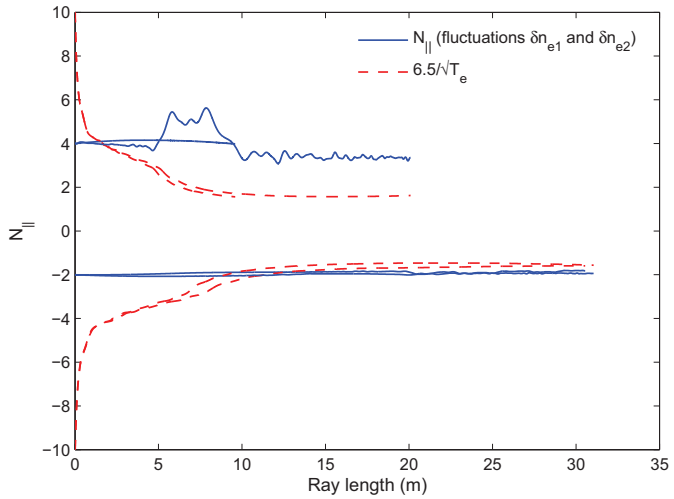

Figure 4.17: Parallel refractive index along the ray: the evolution of $N_{\parallel}$ along the trajectories of the rays used for LHCD calculations considering both the density perturbations $\widetilde{n}_{e1}$ and $\widetilde{n}_{e2}$ is reported in function of the ray length (blue solid lines); the parallel refractive index threshold given by the condition $N_{\parallel} \geq 6.5/\sqrt{T_e(\mathrm{KeV})}$ above which a strong Landau damping occurs is plotted for each ray launched into the plasma (red dashed lines).

As it can be observed in Fig.(4.17), even considering only a low background perturbation level, $N_\parallel$ is affected by the fluctuations, and its evolution presents stochastic oscillations, which are more evident in the case where both $\widetilde{n}_{e1}$ and $\widetilde{n}_{e2}$ are taken into account. In the same figures the following quantity is reported (red dashed lines):

$$N_{\parallel th} = \frac{6.5}{\sqrt{T_e(\mathrm{KeV})}} \tag{4.69}$$

Where the electron temperature T_e is determined at all positions along the rays path. The condition $N_\parallel \geq N_{\parallel th}$ defines a local criterion for having strong Landau damping of the lower hybrid waves on the bulk eletrons [32, 42]. Infact, when this condition is fullfilled, the phase velocity of the wave is close to 3-4 times the thermal velocity, the density of resonant electrons is large enough and the absorption rate becomes very large. Since the inequality $N_\parallel \geq N_{\parallel th}$ is satisfied for all the launched rays before the full absorption, the damping is strong and all the power injected into the plasma is transferred to the electrons. The current density generated by LH waves into the plasma considering only the background process $\widetilde{n}_{e1}$ and both the parturbations $\widetilde{n}_{e1}$ and $\widetilde{n}_{e2}$ is reported in function of the radial coordinate ρ and compared with the current density generated in the case without fluctuations injecting the same power $P_{LH} =$ 20MW and launching the same number of rays with identical initial conditions in Figs.(4.18) and (4.19). These pictures illustrate that the lower hybrid current density profiles, in a scenario with the characteristics of ITER scenario 4, are not strongly modified by density fluctuations effects, even assuming a level of perturbation at the edge of 30%, as in the case with both $\widetilde{n}_{e1}$ and $\widetilde{n}_{e2}$ reported in Fig.(4.19), only the maximum of the peak is slightly lower respect to the case without fluctuations, but the localization and the width of the profiles do not change. This is connected to the fact that also in presence of the perturbations, the power is deposited in the same area of the plasma, near to the plasma edge (peak at $\rho \approx 0.65$) and no broadening of the deposition profile is observed, as it is shown in Figs.(4.20) and (4.21). In Figs.(4.22) and (4.23) the total current I_{tot} generated by LH waves into the plasma is plotted, it is calculated at each quasilinear iteration correspondent to the instants $t_n = n\Delta\tau$ of the uniform temporal grid adopted in the solution of the kinetic equation and introduced in section 2.5. The value $\Delta\tau\nu_c = 10$ is chosen for the quasilinear iteration time step normalized to the collisional period, such that $\Delta\tau > \tau_c$ and the effects of the perturbations satisfying the inequality $\tau_c < \widetilde{\tau}$ on the distribution function evolution and on the current generated into the plasma can be estimated evolving the value of the fluctuations phase at each $t_n = n\Delta\tau$ corresponding to a point of the temporal grid (see section 2.5). I_{tot} is plotted in function of the normalized time $t\nu_c$ and differently from the current density and the power, its evolution is sensitive to density fluctuations, and presents oscillations respect to the case without perturbations.

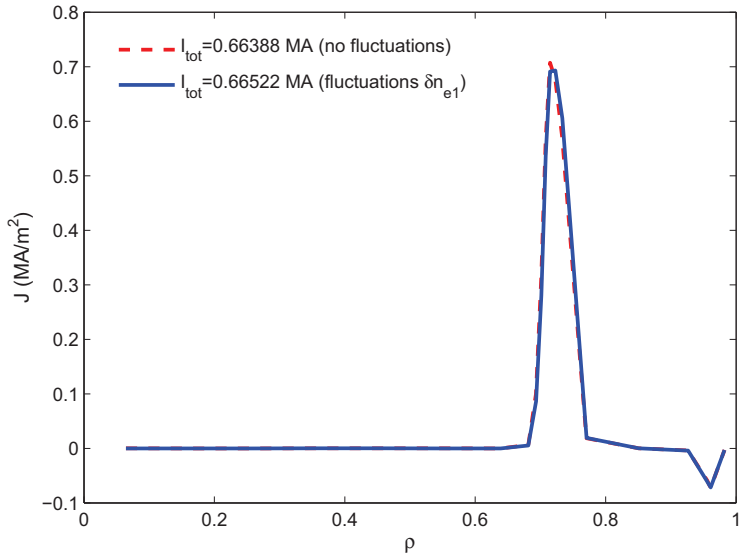

Figure 4.18: Comparison between the current density generated by LH waves in an equilibrium with the background density perturbation $\widetilde{n}_{e1}$ (blue solid line) and the current density generated injecting the same $P_{LH} = 20$MW and launching the same number of rays with the same initial conditions in an unperturbed equilibrium (red dashed line).

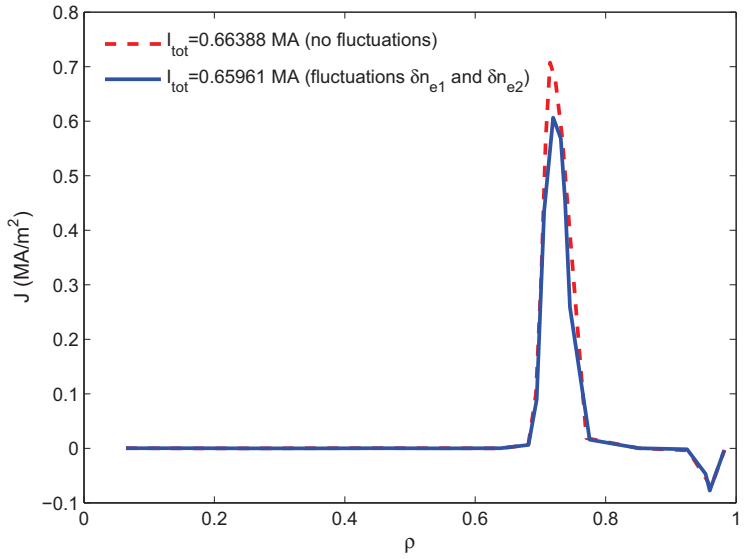

Figure 4.19: Comparison between the current density generated by LH waves in an equilibrium with both the density perturbations $\widetilde{n}_{e1}$ and $\widetilde{n}_{e2}$ (blue solid line) and the current density generated injecting the same $P_{LH} = 20$MW and launching the same number of rays with the same initial conditions in an unperturbed equilibrium (red dashed line).

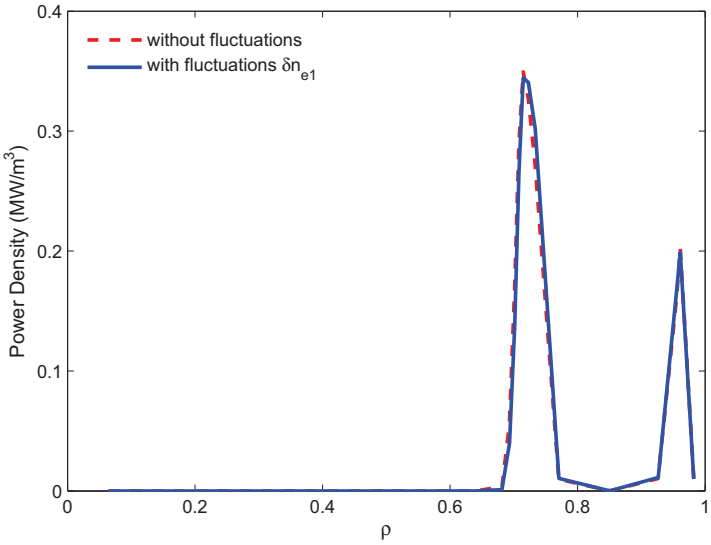

Figure 4.20: Comparison between the LH power deposition profiles evaluated in an equilibrium with the background density perturbation $\widetilde{n}_{e1}$ (blue solid line) and LH power deposition profiles evaluated injecting the same $P_{LH} = 20$MW and launching the same number of rays with the same initial conditions in an unperturbed equilibrium (red dashed line).

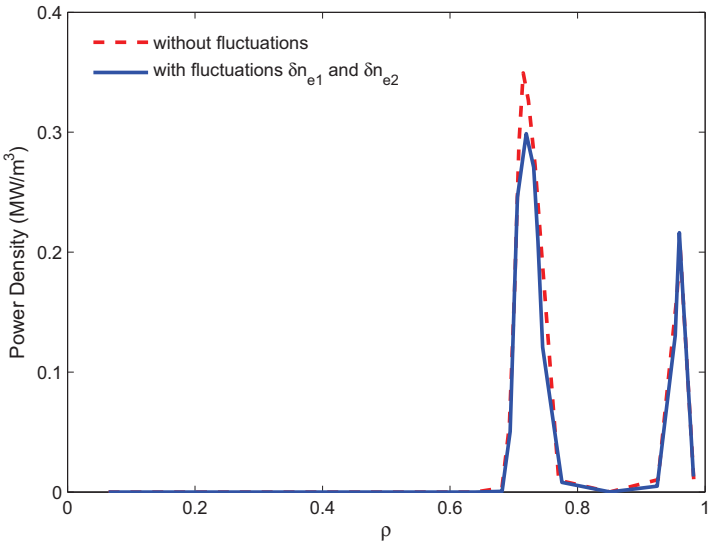

Figure 4.21: Comparison between the LH power deposition profiles evaluated in an equilibrium with both the density perturbations $\widetilde{n}_{e1}$ and $\widetilde{n}_{e2}$ (blue solid line) and LH power deposition profiles evaluated injecting the same $P_{LH} = 20$MW and launching the same number of rays with the same initial conditions in an unperturbed equilibrium (red dashed line).

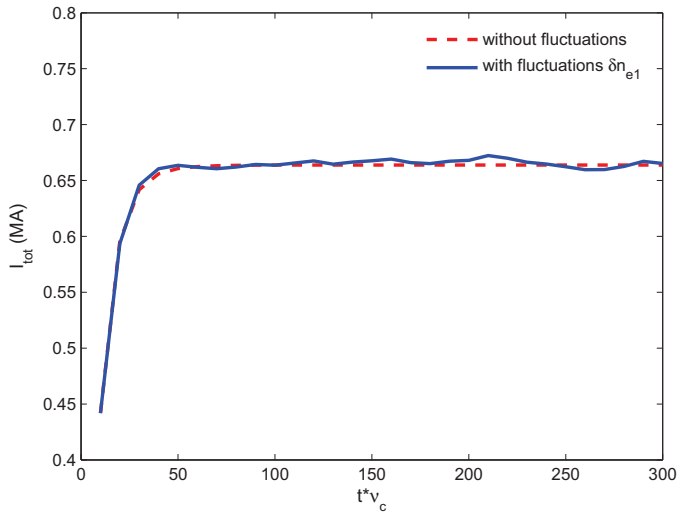

Figure 4.22: Comparison between the total current generated by LH waves in an equilibrium with the background density perturbation $\widetilde{n}_{e1}$ (blue solid line) and the total current generated injecting the same $P_{LH} = 20$MW and launching the same number of rays with the same initial conditions in an unperturbed equilibrium (red dashed line). The total current is plotted in function of the normalized time $t\nu_c$. The quasilinear iteration time step is $\Delta\tau\nu_c = 10$.

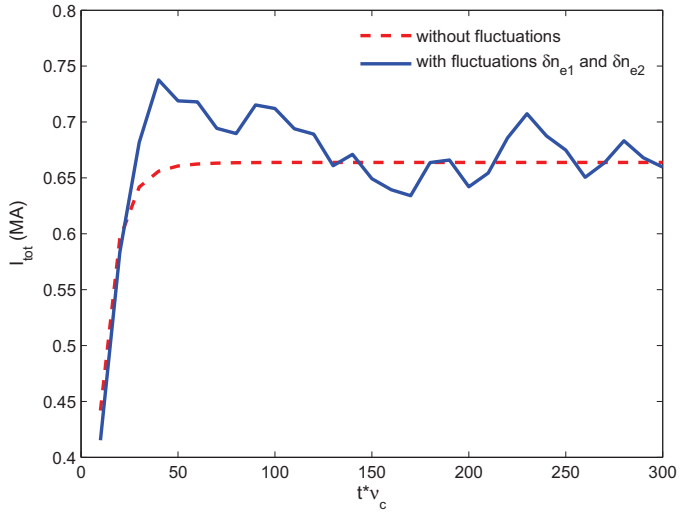

Figure 4.23: Comparison between the total current generated by LH waves in an equilibrium with both the density perturbations $\widetilde{n}_{e1}$ and $\widetilde{n}_{e2}$ (blue solid line) and the total current generated injecting the same $P_{LH} = 20$MW and launching the same number of rays with the same initial conditions in an unperturbed equilibrium (red dashed line). The total current is plotted in function of the normalized time $t\nu_c$. The normalized quasilinear iteration time step is $\Delta\tau\nu_c = 10$.

In Fig.(4.22), the variations respect to the evolution without perturbations, represented by the red dashed line, are visible, even if only the background process $\widetilde{n}_{e1}$ is considered, taking into account also $\widetilde{n}_{e2}$ the oscillations amplitude increase considerably, and a small downshift in the final value of the total current produced is observed ($I_{tot} = 0.66388$MA in the case without fluctuations and $I_{tot} = 0.65961$MA with $\widetilde{n}_{e1}$ and $\widetilde{n}_{e2}$).
The effects of density fluctuations on lower hybrid current drive has been tested in an ITER relevant scenario using two perturbation models having spatial profiles with characteristics similar to fluctuations detected in several experiments [1]. The current density and power deposition profiles are not very sensitive to these fluctuations processes. The power in deposited in a localized area of the plasma near the edge (Figs.(4.20) and (4.21)), and it is fully absorbed before than the rays reach the center of the plasma, then the ray trajectory is not significantly modified by fluctuations. The total current generated by LH waves is the quantity most sensitive to electron density perturbations, and a downshift in the value of I_{tot} can be finally observed.

4.6 ECCD in an ITER scenario with perturbed equilibrium

The effects of density fluctuations on electron cyclotron current drive (ECCD) are investigated with some applications of the model to ITER operational scenario 2 [41]. Plasma parameters characteristics of ITER scenario 2 are reported in table (4.4).

plasma minor radius a_p	1.85m
plasma major radius R_p	6.35m
on-axis magnetic field B_{T0}	5.3T
central electron density $\overline{n}_{e0}$	$10.2 \times 10^{19}\mathrm{m}^{-3}$
edge electron density $\overline{n}_{ea}$	$5.85 \times 10^{19}\mathrm{m}^{-3}$
central electron temperature $\overline{T}_{e0}$	25KeV
edge electron temperature $\overline{T}_{ea}$	2.2KeV
central effective charge Z_{eff0}	1.7
edge effective charge Z_{effa}	1.56

Table 4.4: Parameters of ITER scenario 2

The poloidal section of the magnetic flux surfaces correspondent to ITER scenario 2 equilibrium, evaluated with the 2-D Grad-Shafranov solver HELENA [30], is shown in Fig.(4.24), and the radial profiles of the unperturbed equilibrium quantities are illustrated in Fig.(4.25).

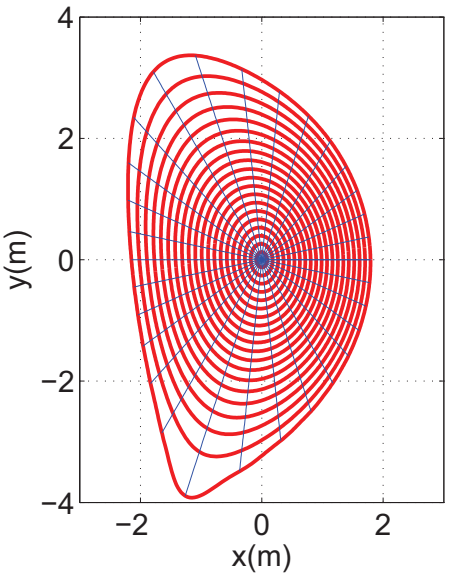

Figure 4.24: Poloidal section of the magnetic flux surfaces correspondent to $\psi = cost$ for the ITER scenario 2 equilibrium. The red and the blue lines are respectively the contours of constant ψ and θ.

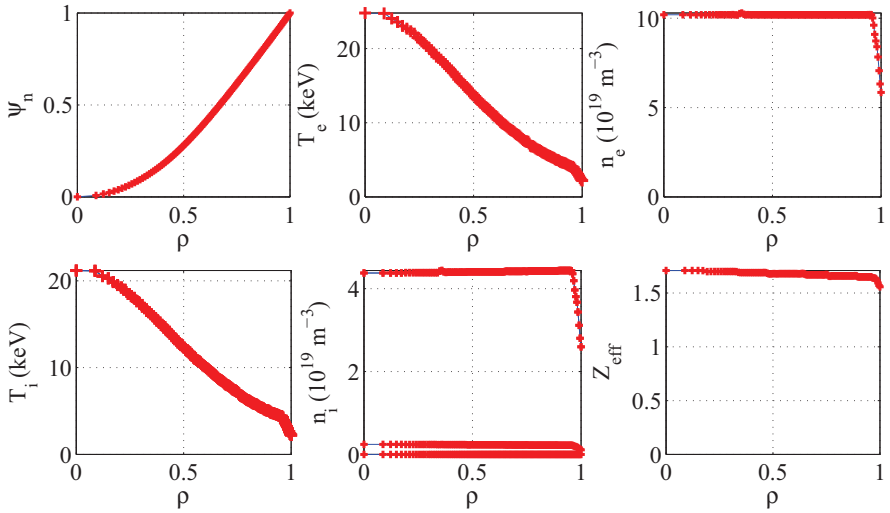

Figure 4.25: Radial profiles of normalized poloidal magnetic flux, electron temperature, electron density, ion temperatures, ion densities, and effective charge for the ITER scenario 2 equilibrium.

The electron cyclotron frequency is $f_{EC} = \omega_{EC}/2\pi = 170$GHz and simulations are performed with first harmonic O-mode and second harmonic X-mode, because the ECCD system projected for ITER is based on the combination of these two modes. The waves are excited from the poloidal launching position $R_L = 6.4848$m,$Z_L = 4.11$m and are described by 246 rays launched from these position. Since simulations are performed just to test the applicability of the model to ECCD calculations, and to give an example of fluctuations effect on EC current density and power deposition profiles, the small non operational value $P_{EC} = 1 \cdot 10^{-6}$MW $= 1$W for the power injected by EC waves into the plasma is taken, and the power carried by each ray is $P_{ray} = P_{EC}/N$ where N is the number of rays. Two different electron density fluctuations processes are considered, and the associated perturbations $\widetilde{n}_{e1}$ and $\widetilde{n}_{e2}$ are both calculated in the local approximation assuming a number of oscillations $N_{\widetilde{k}_\perp} = 900$ with normalized correlation wave vector $a_p k_{\perp c} = 300$. The first process ($\widetilde{n}_{e1}$) is a background perturbation having maximum level $\sigma_{ne1max} = 3\%$ at $\rho = \rho_0 = 0.5$, semi-amplitude parameter $\Delta\rho = 0.5$ and no poloidal dependence ($\lambda = 0$), while the second ($\widetilde{n}_{e2}$) presents a very thin spatial profile peaked at the plasma edge ($\rho_0 = 1$) with a maximum relative level $\sigma_{ne2max} = 50\%$, semi-amplitude parameter $\Delta\rho = 0.02$ and a strong poloidal dependence ($\rho = 0.54$). $\widetilde{n}_{e2}$ describes the fluctuations with high relative level and strong poloidal depencence detected at the plasma edge in many devices [1]. The radial evolution of σ_{ne1} and σ_{ne2} and the poloidal dependence of σ_{ne2} are reported in Fig.(4.26).

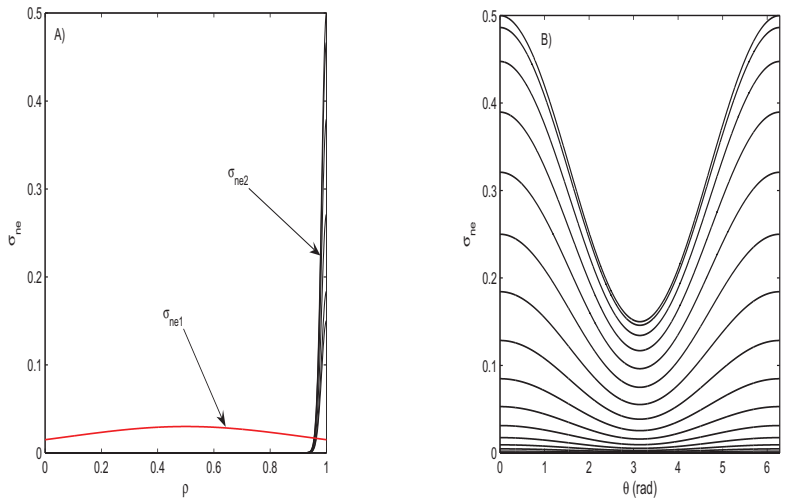

Figure 4.26: A) Radial dependence of the spatial profiles associated with the two fluctuations processes considered in ECCD simulations in ITER scenario 2: the red line corresponds to $\widetilde{n}_{e1}$, peaked at $\rho = \rho_0 = 0.5$ and having $\sigma_{ne1max} = 3\%, \lambda = 0, \Delta\rho = 0.5$, while the black line corresponds to $\widetilde{n}_{e2}$, peaked at the edge and having $\sigma_{ne2max} = 50\%, \lambda = 0.54, \Delta\rho = 0.02$; B) Poloidal depencence of the spatial profile σ_{ne2} correspondent to the perturbation $\widetilde{n}_{e2}$;

In Figs.(4.27) and (4.28) the parallel refractive index of the rays used for ECCD calculations with first harmonic O-mode (Fig.(4.27)) and second harmonic X-mode (Fig.(4.28)) in presence of fluctuations are reported (blue lines) and compared with the case without fluctuations (red lines). As the rays enter into the plasma, they experience immediately the fluctuations effects, and the parallel index of refraction start oscillating respect to the case without perturbations. The behaviour of the refractive index presents a great variation respect to the case without fluctuations at the beginning of the trajectories, near the edge, where the perturbation $\widetilde{n}_{e2}$ has the maximum, when the rays penetrate into the plasma, the value of $\widetilde{n}_{e1}$ vanishes and the small oscillations are due to the background perturbation $\widetilde{n}_{e1}$. In Figs.(4.29) and (4.30) the current density generated by EC waves considering the effects of the perturbations $\widetilde{n}_{e1}$ and $\widetilde{n}_{e2}$ is reported in function of the radial coordinate ρ and compared with the current density generated in the case without fluctuations injecting the same power $P_{EC} = 1 \cdot 10^{-6}$MW and launching the same number of rays with identical initial conditions. An evident drop of the maximum current density level from $J_{max} \approx 7 \cdot 10^{-9}\mathrm{MA/m^2}$ to $J_{max} \approx 2 \cdot 10^{-9}\mathrm{MA/m^2}$ and a consistent spreading of the profiles respect to the case without fluctuations is observed for both O-mode and X-mode, thus the current density generated by EC waves in ITER scenarios is strongly affected by density fluctuations of the level of 50%, and the consequences of these perturbations are a considerable broadening of the current density profiles and a drop of the local maximum of the driven current. Obviously, this behaviour is connected to the broadening of the profiles of the power density deposited by the waves into the plasma, reported in Fig.(4.31) for the O-mode and in Fig.(4.32) for the X-mode. The total current generated by O-mode and X-mode is plotted in Figs.(4.33) and (4.34) in function of the normalized time $t\nu_c$ introduced in the previous section, also for ECCD simulations it has been assumed the value $\nu_c \Delta\tau = 10$ for the normalized quasilinear time step. The effects of the fluctuations on this quantity is very impressive and a downshift ΔI_{tot} in the value of I_{tot} is observed: $\Delta I_{tot}/I_{tot} \approx 18\%$ for the O-mode and $\Delta I_{tot}/I_{tot} \approx 7\%$ for the X-mode.
The lack of localization in the power deposition and the consequent broadening of the current density profiles, the drop of the current density and the downshift in the total current generated by electron density fluctuations may have an important negative consequence on the possibility of controling the MHD instabilities in ITER scenarios generating non-inductive current by means of electron cyclotron waves [39]; with the purpose of indentifying the level of edge density fluctuations above which the current density and the power deposition profiles are consistently modified, several simulations have been performed for the X-mode considering the perturbations $\widetilde{n}_{e1}$ and $\widetilde{n}_{e2}$ and varying the maximum level of the edge fluctuations process $\widetilde{n}_{e2}$, assuming the values $\sigma_{ne2max} = 10\%, 30\%, 50\%$. The current and power density deposition profiles calculated with the different levels of edge fluctuations are reported using different blue graduations in Figs.(4.35) and (4.36).

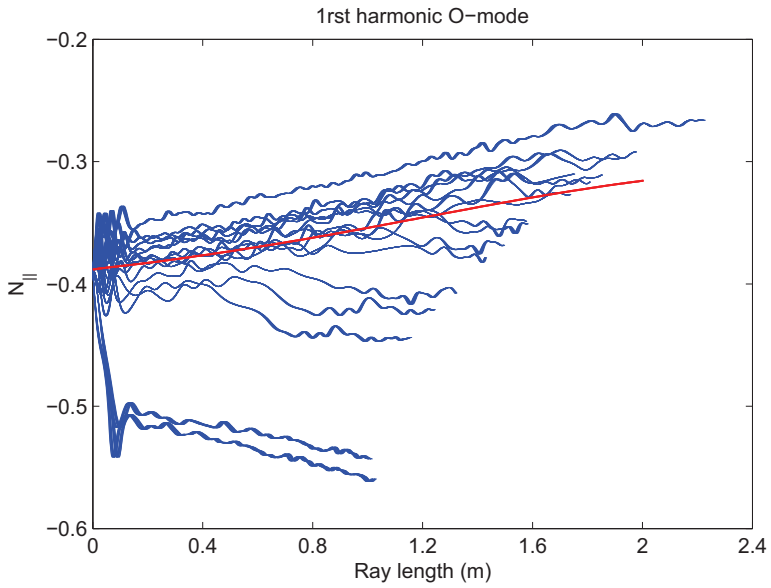

Figure 4.27: Comparison between the evolution of $N_{\parallel}$ along the trajectories of the rays used for ECCD calculations with 1rst harmonic O-mode in presence of fluctuations (blue lines) and the behaviour of $N_{\parallel}$ in the case without fluctuations (red lines).

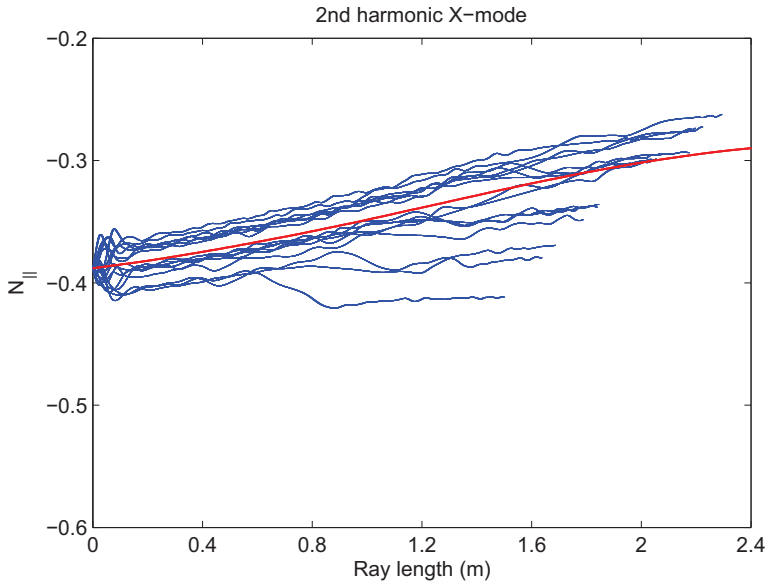

Figure 4.28: Comparison between the evolution of $N_{\parallel}$ along the trajectories of the rays used for ECCD calculations with 2nd harmonic X-mode in presence of fluctuations (blue lines) and the behaviour of $N_{\parallel}$ in the case without fluctuations (red lines).

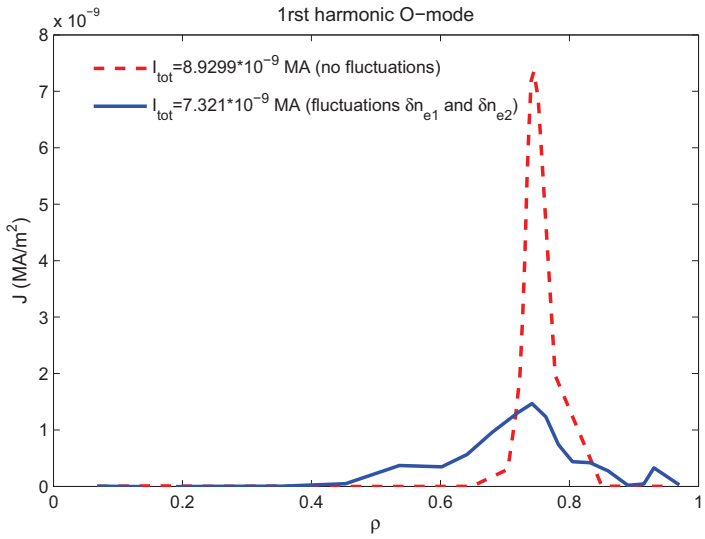

Figure 4.29: Comparison between the current density generated by 1rst harmonic O-mode EC waves in an equilibrium with the density perturbations $\widetilde{n}_{e1}$ and $\widetilde{n}_{e2}$ (blue solid line) and the current density generated injecting the same $P_{EC} = 1 \cdot 10^{-6}$MW and launching the same number of rays with the same initial conditions in an unperturbed equilibrium (red dashed line).

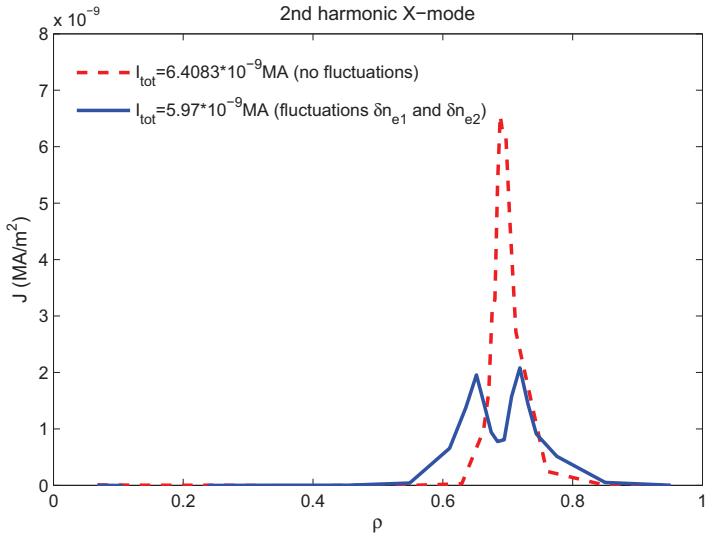

Figure 4.30: Comparison between the current density generated by 2nd harmonic X-mode EC waves in an equilibrium with the density perturbations $\widetilde{n}_{e1}$ and $\widetilde{n}_{e2}$ (blue solid line) and the current density generated injecting the same $P_{EC} = 1 \cdot 10^{-6}$MW and launching the same number of rays with the same initial conditions in an unperturbed equilibrium (red dashed line).

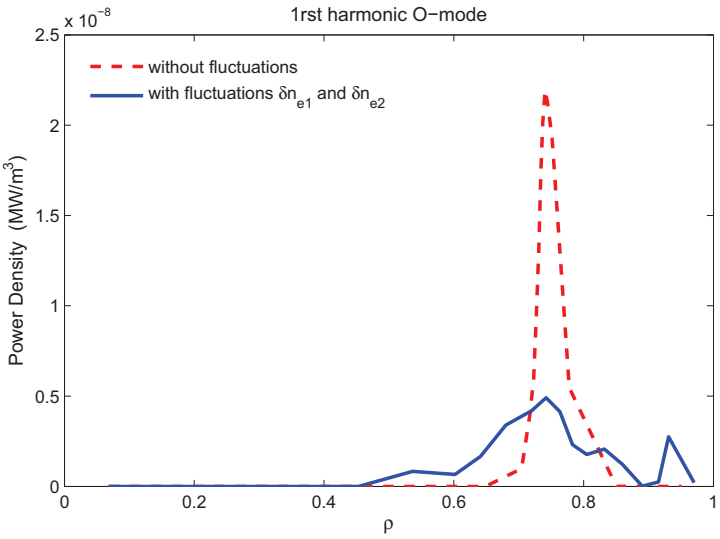

Figure 4.31: Comparison between the EC 1rst harmonic O-mode power deposition profiles evaluated in an equilibrium with the density perturbations $\widetilde{n}_{e1}$ and $\widetilde{n}_{e2}$ (blue solid line) and the EC 1rst harmonic O-mode power deposition profiles evaluated injecting the same $P_{EC} = 1 \cdot 10^{-6}$MW and launching the same number of rays with the same initial conditions in an unperturbed equilibrium (red dashed line).

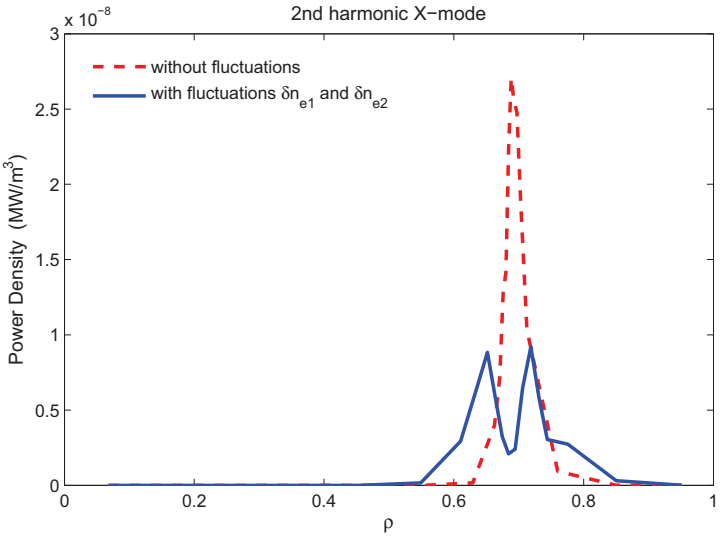

Figure 4.32: Comparison between the EC 2nd harmonic X-mode power deposition profiles evaluated in an equilibrium with the density perturbations $\widetilde{n}_{e1}$ and $\widetilde{n}_{e2}$ (blue solid line) and the EC 2nd harmonic X-mode power deposition profiles evaluated injecting the same $P_{EC} = 1 \cdot 10^{-6}$MW and launching the same number of rays with the same initial conditions in an unperturbed equilibrium (red dashed line).

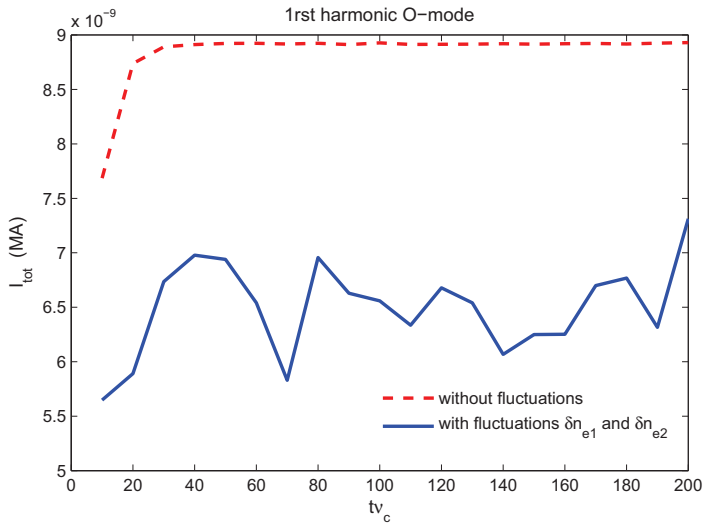

Figure 4.33: Comparison between the total current generated by 1rst harmonic O-mode EC waves in an equilibrium with the perturbations $\widetilde{n}_{e1}$ and $\widetilde{n}_{e2}$ (blue solid line) and the total current generated injecting the same $P_{EC} = 1 \cdot 10^{-6}$MW and launching the same number of rays with the same initial conditions in an unperturbed equilibrium (red dashed line). The total current is plotted in function of the normalized time $t\nu_c$. The quasilinear iteration time step is $\Delta\tau\nu_c = 10$.

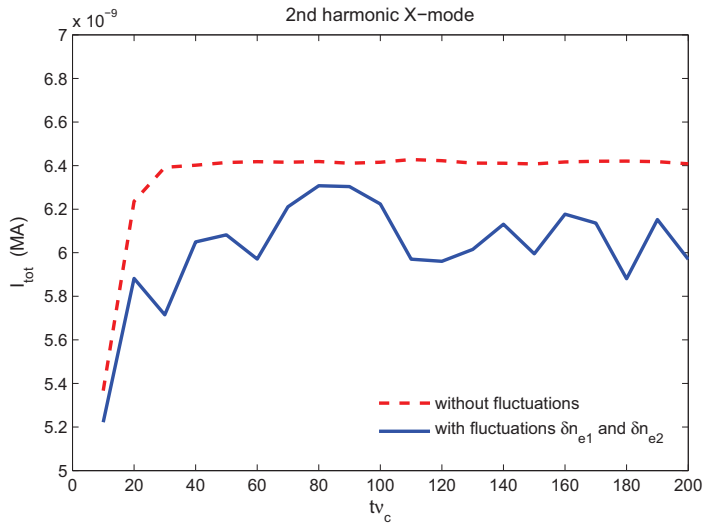

Figure 4.34: Comparison between the total current generated by 2nd harmonic X-mode EC waves in an equilibrium with the perturbations $\widetilde{n}_{e1}$ and $\widetilde{n}_{e2}$ (blue solid line) and the total current generated injecting the same $P_{EC} = 1 \cdot 10^{-6}$MW and launching the same number of rays with the same initial conditions in an unperturbed equilibrium (red dashed line). The total current is plotted in function of the normalized time $t\nu_c$. The quasilinear iteration time step is $\Delta\tau\nu_c = 10$.

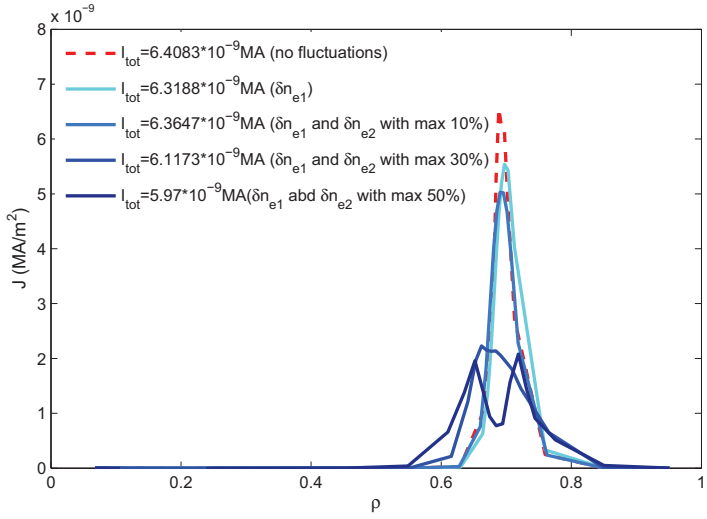

Figure 4.35: Comparison between the current density generated by 2nd harmonic Xmode EC waves in an equilibrium with the density perturbations $\widetilde{n}_{e1}$ and $\widetilde{n}_{e2}$ with different values of the maximum relative level $\sigma_{ne2max} = 10\%, 30\%, 50\%$ (blue colormap lines) and the current density generated injecting the same $P_{EC} = 1 \cdot 10^{-6}$MW and launching the same number of rays with the same initial conditions in an unperturbed equilibrium (red dashed line).

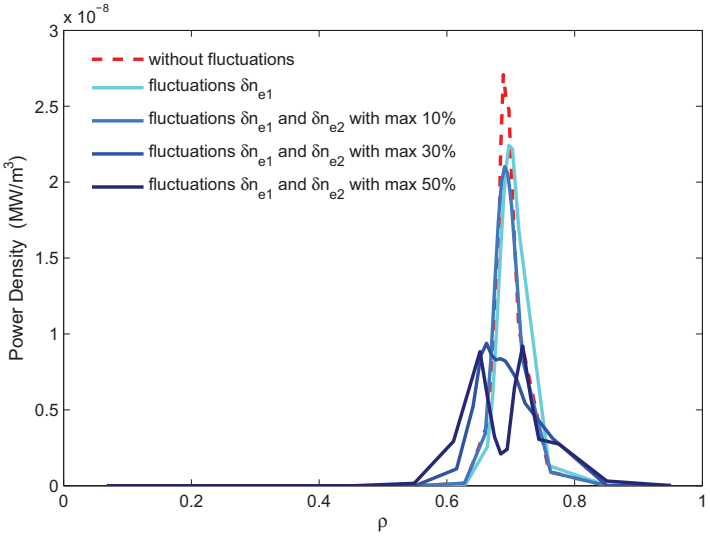

Figure 4.36: Comparison between the power density generated by 2nd harmonic Xmode EC waves in an equilibrium with the density perturbations $\widetilde{n}_{e1}$ and $\widetilde{n}_{e2}$ with different values of the maximum relative level $\sigma_{ne2max} = 10\%, 30\%, 50\%$ (blue colormap lines) and the power density generated injecting the same $P_{EC} = 1 \cdot 10^{-6}$MW and launching the same number of rays with the same initial conditions in an unperturbed equilibrium (red dashed line).

The profiles calculated with the different levels of edge fluctuations are compared with the case without equilibrium perturbations (red dashed line). Considering only the background perturbation $\widetilde{n}_{e1}$ (wich presents $\sigma_{ne1max} = 3\%$), or assuming the maximum relative fluctuations level at the edge $\sigma_{ne2max} = 10\%$, the only effect on the profiles is a little drop of the local current density and power density maximum, no significant broadening is observed. If the maximum relative level of the edge perturbation $\widetilde{n}_{e2}$ becomes 30% or 50%, instead, a great broadening is detected and the profiles are strongly modified for effect of the fluctuations, then if the level of electron density fluctuations is above the $20 - 30\%$ at the edge in an ITER like scenario the current density and the power deposition profiles are significantly affected by the perturbations and the localization of the power deposited by the EC waves into the plasma is changed. Since these modifications in the localization and in the values of the current generated can compromize the possibility of stabilization the neoclassical tearing modes (NTM) in future ITER operative scenarios, a complete analysis of the fluctuations effects, including also magnetic perturbations and ripple and describing them on the base of experimental data taken from other devices, is a crucial issue for modeling ECCD experiments in a more realistic way and individuating the conditions for having an efficient control of the MHD instabilities through electron cyclotron current drive [39].

Chapter 5

Conclusions and future perspectives

In this thesis a general model for studying the fluctuations effects on radiofrequency waves current drive in toroidal plasmas in the framework of the quasilinear description of wave-particle interaction is presented. These effects are represented as time dependent perturbations of the magnetic equilibrium quantities, characterized by a phase and an amplitude, which explicit expressions can be setted on the basis of the physical characteristics of the different fluctuations processes. The corrections to the ray equations due to the perturbations are derived explicitely and implemented in the fast universal raytracing code C3PO [21], coupled with the 3-D Fokker-Planck solver LUKE, developed for radiofrequency current drive simulations in toroidal plasmas with arbitrary magnetic equilibrium [22]. All the fluctuations processes which evolution time scales is much slower than wave propagation time scales and bounce particle motion time scales, preserving the limit of applicability of the WKB eikonal ansatz in the solution of the Maxwell's equation, the validity of the quasilinear description of wave-particle interaction and the bounce-averaging procedure of the kinetic equation, can be described by the proposed model, without any other restriction. Since their time scales are much slower than waves propagation times, fluctuations are considered as static in the time interval over which the ray equations are integrated and the ray path is calculated in the perturbed non-axisymmetric equilibrium, while the quasilinear loop for estimating the radiofrequency diffusion coefficient and calculating the electron distribution function (LUKE code), is setted up taking into account the time evolution of the fluctuations modes, which is comparable with the collisional period. The electron distribution function can then be evaluated solving the kinetic equation and taking into account the effect of the long time scale evolution of the fluctuations, and the value of the current generated by the waves and its density profile can be estimated using the perturbed equilibrium, as far the perturbed magnetic flux surfaces remain nested.
Two examples of fluctuations processes which effects on radiofrequency current

drive can be described using the proposed approach are presented: stochastic fluctuations of the electron density and of the magnetic field, induced by electron drift waves and other MHD modes propagating into the plasma [10, 11, 12], and ripple magnetic field, which is due to the descrete structure of the system for the generation of the toroidal magnetic field in the devices, based on a finite set of bobines [31, 32]. Explicit expressions of the equilibrium perturbations describing the effects of these processes are derived on the basis of their physical characteristics and discussed in details.
The perturbations generated by the MHD modes are periodic time-dependent oscillations having a random contribution to the phase, lying on the magnetic flux surfaces and directed perpendicularly to the unperturbed magnetic field lines. All these characteristics are well described by the global representation based on the Fourier series sum illustrated in subsection 3.1.2, and also the exact relationship between the perturbations amplitude and the wave vector spectral distribution is derived starting from this, nevertheless the implementation of the global representation implies several numerical difficulties, in particular connected with the condition of periodicity of the perturbations. For this reason an alternative local representation, where the fluctuations phase is given by an eikonal-like expression and the amplitude of the pertubations depends by the spectral distribution of the wave vector and by the spatial profile of the relative level of fluctuations is proposed. The local eikonal-like representation is a good approximation of the general non-local model for high values of the fluctuations wave vector, and implies the lack of the periodicity in space of the perturbations, while preserves the other characteristics of the oscillations.
The ripple magnetic field is described by a static perturbation of the equilibrium field which phase is a function of the number of coils N and of the toroidal angle ϕ, and which amplitude depends by the geometrical properties of the bobines. Explicit expressions for the amplitude of the toroidal ripple magnetic field and for the components of the ripple perturbation generated by a set of N identical circular coils are reported and discussed in details [31, 32].
The effects of the fluctuations on lower hybrid rays propagation are tested in a JET-like scenario: ray trajectories and evolution of the refractive index components in presence of density and magnetic field fluctuations and magnetic ripple are reported and compared with the case without perturbations. The rays trajectories and all the components of the refractive index are detected to be very sensitive to electron density fluctuations processes, which in operative scenarios present the maximum relative level at the plasma edge [11, 12], while the only quantity strongly affected by magnetic field fluctuations, generally peaked in the interior of the plasma [12], is the toroidal wave number n. Since the toroidal wave number is no longer a constant of the ray evolution, both density and magnetic fluctutions induce a breaking in the axisymmetry of the system. For effects of density fluctuations the ray trajectory becomes stochastic, this means that the evolution of rays launched by the same posi-

tion with identical initial values of the spectral quantities (ω and N) in the same scenario can be different. The ripple magnetic field modifies also strongly the trajectories and induces a regular modulation of the toroidal wave number n, the frequency of the oscillations is constant and depends by the number of coils present in the magnetic system, while the amplitude is great when the ray propagates in proximity of the plasma edge, where the ripple effect is strong and it is dominant also respect to density drift-like fluctuations, and drops rapidly as the wave penetrates into the core, where the ripple effects are negligible.

Lower hybrid (LH) and electron cyclotron (EC) current drive simulations in ITER operative scenarios 2 and 4 [40, 41] considering drift wave type fluctuations of the electronic density are performed and the results are reported and discussed in details. The fluctuations effects on lower hybrid current density and power deposition profiles in ITER scenario 4 are negligible, the only quantity lightly affected by the perturbations in LHCD simulations is the total current generated by the waves, and a small downshift in the value of I_{tot} $(1-2\%)$ is observed taking a maximum fluctuations level of 30% at the plasma edge. On the contrary, density fluctuations, even if they are well localized at the plasma edge, affect strongly current density and power deposition profiles generated by electron cyclotron waves in ITER scenario 2: significant broadening of the profiles and delocalization of the deposited power are observed for both 1rst harmonic O-mode and 2nd harmonic X-mode taking maximum fluctuations levels of 30% and 50%, in particular the O-mode is found more sensitive to these effects. Through a comparative analysis between the results of several ECCD simulations, a level of density fluctuations at the edge between the 20% and the 30% is individuated as the threshold above which a significant broadening of the current density profiles is detected. Since the broadening of the current density profiles and the delocalization of the deposited power might compromize the possibility of stabilization of the neoclassical tearing modes (NTM) through electron cyclotron current drive in future ITER operative scenarios [39], a complete and detailed analysis of the fluctuations effects, including also magnetic perturbations and ripple, exploring experimental scenarios in existing tokamaks with several levels of fluctuations and comparing experimental data with code predictions is a crucial issue for improving the comprehension and the interpretation of ECCD experiments and individuating the conditions for having an efficient control of the MHD instabilities in future ITER scenarios.

The versatility of the developed model makes possible its application in the analysis of a great number of scenarios, and its extension to the study of fluctuations processes which present different physical properties. Simulations of discharges fully driven by LH waves in Tore Supra tokamak will be performed considering the equilibrium perturbations, and the influence of plasma fluctuations on bridging the spectral gap [33, 35] will be studied in details and discussed. More realistic representations of MHD modes induced perturba-

tions could be implemented in future, defining an expression for the amplitude with a random term (actually the random contribution is contained only in the phase), or coupling the package C3PO-LUKE with gyrokinetic simulation codes. The implementation of the global representation illustrated in the third chapter of the thesis could make possible a more accurated estimation of the effects of the perturbations with small wave vector values, and a coherent modeling of the processes generated by several MHD modes (balooning instabilities). The expressions for the ripple field components could be extended to the general case of non-circular bobines by means of the numerical solution of the magnetic potential equations [31].

Appendix A

Coordinates systems

In this appendix the detailed definition of curvilinear coordinates systems describing the configuration space introduced in section 2.2 is illustrated together with explicit expressions for the position vector and for the covariant and contravariant basis. A more complete description of these sets of coordinates, including also expressions for the metric coefficients, the Christoffel symbols and the differential operators, is reported in reference [22].

A.1 System (R, Z, ϕ)

Definition

The coordinates (R, Z, ϕ) are defined on the following space:

$$\begin{aligned} 0 &\leq R \leq +\infty \\ -\infty &\leq Z \leq +\infty \\ 0 &\leq \phi < 2\pi \end{aligned} \tag{A.1}$$

They are related to the cartesian coordinates (x, y, z) by the expressions:

$$\begin{aligned} R &= \sqrt{x^2 + y^2} \\ Z &= -z \\ \phi &= \arctan(y/x) + \pi H(-x) \quad [2\pi] \end{aligned} \tag{A.2}$$

These relations can be inverted to:

$$\begin{aligned} x &= R\cos\phi \\ y &= R\sin\phi \\ z &= -Z \end{aligned} \tag{A.3}$$

Position vector

The position vector is given by the following expression:

$$\mathbf{X} = R\hat{R} + Z\hat{Z} \tag{A.4}$$

Where the orthonormal basis $\left(\hat{R}, \hat{Z}, \hat{\phi}\right)$ is defined as:

$$\begin{aligned} \hat{R} &= \cos\phi\hat{x} + \sin\phi\hat{y} \\ \hat{Z} &= -\hat{z} \\ \hat{\phi} &= \hat{R} \times \hat{Z} = -\sin\phi\hat{x} + \cos\phi\hat{y} \end{aligned} \tag{A.5}$$

Covariant basis

The covariant vector basis is defined as follows:

$$\begin{aligned} \mathbf{e}_R &= \frac{\partial \mathbf{X}}{\partial R} = \hat{R} \\ \mathbf{e}_Z &= \frac{\partial \mathbf{X}}{\partial Z} = \hat{Z} \\ \mathbf{e}_\phi &= \frac{\partial \mathbf{X}}{\partial \phi} = R\frac{\partial \hat{R}}{\partial \phi} = R\hat{\phi} \end{aligned} \tag{A.6}$$

Such that the covariant basis becomes:

$$(\mathbf{e}_R, \mathbf{e}_Z, \mathbf{e}_\phi) = \left(\hat{R}, \hat{Z}, R\hat{\phi}\right) \tag{A.7}$$

The scaling factors are:

$$(h_R, h_Z, h_\phi) = (1, 1, R) \tag{A.8}$$

And the normalized tangent basis is:

$$(\hat{e}_R, \hat{e}_Z, \hat{e}_\phi) = \left(\hat{R}, \hat{Z}, \hat{\phi}\right) \tag{A.9}$$

Contravariant basis

The contravariant vector basis is defined as follows:

$$\begin{aligned} \mathbf{e}^R &= \nabla R = \hat{R} \\ \mathbf{e}^Z &= \nabla Z = \hat{Z} \\ \mathbf{e}^\phi &= \nabla \phi = \frac{\hat{\phi}}{R} \end{aligned} \tag{A.10}$$

Such that the contravariant basis becomes:

$$\left(\mathbf{e}^R, \mathbf{e}^Z, \mathbf{e}^\phi\right) = \left(\hat{R}, \hat{Z}, \frac{\hat{\phi}}{R}\right) \tag{A.11}$$

And the normalized reciprocal basis is:

$$\left(\hat{e}^R, \hat{e}^Z, \hat{e}^\phi\right) = \left(\hat{R}, \hat{Z}, \hat{\phi}\right) \tag{A.12}$$

In this system, the normalized reciprocal basis coincides with the normalized tangent basis, since both bases are orthogonal.

A.2 System (r, θ, ϕ)

The coordinates (r, θ, ϕ) are referred to the magnetic axis (R_p, Z_p) (see Fig.(2.2)) and are defined on the following space:

$$\begin{aligned} 0 &\leq r \leq +\infty \\ 0 &\leq \theta < 2\pi \\ 0 &\leq \phi < 2\pi \end{aligned} \tag{A.13}$$

They are related to (R, Z, ϕ) by the expressions:

$$\begin{aligned} r &= \sqrt{(R - R_p)^2 + (Z - Z_p)^2} \\ \theta &= \arctan((Z - Z_p)/(R - R_p)) + \pi H(R_p - R) \qquad [2\pi] \end{aligned} \tag{A.14}$$

These relations can be inverted to:

$$\begin{aligned} R &= R_p + r\cos\theta \\ Z &= Z_p + r\sin\theta \end{aligned} \tag{A.15}$$

Position vector

The position vector is given by the following expression:

$$\mathbf{X} = R_p\hat{R} + Z_p\hat{Z} + r\hat{r} \tag{A.16}$$

Where the orthonormal basis $\left(\hat{r}, \hat{\theta}, \hat{\phi}\right)$ is defined as:

$$\begin{aligned} \hat{r} &= \cos\theta\hat{R} + \sin\theta\hat{Z} \\ \hat{\theta} &= \hat{\phi} \times \hat{r} = -\sin\theta\hat{R} + \cos\theta\hat{Z} \end{aligned} \tag{A.17}$$

Since:

$$\begin{aligned} \hat{\phi} \times \hat{r} &= \left(\hat{R} + \hat{Z}\right) \times \left(\cos\theta\hat{R} + \sin\theta\hat{Z}\right) \\ &= \left[\left(\cos\theta\hat{R} + \sin\theta\hat{Z}\right) \cdot \hat{R}\right]\hat{Z} - \left[\left(\cos\theta\hat{R} + \sin\theta\hat{Z}\right) \cdot \hat{Z}\right]\hat{R} \\ &= \cos\theta\hat{Z} - \sin\theta\hat{R} \end{aligned} \tag{A.18}$$

Covariant basis

The covariant vector basis is defined as follows:

$$\begin{aligned} \mathbf{e}_r &= \frac{\partial \mathbf{X}}{\partial r} = \hat{r} \\ \mathbf{e}_\theta &= \frac{\partial \mathbf{X}}{\partial \theta} = r\frac{\partial \hat{r}}{\partial \theta} = r\hat{\theta} \\ \mathbf{e}_\phi &= \frac{\partial \mathbf{X}}{\partial \phi} = R_p\frac{\partial \hat{R}}{\partial \phi} + r\frac{\partial \hat{r}}{\partial \phi} = (R_p + r\cos\theta)\frac{\partial \hat{R}}{\partial \phi} = R\hat{\phi} \end{aligned} \tag{A.19}$$

Such that the covariant basis becomes:

$$(\mathbf{e}_r, \mathbf{e}_\theta, \mathbf{e}_\phi) = \left(\hat{r}, r\hat{\theta}, R\hat{\phi}\right) \tag{A.20}$$

The scaling factors are:

$$(h_r, h_\theta, h_\phi) = (1, r, R) \tag{A.21}$$

And the normalized tangent basis is:

$$(\hat{e}_r, \hat{e}_\theta, \hat{e}_\phi) = \left(\hat{r}, \hat{\theta}, \hat{\phi}\right) \tag{A.22}$$

Contravariant basis

The contravariant vector basis is defined as follows:

$$\begin{aligned} \mathbf{e}^r &= \nabla r = \hat{r} \\ \mathbf{e}^\theta &= \nabla \theta = \frac{\hat{\theta}}{R} \\ \mathbf{e}^\phi &= \nabla \phi = \frac{\hat{\phi}}{R} \end{aligned} \tag{A.23}$$

Such that the contravariant basis becomes:

$$\left(\mathbf{e}^r, \mathbf{e}^\theta, \mathbf{e}^\phi\right) = \left(\hat{r}, \frac{\hat{\theta}}{R}, \frac{\hat{\phi}}{R}\right) \tag{A.24}$$

And the normalized reciprocal basis is:

$$\left(\hat{e}^r, \hat{e}^\theta, \hat{e}^\phi\right) = \left(\hat{r}, \hat{\theta}, \hat{\phi}\right) \tag{A.25}$$

Also in this system, the normalized reciprocal basis coincides with the normalized tangent basis, since both bases are orthogonal.

A.3 System (ψ, s, ϕ)

Definition

The coordinates (ψ, s, ϕ) are in general used to parametrize toroidal magnetic configurations with closed flux surfaces, and are defined from the origin (R_p, Z_p) on the closed space:

$$\begin{aligned} \min(\psi_0, \psi_a) &\leq \psi \leq \max(\psi_0, \psi_a) \\ 0 &\leq \theta \leq s_{\max} \end{aligned} \tag{A.26}$$

Where ψ_0 is the value of the poloidal flux function at the center (R_p, Z_p) and ψ_a is the value at the edge. These flux coordinates are related to (r, θ, ϕ) by the expressions:

$$\begin{aligned} \psi &= \psi(r, \theta) \\ s &= s(r, \theta) \end{aligned} \tag{A.27}$$

These relations can be inverted to:

$$\begin{aligned} r &= r(\psi, s) \\ \theta &= \theta(\psi, s) \end{aligned} \tag{A.28}$$

$\psi(r, \theta)$ must be a monotonic function of the radial coordinate r from ψ_0 at the center to ψ_a at the edge. This is the condition for having nested flux surfaces [25]. The local orthonormal basis $\left(\hat{\psi}, \hat{s}, \hat{\phi}\right)$ is defined as follows:

$$\begin{aligned} \hat{\psi} &= \frac{\nabla\psi}{|\nabla\psi|} \\ \hat{s} &= \hat{\phi} \times \hat{\psi} \end{aligned} \tag{A.29}$$

The trasformation from $\left(\hat{r}, \hat{\theta}\right)$ to $\left(\hat{\psi}, \hat{s}\right)$ is a rotation of angle α such that:

$$\begin{pmatrix} \hat{\psi} \\ \hat{s} \end{pmatrix} = \begin{pmatrix} \cos\alpha & -\sin\alpha \\ \sin\alpha & \cos\alpha \end{pmatrix} \cdot \begin{pmatrix} \hat{r} \\ \hat{\theta} \end{pmatrix} \tag{A.30}$$

Position vector

The expression for the position vector is identical to that defined for (r, θ, ϕ) system:

$$\mathbf{X} = R_p\hat{R} + Z_p\hat{Z} + r(\psi, s)\hat{r} \tag{A.31}$$

Covariant basis

The covariant vector basis is defined as follows:

$$\begin{aligned}
\mathbf{e}_\psi &= \frac{\partial \mathbf{X}}{\partial \psi} = \frac{\partial r}{\partial \psi}\bigg|_s \hat{r} + r\frac{\partial \hat{r}}{\partial \psi}\bigg|_s = \frac{\partial r}{\partial \psi}\bigg|_s \hat{r} + r\frac{\partial \theta}{\partial \psi}\bigg|_s \hat{\theta} \\
\mathbf{e}_s &= \frac{\partial \mathbf{X}}{\partial s} = \frac{\partial r}{\partial s}\bigg|_\psi \hat{r} + r\frac{\partial \hat{r}}{\partial s}\bigg|_\psi = \frac{\partial r}{\partial s}\bigg|_\psi \hat{r} + r\frac{\partial \theta}{\partial s}\bigg|_\psi \hat{\theta} \\
\mathbf{e}_\phi &= \frac{\partial \mathbf{X}}{\partial \phi} = R_p\frac{\partial \hat{R}}{\partial \phi} + r\frac{\partial \hat{r}}{\partial \phi} = (R_p + r\cos\theta)\frac{\partial \hat{R}}{\partial \phi} = R\hat{\phi}
\end{aligned} \tag{A.32}$$

Such that the covariant basis becomes:

$$(\mathbf{e}_\psi, \mathbf{e}_s, \mathbf{e}_\phi) = \left(\frac{\partial r}{\partial \psi}\bigg|_s \hat{r} + r\frac{\partial \theta}{\partial \psi}\bigg|_s \hat{\theta}, \frac{\partial r}{\partial s}\bigg|_\psi \hat{r} + r\frac{\partial \theta}{\partial s}\bigg|_\psi \hat{\theta}, R\hat{\phi}\right) \tag{A.33}$$

The scaling factors are:

$$(h_\psi, h_s, h_\phi) = \left(\sqrt{\frac{\partial r}{\partial \psi}\bigg|_s^2 + r^2\frac{\partial \theta}{\partial \psi}\bigg|_s^2}, \frac{\partial r}{\partial s}\bigg|_\psi^2 + r^2\frac{\partial \theta}{\partial s}\bigg|_\psi^2, R\right) \tag{A.34}$$

And the normalized tangent basis is:

$$(\hat{e}_\psi, \hat{e}_s, \hat{e}_\phi) = \left(\frac{1}{h_\psi}\left[\frac{\partial r}{\partial \psi}\bigg|_s \hat{r} + r\frac{\partial \theta}{\partial \psi}\bigg|_s \hat{\theta}\right], \frac{1}{h_s}\left[\frac{\partial r}{\partial s}\bigg|_\psi \hat{r} + r\frac{\partial \theta}{\partial s}\bigg|_\psi \hat{\theta}\right], \hat{\phi}\right) \tag{A.35}$$

Contravariant basis

The contravariant vector basis is defined as follows:

$$\begin{aligned}
\mathbf{e}^\psi &= \nabla\psi = |\nabla\psi|\hat{\psi} \\
\mathbf{e}^s &= \nabla s = \hat{s} \\
\mathbf{e}^\phi &= \nabla\phi = \frac{\hat{\phi}}{R}
\end{aligned} \tag{A.36}$$

Such that the contravariant basis becomes:

$$\left(\mathbf{e}^\psi, \mathbf{e}^s, \mathbf{e}^\phi\right) = \left(|\nabla\psi|\hat{\psi}, \hat{s}, \frac{\hat{\phi}}{R}\right) \tag{A.37}$$

And the normalized reciprocal basis is:

$$\left(\hat{e}^\psi, \hat{e}^s, \hat{e}^\phi\right) = \left(\hat{\psi}, \hat{s}, \hat{\phi}\right) \tag{A.38}$$

Explicit expressions for the components of the tangent basis $(\mathbf{e}_\psi, \mathbf{e}_s, \mathbf{e}_\phi)$ can be derived from the reciprocal basis elements:

$$\begin{aligned} \mathbf{e}_\psi &= \frac{\mathbf{e}^s \times \mathbf{e}^\phi}{\mathbf{e}^\psi \cdot \mathbf{e}^s \times \mathbf{e}^\phi} = \frac{\hat{\psi}}{|\nabla\psi|} \\ \mathbf{e}_s &= \frac{\mathbf{e}^\phi \times \mathbf{e}^\psi}{\mathbf{e}^s \cdot \mathbf{e}^\phi \times \mathbf{e}^\psi} = \hat{s} \\ \mathbf{e}_\phi &= \frac{\mathbf{e}^\psi \times \mathbf{e}^s}{\mathbf{e}^\phi \cdot \mathbf{e}^\psi \times \mathbf{e}^s} = R\hat{\phi} \end{aligned} \tag{A.39}$$

Then the covariant basis becomes:

$$(\mathbf{e}_\psi, \mathbf{e}_s, \mathbf{e}_\phi) = \left(\frac{\hat{\psi}}{|\nabla\psi|}, \hat{s}, R\hat{\phi} \right) \tag{A.40}$$

Where the scaling factors are:

$$(h_\psi, h_s, h_\phi) = \left(\frac{1}{|\nabla\psi|}, 1, R \right) \tag{A.41}$$

And the normalized tangent basis is the following:

$$(\hat{e}_\psi, \hat{e}_s, \hat{e}_\phi) = (\hat{\psi}, \hat{s}, \hat{\phi}) \tag{A.42}$$

Also in this case the normalized tangent basis coincides with the normalized reciprocal basis, since both bases are orthogonal. By comparing expressions (A.32) and (A.39) the following relations are derived:

$$\begin{aligned} \left.\frac{\partial r}{\partial \psi}\right|_s &= \frac{\cos\alpha}{|\nabla\psi|} \\ \left.\frac{\partial \theta}{\partial \psi}\right|_s &= \frac{-\sin\alpha}{r|\nabla\psi|} \end{aligned} \tag{A.43}$$

$$\begin{aligned} \left.\frac{\partial r}{\partial s}\right|_\psi &= (\hat{s} \cdot \hat{r}) = \sin\alpha \\ \left.\frac{\partial \theta}{\partial s}\right|_\psi &= \frac{\left(\hat{s} \cdot \hat{\theta}\right)}{r} = \frac{\cos\alpha}{r} \end{aligned} \tag{A.44}$$

A.4 System (ψ, θ, ϕ)

Definition

The coordinates (ψ, θ, ϕ) are defined from the origin (R_p, Z_p) on the space:

$$\min(\psi_0, \psi_a) \leq \psi \leq \max(\psi_0, \psi_a) \tag{A.45}$$

Where ψ_0 is the value of the poloidal flux function at the center (R_p, Z_p) and ψ_a is the value at the edge. These coordinates are related to (r, θ, ϕ) by the expression:

$$\psi = \psi(r, \theta) \tag{A.46}$$

This relation can be inverted to:

$$r = r(\psi, \theta) \tag{A.47}$$

$\psi(r, \theta)$ must be a monotonic function of the radial coordinate r from ψ_0 at the center to ψ_a at the edge. This is the condition for having nested flux surfaces [25].

Position vector

The expression for the position vector is identical to that defined for (r, θ, ϕ) system:

$$\mathbf{X} = R_p\hat{R} + Z_p\hat{Z} + r(\psi, \theta)\hat{r} \tag{A.48}$$

Covariant basis

The covariant vector basis is defined as follows:

$$\begin{aligned}
\mathbf{e}_\psi &= \frac{\partial \mathbf{X}}{\partial \psi} = \frac{\partial r}{\partial \psi}\bigg|_\theta \hat{r} \\
\mathbf{e}_\theta &= \frac{\partial \mathbf{X}}{\partial \theta} = \frac{\partial r}{\partial \theta}\bigg|_\psi \hat{r} + r\frac{\partial \hat{r}}{\partial \theta} = \frac{\partial r}{\partial \theta}\bigg|_\psi \hat{r} + r\hat{\theta} \\
\mathbf{e}_\phi &= \frac{\partial \mathbf{X}}{\partial \phi} = R_p\frac{\partial \hat{R}}{\partial \phi} + r\frac{\partial \hat{r}}{\partial \phi} = (R_p + r\cos\theta)\frac{\partial \hat{R}}{\partial \phi} = R\hat{\phi}
\end{aligned} \tag{A.49}$$

Such that the covariant basis becomes:

$$(\mathbf{e}_\psi, \mathbf{e}_\theta, \mathbf{e}_\phi) = \left(\frac{\partial r}{\partial \psi}\bigg|_\theta \hat{r}, \frac{\partial r}{\partial \theta}\bigg|_\psi \hat{r} + r\hat{\theta}, R\hat{\phi}\right) \tag{A.50}$$

The scaling factors are:

$$(h_\psi, h_\theta, h_\phi) = \left(\frac{\partial r}{\partial \psi}\bigg|_\theta, \sqrt{\frac{\partial r}{\partial \theta}\bigg|_\psi^2 + r^2}, R\right) \tag{A.51}$$

And the normalized tangent basis is:

$$(\hat{e}_\psi, \hat{e}_\theta, \hat{e}_\phi) = \left(\hat{r}, \frac{1}{h_\theta}\left[\frac{\partial r}{\partial \theta}\bigg|_\psi \hat{r} + r\hat{\theta}\right], \hat{\phi}\right) \tag{A.52}$$

Contravariant basis

The contravariant vector basis is defined as follows:

$$\begin{aligned} \mathbf{e}^{\psi} &= \nabla\psi = |\nabla\psi|\hat{\psi} \\ \mathbf{e}^{\theta} &= \nabla\theta = \frac{\hat{\theta}}{r} \\ \mathbf{e}^{\phi} &= \nabla\phi = \frac{\hat{\phi}}{R} \end{aligned} \tag{A.53}$$

Such that the contravariant basis becomes:

$$\left(\mathbf{e}^{\psi}, \mathbf{e}^{\theta}, \mathbf{e}^{\phi}\right) = \left(|\nabla\psi|\hat{\psi}, \frac{\hat{\theta}}{r}, \frac{\hat{\phi}}{R}\right) \tag{A.54}$$

And the normalized reciprocal basis is:

$$\left(\hat{e}^{\psi}, \hat{e}^{\theta}, \hat{e}^{\phi}\right) = \left(\hat{\psi}, \hat{\theta}, \hat{\phi}\right) \tag{A.55}$$

Explicit expressions for the components of the tangent basis $(\mathbf{e}_{\psi}, \mathbf{e}_{\theta}, \mathbf{e}_{\phi})$ can be derived from the reciprocal basis elements:

$$\begin{aligned} \mathbf{e}_{\psi} &= \frac{\mathbf{e}^{\theta} \times \mathbf{e}^{\phi}}{\mathbf{e}^{\psi} \cdot \mathbf{e}^{\theta} \times \mathbf{e}^{\phi}} = \frac{\hat{r}}{|\nabla\psi| \cos\alpha} \\ \mathbf{e}_{\theta} &= \frac{\mathbf{e}^{\phi} \times \mathbf{e}^{\psi}}{\mathbf{e}^{\theta} \cdot \mathbf{e}^{\phi} \times \mathbf{e}^{\psi}} = \frac{r\hat{\theta}}{\cos\alpha} \\ \mathbf{e}_{\phi} &= \frac{\mathbf{e}^{\psi} \times \mathbf{e}^{\theta}}{\mathbf{e}^{\phi} \cdot \mathbf{e}^{\psi} \times \mathbf{e}^{\theta}} = R\hat{\phi} \end{aligned} \tag{A.56}$$

Then the covariant basis becomes:

$$(\mathbf{e}_{\psi}, \mathbf{e}_{\theta}, \mathbf{e}_{\phi}) = \left(\frac{\hat{r}}{|\nabla\psi| \cos\alpha}, \frac{r\hat{\theta}}{\cos\alpha}, R\hat{\phi}\right) \tag{A.57}$$

Where the scaling factors are:

$$(h_{\psi}, h_{\theta}, h_{\phi}) = \left(\frac{1}{|\nabla\psi| \cos\alpha}, \frac{r}{\cos\alpha}, R\right) \tag{A.58}$$

And the normalized tangent basis is the following:

$$(\hat{e}_{\psi}, \hat{e}_{\theta}, \hat{e}_{\phi}) = (\hat{r}, \hat{\theta}, \hat{\phi}) \tag{A.59}$$

It is important to observe that in this coordinates system the normalized tangent basis (A.59) does not coincide with the normalized reciprocal basis (A.55), since both bases are not orthogonal. By comparing expressions (A.54) and (A.57) the following relations are derived:

$$\begin{aligned} \left.\frac{\partial r}{\partial\psi}\right|_{\theta} &= \frac{1}{|\nabla\psi| \cos\alpha} \\ \left.\frac{\partial r}{\partial\theta}\right|_{\psi} &= r\sqrt{\frac{1}{\left(\hat{\theta} \cdot \hat{s}\right)} - 1} = r \tan\alpha \end{aligned} \tag{A.60}$$

Appendix B

Derivatives of the equilibrium

In this appendix are reported explicit expressions for the derivatives of the equilibrium quantities $\beta_{T\alpha}, \overline{\omega}_{p\alpha}$ and $\overline{\omega}_{c\alpha}$ calculated considering the equilibrium perturbations generated by the fluctuations and implemented in the raytracing routine C3PO [21]. Remembering that the fluctuations processes time scales are slow compared to the propagation times the perturbation are considered static respect to the ray evolution and no explicit time dependence is introduced in the dispersion relation. Remebering the general expressions for the perturbed equilibrium quantities illustated in chapter 2, the derivatives become:

$$\begin{aligned}
\frac{\partial \beta_{T\alpha}}{\partial \rho} &= \frac{\beta_{T\alpha}}{2T_\alpha}\frac{\partial T_\alpha}{\partial \rho} = \frac{\beta_{T\alpha}}{2T_\alpha}\left(\frac{\partial \overline{T}_\alpha}{\partial \rho} + \frac{\partial \widetilde{T}_\alpha}{\partial \rho}\right); \\
\frac{\partial \beta_{T\alpha}}{\partial \theta} &= \frac{\beta_{T\alpha}}{2T_\alpha}\frac{\partial T_\alpha}{\partial \theta} = \frac{\beta_{T\alpha}}{2T_\alpha}\frac{\partial \widetilde{T}_\alpha}{\partial \theta}; \\
\frac{\partial \beta_{T\alpha}}{\partial \phi} &= \frac{\beta_{T\alpha}}{2T_\alpha}\frac{\partial T_\alpha}{\partial \phi} = \frac{\beta_{T\alpha}}{2T_\alpha}\frac{\partial \widetilde{T}_\alpha}{\partial \phi};
\end{aligned} \tag{B.1}$$

$$\begin{aligned}
\frac{\partial \overline{\omega}_{p\alpha}}{\partial \rho} &= \frac{\overline{\omega}_{p\alpha}}{2n_\alpha}\frac{\partial n_\alpha}{\partial \rho} = \frac{\overline{\omega}_{p\alpha}}{2n_\alpha}\left(\frac{\partial \overline{n}_\alpha}{\partial \rho} + \frac{\partial \widetilde{n}_\alpha}{\partial \rho}\right); \\
\frac{\partial \overline{\omega}_{p\alpha}}{\partial \theta} &= \frac{\overline{\omega}_{p\alpha}}{2n_\alpha}\frac{\partial n_\alpha}{\partial \theta} = \frac{\overline{\omega}_{p\alpha}}{2n_\alpha}\frac{\partial \widetilde{n}_\alpha}{\partial \theta}; \\
\frac{\partial \overline{\omega}_{p\alpha}}{\partial \phi} &= \frac{\overline{\omega}_{p\alpha}}{2n_\alpha}\frac{\partial n_\alpha}{\partial \phi} = \frac{\overline{\omega}_{p\alpha}}{2n_\alpha}\frac{\partial \widetilde{n}_\alpha}{\partial \phi};
\end{aligned} \tag{B.2}$$

$$
\begin{aligned}
\frac{\partial \overline{\omega}_{c\alpha}}{\partial \rho} &= \frac{\overline{\omega}_{c\alpha}}{B^2}\left[\widetilde{B}_\rho \frac{\partial \widetilde{B}_\rho}{\partial \rho} + \left(\sigma_I B_p + \widetilde{B}_s\right)\left(\sigma_I \frac{\partial B_P}{\partial \rho} + \frac{\partial \widetilde{B}_s}{\partial \rho}\right) + \right. \\
&+ \left.\left(\sigma_B B_T + \widetilde{B}_\phi\right)\left(\sigma_I \frac{\partial B_T}{\partial \rho} + \frac{\partial \widetilde{B}_\phi}{\partial \rho}\right)\right]; \\
\frac{\partial \overline{\omega}_{c\alpha}}{\partial \theta} &= \frac{\overline{\omega}_{c\alpha}}{B^2}\left[\widetilde{B}_\rho \frac{\partial \widetilde{B}_\rho}{\partial \theta} + \left(\sigma_I B_p + \widetilde{B}_s\right)\left(\sigma_I \frac{\partial B_P}{\partial \theta} + \frac{\partial \widetilde{B}_s}{\partial \theta}\right) + \right. \\
&+ \left.\left(\sigma_B B_T + \widetilde{B}_\phi\right)\left(\sigma_I \frac{\partial B_T}{\partial \theta} + \frac{\partial \widetilde{B}_\phi}{\partial \theta}\right)\right]; \qquad \text{(B.3)} \\
\frac{\partial \overline{\omega}_{c\alpha}}{\partial \phi} &= \frac{\overline{\omega}_{c\alpha}}{B^2}\left[\widetilde{B}_\rho \frac{\partial \widetilde{B}_\rho}{\partial \phi} + \left(\sigma_I B_p + \widetilde{B}_s\right)\frac{\partial \widetilde{B}_s}{\partial \phi} + \left(\sigma_B B_T + \widetilde{B}_\phi\right)\frac{\partial \widetilde{B}_\phi}{\partial \phi}\right];
\end{aligned}
$$

Bibliography

[1] S. J. Zweben, J. A. Boedo, O. Grulke, C. Hidalgo, B. LaBombard, R. J. Maqueda, P. Scarin, and J. L. Terry. Edge turbulence measurements in toroidal fusion devices. *Plasma Phys. Control. Fusion*, 49:S1–S23, 2007.

[2] X. L. Zou, L. Colas, M. Paume, J. M. Chareau, L. Laurent, P. Devynck, and D. Gresillon. Internal magnetic turbulence measurement in plasma by cross polarization scattering. *Phys. Rev. Lett.*, 75(6):pp. 1090–1093, 1995.

[3] T. Gerbaud, F. Clairet, R. Sabot, A. Sirinelli, S. Heuraux, G. Leclert, and L. Vermare. Comparison of density fluctuation measurements between O-mode and X-mode on Tore Supra. *Rev. Sci. Instrum.*, 77(10):E928, 2006.

[4] R. E. Slusher and C. M. Surko. Study of plasma density fluctuations by the correlation of crossed CO2 laser beams. *Phys. Fluids*, 23(12):pp. 2426–2439, 1980.

[5] R. E. Slusher and C. M. Surko. Study of density fluctuations in the absorption of the oxygen on silicon. *Phys. Rev. Lett.*, 40(6):pp. 400–403, 1978.

[6] A. G. Sitenko. *Electromagnetic Fluctuations in Plasma*. Academic Press, New York, 1967.

[7] L. Vahala, G. Vahala, and N. E. Bretz. Electromagnetic wave scattering from magnetic fluctuations in tokamaks. *Phys. Fluids B*, 4(3):pp. 619–629, 1992.

[8] H. Bindslev. Three-wave mixing and Thomson scattering in plasmas. *Plasma Phys. Control. Fusion*, 35:pp. 1615–1640, 1993.

[9] E. Ott. Lower hybrid wave scattering by density fluctuations. *Phys. Fluids*, 25(2):pp. 359–375, 1982.

[10] P. L. Andrews and F. W. Perkins. Scattering of lower-hybrid waves by drift-wave density fluctuations: solution of the radiative transfer equation. *Phys. Fluids*, 26(9):pp. 2537–2545, 1983.

[11] P. T. Bonoli and E. Ott. Toroidal and scattering effects on lower-hybrid wave propagation. *Phys. Fluids*, 25(2):pp. 359–375, 1982.

[12] L. Vahala, G. Vahala, and P. T. Bonoli. Effects of magnetic and density fluctuations on the propagation of lower-hybrid waves in tokamaks. *Phys. Fluids B*, 4(12):pp. 4033–4045, 1992.

[13] C. Tsironis, A. G. Peeters, H. Isliker, D. Strintzi, I. Chatziantonaki, and L. Vlahos. Electron-cyclotron wave scattering by edge density fluctuations in iter. *Phys. Plasmas*, 16(11):pp. 619–629, 2009.

[14] K. Hizanidis, A. K. Ram, Y. Kominis, and C. Tsironis. Fokker-Planck description of the scattering of radio-frequency waves at the plasma edge. *Phys. Plasmas*, 17(1):pp. 1–10, 2010.

[15] F. Imbeaux and Y. Peysson. Ray-tracing and Fokker-Planck modeling of the effect of plasma current on the propagation and absorption of lower hybrid waves. *Plasma Phys. Control. Fusion*, 47(11):pp. 2041–2065, 2005.

[16] P. T. Bonoli, R. Parker J. Ko, A. E. Schmidt, G. Wallace, C. L. Fiore J. C. Wright, A. E. Hubbard, J. Hirby, E. Marmar, M. Porkolab, D. Terry, S. M. Wolfe, S. J. Wukitch, the Alcator C-Mode Team, J. R. Wilson, S. Scott, E. Valeo, C. K. Phillips, and R. W. Harvey. Lower hybrid current drive experiments on Alcator C-Mode: comparison with theory and simulation. *Phys. Plasmas*, 15:056117, 2008.

[17] M. Brambilla. *Kinetic Theory of Plasma Waves: Homogeneous Plasmas*. Oxford University Press, Oxford, first edition, 1998.

[18] T. H. Stix. *Waves in Plasmas*. Springer Verlag, New York, 1992.

[19] Y. Peysson and J. Decker. Calculations of rf current drive in tokamaks. In *Theory of Fusion Plasmas*, volume 1069 of *AIP Conference Proceedings*. AIP, 2008.

[20] J. Decker and A. K. Ram. Relativistic description of electron Bernstein waves. *Phys. Plasmas*, 13:112503, 2006.

[21] Y. Peysson and J. Decker. C3PO, a ray-tracing code for arbitrary axisymmetric magnetic equilibrium. Report EUR-CEA-FC-1739, 2008.

[22] J. Decker and Y. Peysson. DKE : a fast numerical solver for the 3D drift kinetic equation. Report EUR-CEA-FC-1736, 2004.

[23] J. A. Heikkinen, T. J. J. Tala, T. J. H. Pattikangas, A. D. Piliya, A. N. Saveliev, and S. J. Karttunen. Role of fast waves in the central deposition of lower hybrid power. *Plasma Phys. Control. Fusion*, 41:pp. 1231–1249, 1999.

[24] H. Goldstein, C. Poole, and J. Safko. *Classical Mechanics*. Addison-Wesley, New York, third edition, 2002.

[25] J. Wesson. *Tokamaks*. Oxford University Press, Oxford, second edition, 1997.

[26] A. Truc, A. Quemeneur, P. Hennequin, D. Gresillon, F. Gervais, C. Laviron, J. Olivain, S. K. Saha, and P. Devynck. ALTAIR: an infrared laser diagnostic on the Tore Supra tokamak. *Rev. Sci. Instrum.*, 63(7):pp. 3716–3724, 1992.

[27] Ch. P. Ritz, E. J. Powers, T. L. Rhodes, R. D. Bengston, K. W. Gentle, H. Lin, P. E. Phillips, A. J. Wootton, D. L. Brower, N. C. Luhmann Jr., W. A. Peebles, P. M. Schoch, and R. L. Hickock. Advanced plasma fluctuation analysis techniques and their impact on fusion research. *Rev. Sci. Instrum.*, 59(8):pp. 1739–1744, 1988.

[28] S. J. Zweben and S. S. Medley. Visible imaging of edge fluctuations in the TFTR tokamak. *Phys. Fluids B*, 1(10):pp. 2058–2065, 1989.

[29] R. Epstein and R. S. Craxton. Statistical ray tracing in plasmas with random density fluctuations. *Phys. Rev. A*, 33(3):pp. 1892–1902, 1986.

[30] G. T. A. Huysmans, J. P. Goedbloed, and W. Kerner. Helena code. In *Proceedings of the CP90 Europhysics Conference on Computational Physics, Amsterdam, the Netherlands, 10-13 September 1990*, page 371. Word Scientific, Singapore, 1991.

[31] P. N. Yushmanov. Diffusive transport processes caused by ripple in tokamaks. In *Reviews of Plasma Physics*, volume 16, pages 117–223. Consultants Bureau, New York, 1990.

[32] Y. Peysson, R. Arslanbekov, V. Basiuk, J. Carrasco, X. Litaudon, and J. P. Bizarro. Magnetic ripple and modeling of the lower-hybrid current drive in tokamaks. *Phys. Plasmas*, 3(10):pp. 3668–3688, 1996.

[33] N. J. Fisch. Theory of current drive in plasmas. *Rev. Mod. Phys.*, 59(1):pp. 175–234, 1987.

[34] Y. Peysson and the Tore Supra Team. High power lower hybrid current drive experiments in the Tore Supra tokamak. *Nucl. Fusion*, 41(11):pp. 1703–1713, 2001.

[35] S. Bernabei, C. Daughney, P. Efthimion, W. Hooke, J. Hosea, F. Jobes, A. Martin, E. Mazzuccato, E. Meservey, R. Motley, J. Stevens, S. Von Goeler, and R. Wilson. Lower-hybrid current drive in the PLT tokamak. *Phys. Rev. Lett.*, 49(17):pp. 1255–1258, 1982.

[36] R. Cesario, A. Cardinali, C. Castaldo, F. Paoletti, and D. Mazon. Modeling of a lower-hybrid current drive by including spectral broadening induced by parametric instability in tokamak plasmas. *Phys. Rev. Lett.*, 92(17):175002, 2004.

[37] R. Cesario, A. Cardinali, C. Castaldo, F. Paoletti, W. Fundamenski, S. Hacquin, and the JET-EFDA workprogramme contributors. Spectral broadening of lower hybrid waves produced by parametric instability in current drive experiments of tokamak plasmas. *Nucl. Fusion*, 46(4):pp. 462–476, 2006.

[38] N. J. Fisch and A. H. Boozer. Creating an asymmetric plasma resistivity with waves. *Phys. Rev. Lett.*, 45(9):pp. 720–722, 1980.

[39] S. Gunther, G. Giruzzi, A. Gude, R. J. La Haye, K. Lackner, M. Maraschek, S. Schade, S. Sesnic, R. Wolf, Q. Yu, H. Zohm, and the ASDEX Upgrade Team. MHD modes in regular and reversed shear scenarios and possibilities for their control through current drive. *Plasma Phys. Control. Fusion*, 41(12B):B231–B241, 1999.

[40] P. T. Bonoli, R. W. Harvey, C. Kessel, F. Imbeaux, T. Oikawa, M. Schneider, E. Barbato, J. Decker, G. Giruzzi, C. B. Forest, S. Ide, Y. Peysson, A. E. Schmidt, A. C. C. Sips, A. P. Smirnov, and J. C. Wright. Benchmarking of Lower Hybrid Current Drive codes with applications to ITER-relevant regimes. In *In Proceedings of the 21st IAEA Conference, Chengdu,China, 16-21 October 2006*, 2006.

[41] *Summary of the ITER Final Design Report*, 2001. Available on line at http://fire.pppl.gov/.

[42] D. W. Ignat, E. J. Valeo, and S. C. Jardin. Dynamic modelling of lower hybrid current drive. *Nucl. Fusion*, 34(6):pp. 837–852, 1994.

Acknowledgements

I would particularly like to thank Dr. Y. Peysson for his careful and instructive advices during my third year of Ph.D course, always stimulating my work and helping me in difficult moments with great patience and persistence. In this thesis are presented the results of the work done about the effects of fluctuations on radiofrequency current drive under his supervision at Institut de Recherche sur la Fusion Magnetique (IRFM), CEA, Cadarache (France). I thank the Plasma Heating and Confinement Department and the Experimental Support and Modeling Group of the IRFM for their hospitality and I wish to give a special thank to Dr. J. Decker for his friendly and fruitful suggestions during my year in Cadarache.
I am grateful to Prof. M. Carfora of the University of Pavia for his support and his valuable suggestions during these three years of work and expecially for giving me the opportunity of spending my third year at IRFM in Cadarache.
I would like to thank also Prof. M. Bornatici of the University of Pavia for the diligent supervision of my work during the first part of my Ph.D course.
I thank also Dr. C. Castaldo, the external referee of my thesis, for his availability and the valuable discussions, and Dr. A. Cardinali, for his helps and advices and his friendship during all these years.
I want to give a special thank to Prof. Turchetti, my first supervisor during my bachelor and master, for devoting so much time and attention to teaching and to introduce students to research.
Moreover I thank the Physics Department "A. Volta" of the University of Pavia together with all Ph.D students which have shared with me these three years.

Alla fine di questa avventura, voglio innanzitutto ringraziare tutta la mia famiglia e Carla per essermi sempre stati vicini ed essere sempre stati dalla mia parte, in ogni momento, se sono arrivato a questo traguardo lo devo a loro, ed è a loro che dedico la mia tesi. Grazie ai miei genitori, per avermi sempre aiutato e sostenuto nel cercare la mia strada e nel seguire i miei sogni, anche nei momenti più duri, in cui io stesso dubitavo di potercela fare, loro hanno sempre avuto fiducia in me, e questo mi ha aiutato a non mollare mai, fino alla meta. Grazie a mia sorella Margherita, che mi sopporta, mi ascolta e cerca di

capirmi ogni giorno, e so che non è facile. Grazie ai miei nonni e a tutto il resto della mia famiglia per esserci, sempre. Un grazie immenso a Carla, per tutto quello che è nato ed è maturato fra noi in questi anni, per avermi incontrato, cercato e aspettato, per la dolcezza con cui mi è stata vicino sempre, anche quando siamo stati lontani, per avere intrapreso questo splendido cammino insieme.
Ringrazio tutti i miei colleghi di dottorato e di studi universitari, in modo particolare il Toscano e il Tenti, per tutti i momenti trascorsi insieme, anche di studio, e le belle serate passate fra i giorni di lavoro, a loro mando un grande in bocca al lupo per il futuro e un arrivederci in giro da qualche parte, per un' altra delle nostre solite cene.
Voglio ricordare i miei amici, senza i quali tante cose in questi anni non avrebbero avuto lo stesso significato. Grazie a Teo e ad Andre per i tantissimi momenti vissuti insieme, fin dagli anni del liceo, per i viaggi, le serate, le risate, le discussioni, anche per le liti, che ogni tanto in fondo ci vogliono e fanno crescere...Grazie ad Alberto e Claudio per esserci sempre, con la loro generosità e semplicità, e per essere due grandi esempi di persone coerenti e a loro modo controcorrente, in un mondo dove non è tanto semplice andare contromano. Grazie all' Eli per aver sempre cercato di capirmi, ascoltarmi e in certi momenti anche sopportarmi. Grazie a Chiara per la sua amicizia sempre sincera, la sua grande saggezza e i tanti buoni consigli. Grazie ad Ale per essere stato il miglior coinquilino che abbia mai sperato di incontrare, oltre ad essere un signor musicista e un grande amico, le nostre serate fra Torrenova e San Lorenzo con Guccini in sottofondo resteranno nella storia...Grazie a Michele per essere l'informatico smanettone più simpatico e antagonista che conosca, altro che wikileaks!! Grazie a tutti i compagni d'avventura incontrati durante lo splendido periodo passato oltr'alpe, a Cadarache, in modo particolare a Joao, Michal, Clemente, Blaise e François-Xavier. Un grazie enorme anche all' Ali, alla Susi, a Kekko, a Tano, a Nicola e a tutti gli altri amici incontrati e conosciuti in questi anni, con cui ho camminato insieme lungo un pezzo della strada.